DEVELOPMENT AND CHARACTERIZATION OF POLYDIMETHYLSILOXANE AND CARBON BLACK COMPOSITES FOR PHOTO ACTUATION

Thesis

Submitted in partial fulfillment of the requirements for the degree of

DOCTOR OF PHILOSOPHY

By

SHIVASHANKARAYYA HIREMATH

DEPARTMENT OF MECHANICAL ENGINEERING

NATIONAL INSTITUTE OF TECHNOLOGY KARNATAKA,

SURATHKAL MANGALURU - 575 025

May, 2020

DECLARATION

I hereby *declare* that the Research Thesis titled "**Development and Characterization of Polydimethylsiloxane and Carbon black Composites for Photo Actuation**" Which is being submitted to the **National Institute of Technology Karnataka, Surathkal,** in the partial fulfilment of the requirements for the award of the Degree of **Doctor of Philosophy** in the Department of Mechanical Engineering, is a *bonafide report of the work carried out by me*. The material contained in this Research Thesis has not been submitted to any University or Institution for the award of any degree.

Register Number: **155132ME15F11**

Name of the Research Scholar: **SHIVASHANKARAYYA HIREMATH**

Signature of the Research Scholar:

Department of Mechanical Engineering

Place: NITK, SURATHKAL

Date: 15/05/2020

CERTIFICATE

This is to *certify* that the Research Thesis titled "**Development and Characterization of Polydimethylsiloxane and Carbon black Composites for Photo Actuation**" submitted by **Mr. Shivashankarayya Hiremath (Register number: 155132ME15F11**) as the record of the research work carried out by him, is *accepted as the Research Thesis submission* in partial fulfilment of the requirements for the award of degree of Doctor of Philosophy.

Research Guide

Dr. S.M. Kulkarni
Professor
Dept. of Mechanical Engineering,
NITK, Surathkal.

Chairman – DRPC

DEDICATION

**"Guru Brahma Guru Vishnu, Guru Devo Maheshwara
Guru Sakshat, Param Brahma, Tasmai Shri Guravay Namah"**

To all my Teachers,
To my beloved Parents,
To my Brothers and Sisters,
To my Wife and little Daughter

ACKNOWLEDGMENTS

ABSTRACT

There has been a rapid increase in the number of multidisciplinary research activities in the last two decades. The limits between disciplines are narrowing, as scientists in distinct areas coming up with intriguing concepts that combine expertise in a distinct field. The motive behind this multidisciplinary research arises from nature. Nature inspires us to mimic or generate thoughts for different applications that can enhance or change the requirements of society.

The objective of the present research is to develop a photo actuator using composite material for microcantilevers, micro-grippers, micro-robots, photo-switches, micro-motors, energy harvesting, and other smart photo devices. The cantilever beam is designed as a single and bilayer structure, actuated by photothermal action. It consists of polydimethylsiloxane and carbon black composites. Thus, there is thermomechanical deformation owing to the difference in the coefficient of thermal expansion as well as the rise in the thermal conductivity of the composite material. The composite beam also induces thermal stress due to differences in the temperature of the beam involved in the adsorption of the light source. The methods engaged in the current investigation of the photo actuator are empirical, numerical (Finite Element) modeling, analytical, and composite material processing and characterization. The empirical model has been used to comprehend and compare the properties of the composite material. Also, material modeling of more significant characterizations is being studied using numerically. The carbon black and polydimethylsiloxane materials have been procured, and the composites have been synthesized using the solution casting technique. Composite properties have been studied by performing various characterization tests for physical, mechanical, thermal, optical, dielectric, and microstructure. Analytical and numerical studies were implemented to investigate the optimum value by varying the thickness and volume percentage of the filler material at different temperatures. The photo actuation test setup was built, and the

composite beam has been tested. Finally, the proposed conceptual model was developed and tested in the laboratory environment.

The approach of empirical and numerical (Finite Element) material modeling, composite material characterization, analytical and numerical modeling of actuator models, and proposed prototypes have been discussed. The empirical models were used to estimate the density, elastic modulus, thermal conductivity, coefficient of thermal expansion, and dielectric permittivity of the composite material, and numerical (FE) modeling is also performed for the more influencing parameters of the actuator. The results of material modeling were compared with experimental results. The carbon black particulate-filled polymer composite is developed for the investigation of density, mechanical, thermal, optical, and dielectric characteristics. The inclusion of the filler significantly improves the features of the matrix material. The density of the composite enhanced as the content of the reinforcement is increased from 5 to 25 Vol %. The elastic modulus of the composite is 57% higher than the plain matrix material. The thermal conductivity of the composite was substantially improved both numerically and experimentally. The inclusion of carbon black fillers into the PDMS leads to the reduction of the coefficient of thermal expansion. Also, the same is proved using the numerical method. The dielectric constant of the composite is improved significantly more by varying filler concentration.

Analytical and numerical modeling has been carried out using commercially accessible software. Analytical findings on the deflection of the composite beam are validated with numerical modeling. The results are almost similar to each other, with a varying percentage of carbon black content and a change in the thicknesses of the layers. The bilayer composite beam is significantly more deflective than the single-layer beam. Also, by altering the temperature of the layers, the bilayer composite beam indicates considerably more deflection than the single layer. In continuing with this, the single and bilayer composite beams are tested experimentally, and it is a good agreement with numerical results. Finally, the proposed conceptual model of the photo actuator tested successfully. Attempts are

being made in the present research to use a polymer composite beam for photo actuation and testing for the suggested prototype system. The dissertation is typically composed of empirical, numerical (FE), analytical modeling, and experimental approaches. Also, the characterization of the composite material and the efficiency of the photo actuator have been highlighted. As a result, PDMS and CB composites could be suggested for one of the photo actuator material.

TABLE OF CONTENTS

LIST OF FIGURES

xvii

LIST OF TABLES

NOMENCLATURE

MEMS	Micro electro-mechanical system
MOMS	Micro optomechanical system
GPS	Global Position System
MMC	Metal Matrix Composites
CMC	Ceramic Matrix Composites
PMC	Polymer Matrix Composites
PRP	Particle Reinforced Polymer
FRP	Fibre Reinforced Polymer
FE	Finite element
UV	Ultraviolet
NIR	Near-infrared
FEA/M	Finite element analysis/method
SWCNT	Single-wall carbon nanotube
VO_2	Vanadium dioxide
GNP	Graphene nanoparticles
CNT	Carbon nanotube
PDMS	Polydimethylsiloxane
LC	Liquid crystalline
rGO	Reduced graphene oxide
PET	Polyethylene terephthalate
LAP	Light active polymer
CB	Carbon black
LCE	Liquid crystal elastomer
TEM	Thermally expanding microspheres
MoS_2	Molybdenum disulfide
HDPE	High-density polyethylene
SMA	Shape memory alloy

CTE	Coefficient of thermal expansion
TC	Thermal conductivity
ASTM	American Society for Testing and Materials
UTM	Universal testing machine
TMA	Thermomechanical analyser
TPS	Transient Plane Source
XRD	X-ray diffraction
TEM	Transmission electron microscopy
DLS	Dynamic light scattering
SEM	Scanning electron microscope
UV-Vis-IR	Ultraviolet-Visible Infrared
3-D	Three Dimensional

SYMBOLS

ρ	Density
E	Young modulus
ν	Poison's ratio
k	Thermal conductivity
Cp	Specific heat capacity
α	Coefficient of thermal expansion
I_{in}	Intensity of light
m	Mass
A	Absorption coefficient
h	Convective coefficient
δ	Deflection
T	Temperature
t	Time
R	The radius of the curvature
b	Thickness
θ	Bending angle
L	Length
V_f	Volume fractions of the reinforcement
V_m	Volume fractions of the matrix
Q	Heat flux
F	Force
T_s	Tear strength
ε	Dielectric constant
σ	Electric conductivity
ω	Angular Frequency

CHAPTER 1

INTRODUCTION

1.1 General

In the past two decades, there is a tremendous rise in the number of multidisciplinary research. The boundaries between disciplines are getting narrower, as researchers in different fields come up with fascinating ideas that combine knowledge in different areas. Such collaborations have opened new avenues, especially in science and engineering, where fundamental knowledge is applied in solving practical problems. In the present work, such multidisciplinary research is attempted to develop a polymer composite based photothermal actuator.

Nature is inspiring us to mimic or create ideas for different applications; Nature motivated research is a new era in science and technology. Sunflower is one of the best examples of natural orientation, and its tilt mechanism is based on the sunlight. Much research is going on the development of the light-based actuator devices. Nevertheless, the device depends on the mechanical arrangement, materials, and source of stimulus.

The primary motivation of an actuation phenomenon is due to sunflower bending. Hence, currently, light-based actuation, research is one of the emerging fields of study for orienting, deflecting, and tilting of an object. The goal of work is to develop a novel actuator, whose movements are based on a light source. Presently, the researchers are developing actuators using different stimuli, like electrical, magnetic, thermal, and pneumatic/hydraulic. There is limited research carried out in light-based actuation. Few researchers have implemented light stimulated sensor and actuator, switches, micro-motors, robotics, artificial muscle, Micro electro-mechanical system (MEMS), energy harvesting, Micro optomechanical system (MOMS), optical telecommunication (Zhu et al. 2018) applications.

The development of composites-based actuators are required an essential engineering background and material background as one of the key components for photo actuation. Thus, primary materials such as metals, ceramics, polymers, alloys, and composites are

used in the development of the above applications. In that, the recent year polymers are replacing other material due to less weight, less cost, natural way of tailoring the properties (i.e., mechanical, thermal, optical and dielectric), and simple fabrication. Hence, the present study is focused on polymer-based composite for the development of the actuator. Understanding the actuation mechanism due to light source requires the knowledge of material science, physics, modeling, and simulation. The development of a prototype and testing of the composite actuator follows steps like idea generation, a development of the model, selection of material, implementation or fabrication of the actuator, experimental testing, and validating the system.

1.2 Motivation

A renewable source of energy, such as solar, wind, geothermal, biomass, or wave energy, does not cause pollution. Also, renewable sources are of low cost; they eliminate the uncertainty and the expenses of material, then increase the output energy. A renewable energy source is a perfect solution to the alternate source of energy. Solar power is one of the world's most promising sources of renewable energy. The location of the sun in the sky changes from season to time as the earth moves across the sky. The light power of the sun is about 1000 to 1300 W/m², as the sun rays come perpendicular to a plane. Every day, dynamically focused solar panels will monitor the sun to improve the collection of power significantly. To optimize irradiation, a solar monitor orients a solar panel or focus solar reflector or lens towards the sun.

The way of maximizing solar energy is by orienting the solar panel appropriately. The panel angles, such as azimuth and elevation, are kept at the desired position during the daytime and generate desired values of elevation, and azimuth angles between 6 am to 6 pm. Hence, the panel orientation/tilting approach is an effective and predictable way of increasing solar energy. Nowadays, researchers are mimicking nature components for getting a better, robust, and efficient system for the development of sensors and actuators. Few researchers have developed a new solar energy system inspired by the action of

sunflowers. It is at least 10% more effective than traditional solar panels have shown (Li et al. 2012).
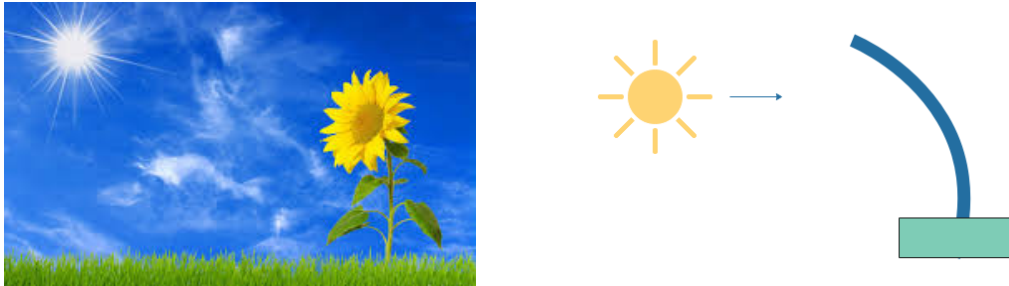
Figure 1.1 Sunflower inspired bending

The sunflower inspired behavior is known as heliotropism - the tracking of the sun rays throughout the day and then positioning the panel to grab the most sunlight shown in Figure 1.1. There are many other solar power systems that use GPS and motors to reposition solar panels for the whole day. Still, this new system is unique because it uses state-of-the-art material technology to take a more passive approach to sunlight monitoring.

The sunflower orientation or tilting is to motivate the implementation of the actuator system by a light source. The actuator needs to be developed by selecting the appropriate material and mechanism. In the present work, a composite beam has been implemented based on a light source.

1.3 Actuators

The function of the actuator is to transfer the input energy (i.e., electrical, thermal, magnetic, light) into output work (i.e., mechanical motion/displacement, shifting, phase changing). The direct transformation of various types of energy into mechanical energy is of paramount importance in a wide range of actuation applications such as robots, artificial muscles, valves, switches, optical displays, MEMS, and MOMS. Actuators are categorized according to the input type, a material used, process, and operation. Some of the soft actuation listed out in Table 1.1 (Asaka and Okuzaki 2013).

Table 1.1 Some of the soft actuators

Type of Input	Material	Mechanism
Electric/mechanical	Piezoelectric materials, dielectric material	Compressed/expansion
Thermal/electric	Shape memory alloys	Bending/deflection
Thermal/light/electric	polymers	Bending/deflection/phase change

Materials in response to external stimuli such as temperature, electrical field, magnetic field, or a light source, may alter their properties and dimensions. Material is one of the vital constituents to implement the actuator device for different applications based on the requirement. Modern-day actuators include electromagnetic motors, hydraulic actuators, pneumatic actuators, shape memory alloys, electroactive polymers, piezoelectric and magnetic actuators. In recent years, light-driven actuators are developed and light as a form of energy to drive the polymer-based actuation system (Ahir and Terentjev 2005b; Li et al. 2003).

1.3.1 Photo actuators

The photo actuator can be divided into three groups; these are optical force, photochemical effect, and photothermal action, as shown in Figure 1.2. The actuation of optical force is based on the direct transfer of momentum from radiation to matter; it can transform optical energy into mechanical work (Maragò et al. 2013). Photochemical effects, such as photoisomerization and photodimerization, make full use of the different photoreactions of light-sensitive groups (Camacho-Lopez et al. 2004), whereas photothermal results depend on light-to-heat conversion, including photothermal expansion or contraction, absorption or desorption, and phase transition (Maggi et al. 2015).

```
                    ┌──────────┐
                    │  Light   │
                    └──────────┘
          ┌──────────────┼──────────────┐
          ▼              ▼              ▼
   ┌──────────┐   ┌──────────────┐  ┌──────────────┐
   │ Optical  │   │Photochemical │  │ Photo thermal│
   │ force    │   │              │  │ Effects      │
   │          │   │ Effects      │  │              │
   └──────────┘   └──────────────┘  └──────────────┘
```
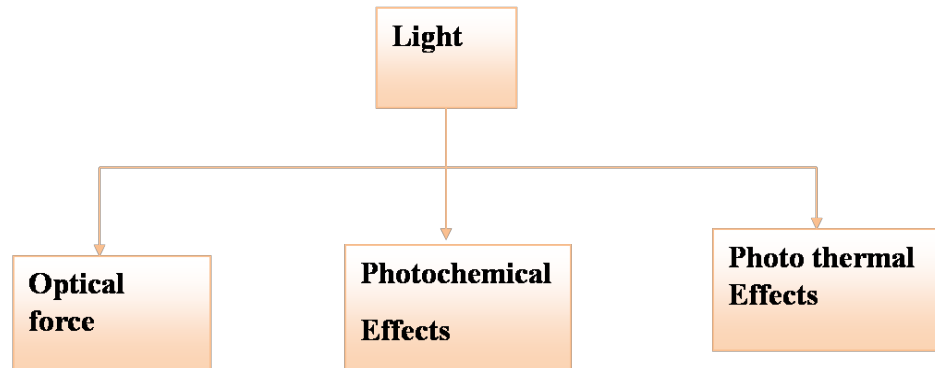
Figure 1.2 Classification of the photo actuators

The photothermal effect has been commonly used in actuators since various photosensitive materials can convert light to heat. For example, carbon materials (Han et al. 2018), noble metal nanoparticles, and photothermal polymers (Luo et al. 2015) are usually used in photothermal mechanical actuation strategies. Photothermal strategies are classified into three categories: (i) Photothermal phase transition using shape-memory materials, (ii) Photothermal surface tension gradient, and (iii) Photothermal expansion or contraction. A general mechanism for multilayer photo actuators is the photothermal effect mediated by expansion or contraction and bending of the material. Differences in the thermal expansion of the two layers induce deformation by light irradiation. Also, the photothermal effect, the change in size, the change in phase are all lead to the smart actuation. In the current work, the main focus is on proposing composite material, testing the characteristics of the composite material, and the photo actuator bending test.

1.4 Materials

Conventional engineering materials are still unable to fulfill the requirements of these unique properties, such as high strength, high density, lower expansion coefficient, and higher conductivity. Demand for structurally stable, cost-effective, and lightweight, and absorbent materials is growing daily. Research efforts are thus directed towards the development of a polymer matrix composite, eventually enabling the production of a new class of inexpensive, high thermal conductivity and a lower coefficient of thermal

expansion material. At present, the commonly used material for the photo actuator is of polymer-based. Smart polymer-based materials are, therefore, of increasing interest due to their ability to perform specific functions in response to environmental changes. A composite material is, therefore, necessary to adapt the properties of the polymer according to its functionality.

1.4.1 Composite material

A composite is a structural substance composed of two or more elements combined at a macroscopic level and not soluble in each other. One part is called the reinforcement stage and is called the matrix in which it is integrated. The form of the fibers, particles, or flakes may be the reinforcement stage material. In general, the matrix stage materials are continuous. Matrix's primary function is to transfer stress between reinforcement (flakes/fiber/ particle) materials and to prevent them from mechanical and environmental damage, where the existence of this filler in the composite can improve or modify its mechanical and thermal characteristics such as strength, stiffness and thermal conductivity. Composites have been effectively substituted in the conventional product due to the lightweight, easily adjustable, and simple manufacturing processes involved. Therefore, the strength of the composite depends primarily on the amount, arrangement, and form of filler used in the resin material (Kausar et al. 2016).

Types of Composites

Depending on the matrix material, composites can be categorized into three classes. They are:

    a) Metal matrix composite (MMC)
    b) Ceramic matrix composite (CMC)
    c) Polymer matrix composite (PMC)

a) Metal Matrix Composites:

Because of their high specific strength, metal matrix composites have many advantages over monolithic metals; they can work in a wide range of temperatures, good electrical and thermal conductivity, higher specific modules, and low thermal expansion coefficient. Material matrix composites are used for a wide range of applications due to these attributes such as combustion chamber nozzle (in a rocket, space shuttle), housings, pipes, wires, heat exchangers, tank loves, modern high-performance sports cars, and many more.

b) Ceramic Matrix Composites:

Increasing strength and crack resistance are some of the main goals for manufacturing ceramic matrix composites. Typically, it is found that the strength and rigidity of ceramic matrix composites are simultaneously increased. The ceramic matrices generally are glass, glass ceramics (aluminosilicate lithium), carbides (SiC), nitrides (SiN4, BN), oxides (Al_2O_3, Zr_2O_3, Cr_2O_3, Y2O3, CaO, and ThO_2) and borides (ZrB_2, TiB_2). The reinforcements are inorganic materials of high temperature, like ceramics, perhaps in the form of particle flakes, whiskers, and fibers. Carbon, silicon carbide, silica, and alumina are frequently used fibers. Carbon-carbon composites are a large group of composites of the ceramic matrix that can withstand temperatures of up to 3000 ºC. Ceramic composites are primarily used in high-temperature applications, higher strength, and high dielectric applications.

c) Polymer Matrix Composites (PMC)

Commercial composite production is often referred to as polymer matrix composites using resin solutions. Polymers are repeated structural units for macromolecular binding covalently. Therefore, for various structural purposes, their mechanical property is inadequate. Compared to metals and ceramics, their strength and stiffness are particularly low. This challenge is overcome, however, by improving other constituent materials such as iron, ceramics, or organic compounds. The most common advanced polymer matrix composites (e.g., epoxy, polyester, polydimethylsiloxane, polyurethane) are thus

strengthened by filler (e.g., graphene, carbon nanotube, chromium powder, carbon) (Bakshi et al. 2010),(Huang 2002).

Composites are nearly five times stronger than the primary material on a weight-to-weight ratio. The most popular composites have low cost, high strength, and simple manufacturing principles. The major drawbacks of PMCs are low operating temperatures, high thermal and moisture expansion coefficients, and poor elastic properties in specific directions (Kaw 2005). The polymers are also graded according to the specification by low pressure and high/low temperature. The material may be a thermoset (processing temperature 200°C) or a thermoplastic (processing temperature 300°C to 400°C). Still, together with more straightforward manufacturing equipment for the production of these composites, it is concatenated in real-life applications to its suitability.

1.4.2 Polymer composite

Figure 1.3 indicates a further grouping of polymer composite into three groups based on the reinforcement material used. They are:

- Particle reinforced polymer
- Fiber-reinforced polymer
- Hybrid composites/structural composite

Particle reinforced polymer:

These are composites formed using a particle as a constituent reinforcement material. Particles may be minerals, ceramics, amorphous material, and other organic compounds that are unavailable in the neat polymer matrix medium to achieve the desired product. In particular, particles are used to increase modulus, thermal conductivity, and deduction of elasticity, weight reduction, and overall cost. Some of the main properties are low density, high melting point, corrosion resistance, high strength and stiffness, wear-resistant. Many ceramic filler particles also possess excellent electrical and thermal insulation properties; some are piezoelectric materials, while some behave as superconductors at very low temperatures. Many polymeric particles of materials, such as carbon nanotube, graphite

flake, graphene oxide, zinc oxide, barium titanate (BaTiO3) and carbon powder, etc., are commonly used in the generation of micropower, sensor and actuators. They serve as additives to adjust the composite's creep, effect, thermal, electrical, and magnetic properties and wear resistance, flammability, and other such characteristics.
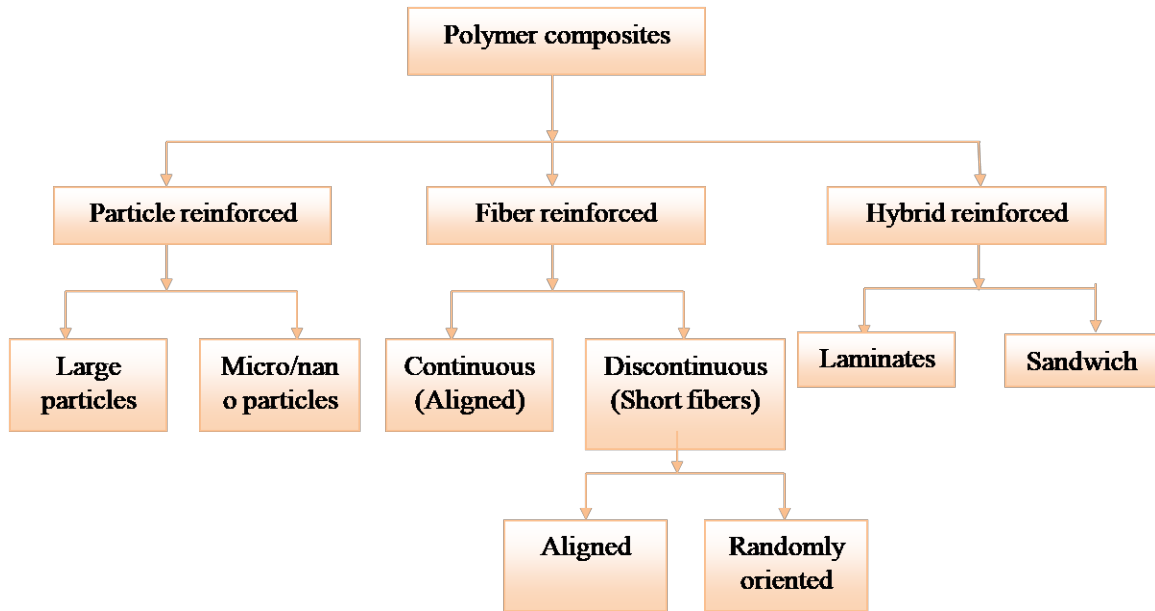
Figure 1.3 Classification of polymer composites based on the method of reinforcement

At present, particle reinforced composites are making rapid progress in the development of soft materials. Nonetheless, considering malnutrition as a challenge and enhancing the properties of the particulate composite material for actuation purposes.

1.4.3 Materials for photo actuation

The light-driven materials are those; which can absorb the light by photoresponsive materials. These composite materials can raise the internal temperature by non-radiative decaying. For example, carbon-based material absorbs a wide range of light from the ultraviolet (UV) to near-infrared (NIR) range of wavelength. The carbon material functions as a composite material to absorb the NIR light and then convert light energy into thermal

energy. Light on the material may scatter, absorbs, and transmits across the area. Transmitted light propagating in the same direction as the incident light. The scattered light is spread over the direction of light. Whereas absorbed light energy is stored in the form of heat energy in the volume of the materials. In materials, absorption and scattering take place at the molecular and atomic levels. Light intensity profile/ absorption in the material along the thickness can be calculated using Beer-Lambert's law. Finally, transverse bending is due to the impact of the light source on the material. Thus, this multidisciplinary transduction leads to mainly three steps for the overall analysis of the system.

- Photo energy into heat energy
- Material elongation or transverse bending is due to heat
- Displacement is due to a change in temperature

Light absorbing material: light intensity decreases as it passes through the material, generally due to its conversion to another form of energy. Whereas dark material such as carbon black, carbon nanotubes, and graphene absorb more visible and IR light than UV light. The intensity of light absorbance is measured using a spectrophotometer. The light passes through the sample, and the absorbance constant is detected based on the wavelength of light.

1.5 Analysis and modeling of photo actuator

A well-designed model of simulation can help to build consensus and trust. The new, improved model is developed, which has never been used before "tried & tested." Computerized simulation models can provide powerful visual resources that can make many complicated, interdependent decisions quickly and efficiently. Often, with executing scenarios and analyzing results, a user gains essential insight and a higher knowledge of their issue from the very process of model construction. Simulation models can sometimes be designed to discover the ideal solution with a high level of trust. There is distinct modeling software used for analytical and numerical (FE) analysis of photo actuators. For

the proposed research study, commercially available Finite Element Analysis (FEA) software is used. Understand the software tools and implement the models/equation for the analysis of the actuator system.

The light-based actuation depends on the material and mode of transduction. An extended block diagram of the light actuation method is as shown in Figure 1.4. Due to the material behavior or internal transduction of the system; the stack (beam) gets heated up based on the intensity of the light, and then a change in temperature occurs in the order. The difference in temperature leads to compressing, bending, tension, phase changes in the system. Also, the proper selection of material and assembling depends on a rise in temperature. Hence, the system is combined with the interdisciplinary branches to define the photo actuator system using composite material.
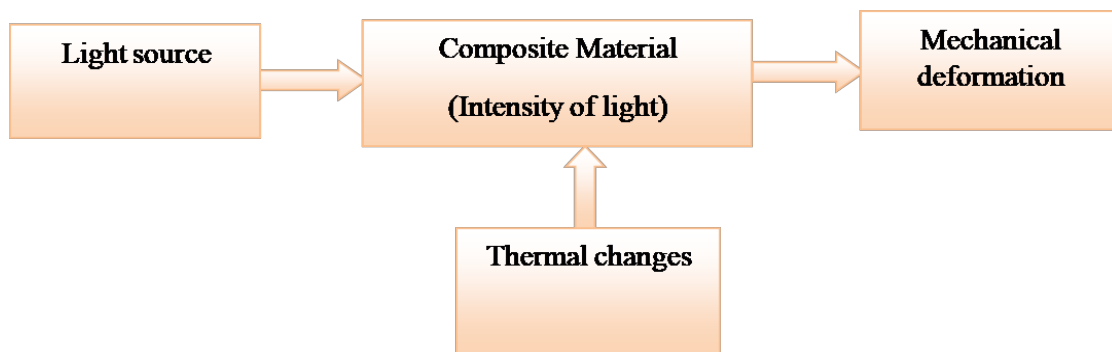
Figure 1.4 A functional diagram of a photo actuator

Summary

Nature has given many resources to utilize in an appropriate way for the development of humankind. The nature-inspired heliotropic actuator development is considered, which will mimic the sunflower and tracking the sunlight. In this phenomenon, two transduction methods occur i) photothermal conversion ii) thermal to mechanical conversion. Thus this photothermal actuator, deflection, is based on natural light, which consists of ultraviolet to an infrared range of wavelengths. Also, there is a need to understand and study the light to actuation methods. For the actuation, appropriate material is required to mimic the sunflower. Hence polymer composite materials were used for the development of

11

photothermal actuator. The desired properties of polymer composite are to be explored. Simultaneously analytical and numerical methods are used for a better understanding of actuator behavior using commercially available tools. Finally, the photothermal actuator has to develop and prototype tests to be conducted for a tracking and switching system.

1.6 Literature survey

The detailed review of the published literature is very relevant to identify the area and gaps in the present study. The literature study discussed is concerning to the development of a composite photo actuator. The literature is focused on polymer composite material, photo-actuators, numerical modeling of the actuator, and application are surveyed.

1.6.1 Materials for the photo actuator

The photo actuator system combines both transductions and actuation functions into a compact system. The actuation material directly transforms photo energy into heat and mechanical deformation. In the development of the actuator, the type of energy for movement and actuation becomes an important consideration. The light energy to mechanical energy conversion can be performed by choosing various photoresponsive materials for the actuator. Presently, the polymer-based composites are replacing the conventional material for the photothermal applications. Hence, some of the recent literature on photoresponsive materials has shown a tremendous response to photo actuation.

Zhang et al. (2014) had fabricated polycarbonate and single-wall carbon nanotube of bilayer photo actuators with highly unique light-responsive properties. A low-cost and the straight forward room-temperature process was adopted. In these double layers, the material showed a quick response, extreme light sensitivity, large deflection, and also a reversible actuation. As a benchmark for rapid and reversible light-responsive properties, a bright curtain was demonstrated to highlight the typical application of the proposed double layers. A bilayer was prepared and directly under sun intensity (100mW/cm²), the

sample is bent ~90 degrees within ~0.67 s and reverts to the relaxed state in ~0.87 s after the light is turned on and off, which is shown in Figure 1.5.
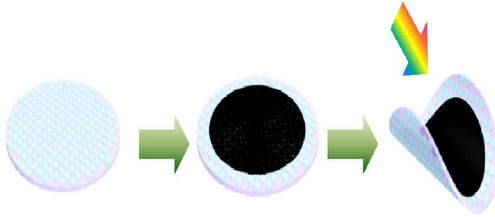
Figure 1.5 Bilayer polycarbonate and single-wall carbon nanotube composite. (Zhang et al. 2014b)

Torres et al. (2015) presented a new approach to increase the efficiency, responsivity, and speed of Vanadium Dioxide and, Single-Wall Carbon Nanotube based photo-thermally driven actuators. It utilizes the excellent light-absorbing properties of the carbon nanotube films. The film was prepared using a simple vacuum filtration process. The improvements in SWCNT/VO$_2$ composite actuators have demonstrated excellent performance in terms of strain energy density, speed, reversible actuation, programming capabilities, and large deflection compared to Vanadium Dioxide film. The images of Vanadium Dioxide and SWCNT/VO$_2$ composite cantilever deflection are shown in Figure 1.6.
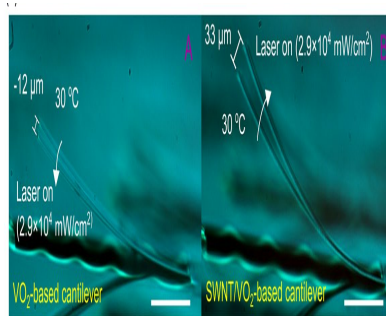
Figure 1.6 Vanadium dioxide and vanadium dioxide /single-wall carbon nanotube composite photo-thermally driven actuators (Torres et al. 2015)

Loomis et al. (2013) fabricated a composite of graphene nanoplatelets dispersed within the polydimethylsiloxane matrix. The authors have reported that the GNPs in the matrix showed efficient light absorption. The subsequent energy transduction to polymeric chains was utilized to produce in a controlled manner, significant amounts of motion due to the entropic elasticity of the pre-strained composite. Maximum actuator efficiency values

measured were observed to be 1000 times higher than recently reported actuator efficiency for light-thermal-driven polymer systems.

Baglio et al. (2002), in their work, proposed a photothermal mechanical actuation strategy. A bi-layer cantilever was designed with a micro-machined lens placed over it. Laser beams were used as a power source for photothermal actuation, causing the cantilever to heat up and bend, on account of difference in values of the coefficient of thermal expansion of two layers. The authors stated that "this kind of actuation system can be used in applications where high actuation power is required, and an electrical power supply is neither accessible nor feasible.

Levitsky et al. (2006) prepared a double layer composite by depositing single-walled carbon nanotubes into nafion. The composite exhibited substantial mechanical motion upon exposure to visible and near-infrared light. The absorption spectrum of single-walled carbon nanotube in near-infrared was found to be in parallel to the magnitude of actuation, but the actuation diminished in the visible portion of the spectrum and disappeared in the UV portion of the spectrum. It was observed that the actuation in near-infrared was linear to the light intensity. The authors concluded that the band bending of the semiconducting SWCNTs induces the polarization of the mobile hydrogen ions at the Nafion interface, causing swelling of the polymer, and the swelling of the polymer was the mechanism for actuation.

Xu and Allen (2009), in their research on patterned carbon nanotube (CNT), have reported the fabrication process for realizing localized regions of highly-loaded carbon nanotube networks within the surface layers of polydimethylsiloxane. At room temperature, the method was performed. The double-layer microstructures were formed by electrophoretic deposition of CNTs into a patterned mould. The double-layer exhibited flexibility maintained high local CNT concentration and preserved the spatial orientation. This material was characterized for sensor applications.

(Jeong and Konishi 2005) have enumerated while understanding the response of design, fabrication, and characteristics of polydimethylsiloxane pneumatic balloon actuators for the bidirectional motion of the micro finger. The authors have reported that "the actuation mechanism of the balloon actuator was based on pressure-dependent swelling and saturation phenomena of two flexible diaphragms with different thicknesses. Two types of micro fingers with balloon actuators were fabricated by the simple silicon molding process and pneumatically tested." At the applied pressure values of 50kPa, it was observed that the force generated and the angle of bending of the finger was found to be 0.17 rnN and 59º, respectively. The proposed actuation mechanism and all PDMS micro fingers are applicable to various kinds of microdevices with the out-of-plane motion in the micro-robotics and Bio-MEMS field.

The intrinsic photomechanical actuation of graphene-based polymer composites is demonstrated by (Loomis et al. 2013). The authors have stated that "homogeneous mixtures of graphene nanoparticles and polydimethylsiloxane (GNP/ PDMS) composites (0.1–5 wt. %) were prepared and their infrared (IR) mechanical responses were studied with increasing pre-strains. Actuation was witnessed due to the presence of graphene. Dispersion of GNPs into a PDMS silicone elastomer matrix resulted in a novel GNP-based photomechanical actuator that showed reversible light-induced elastic expansion and contraction."

Wang et al. (2013), in their work, demonstrated the creation of macroscale functional materials by combining rationally designed proteins with synthetic nanoparticles. Near-infrared light-driven hydrogel actuators were synthesized. Genetically engineered elastin-like polypeptides and reduced graphene oxide sheets were interfaced. The resulting nanocomposites exhibited rapid and tuneable motions controlled by light path and intensity, including finger-like flexing and crawling.

Van Oosten et al. (2008) showed the typical bending of liquid crystalline (LC) photo actuators toward the light source, driven by the isomerization of azobenzene. In samples with relatively large thickness and high azobenzene loading, intense optical beams were seen to be absorbed in spatially non-exponential ways. As shown in Figure 1.7, the actuator reaches a maximum bend prior to unbending again to its equilibrium deformed state. Further, the authors have reported that "this effect was observed to be amplified when an internal composition gradient is created by using a mixture of mono- and dysfunctional reactive mesogens, leading to a reversal of the bending direction away from the light source. This two-way bending opens the road to new potential applications for light-driven LC network actuators."
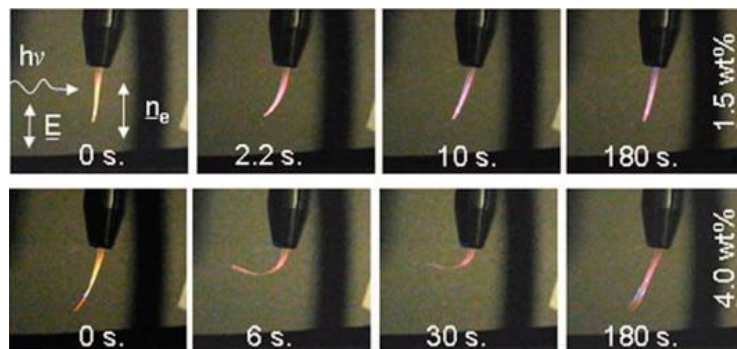
Figure 1.7 The bending of the films containing liquid crystalline elastomer. (Van Oosten et al. 2008)

Ahir and Terentjev (2005a) fabricated composites of silicone elastomer reinforced with multiwall carbon nanotubes. The composites were irradiated with near IR light to understand their actuation response. However, it was observed that "the relaxation after switching off the light source follows the simple-exponential relaxation, as does the stimulated reaction at deficient nanotube concentration. The preferred explanation considers nanotubes as photon absorbers that locally redistribute the energy as heat, causing contraction of anisotropic polymer chains aligned near the nanotube walls. The demonstration shows how nanotubes can impart photomechanical properties in otherwise suitable materials; the role of the nanotube-polymer interface is shown to be of great

interest and the speed of the photo actuation response warrants much further experimental and theoretical investigation.

Kim et al. (2016), have achieved full bending motion upon visible light exposure, and successfully fabricated and tested the actuation system in response to solar radiation. Figure 1.8 shows the bilayer-type photo-actuators. The poly (N-isopropyl acrylamide) incorporating into the reduced graphene oxide (PNIPAm/rGO) as an active layer and poly (acrylamide) passive layer was fabricated. On exposure to the light source, high bending and cooling are observed.
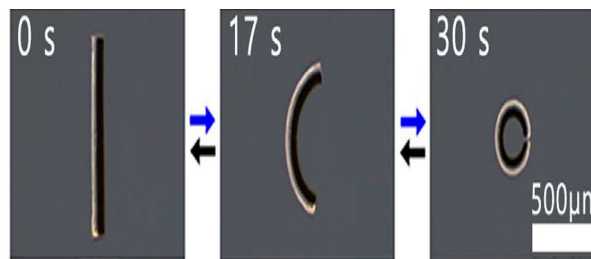
Figure 1.8 Bilayer bending of photo actuator. (Kim et al. 2016)

In (Zhang et al. 2013) paper various applications of different carbon-based nano-materials as reinforcements like Graphene, Nanodiamonds, Nano cones/discs, and nano horns, Fullerenes, and nanotubes, their functionalized forms, in sample preparation is provided. These materials can be used as sorbent agents. But it was also found that these materials can be costly and not readily available for laboratory work.

Mu et al. (2015) designed a light-activated polymer-based laminate composite to provide the pre-programmed stress field, which is used for photo-induced deformation. To overcome the drawback of prior approaches where the strain was caused by maintaining an external load during irradiation. The laminate is fabricated by bonding a stretched elastomer between two LAP layers. Compressive stresses were introduced in LAPs by contraction of elastomer. The laminate deformed to designed shape by optically relaxing the LAPs. A theoretical model was also developed to assist in the design. Curling of the

samples towards the light to a limiting value due to the illumination of one side of the laminate was observed, and it was in good agreement with theoretical results.

Nakamura and Kawakami (2019), had proposed a device and is hybridized with an electrothermal actuator which bends with temperature-compensating ability, which can serve as a self-sensing system, which is shown in Figure 1.9. The sample is fabricated using multiwall carbon nanotube and polydimethylsiloxane composite material. The bending of the composite beam due to electrothermal heating is observed.
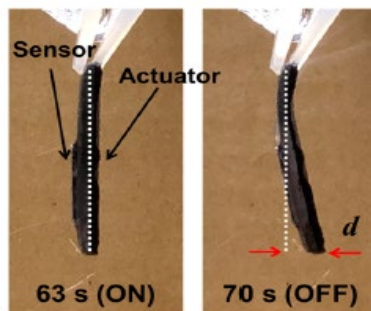
Figure 1.9 Composite beam bending due to electrothermal heating. (Nakamura and Kawakami 2019)

A new strategy exploiting IR light-driven double-layer polymeric composites for the autonomic origami assembly of 3D structures is studied by (Tang et al. 2017). The double-layer sheet comprising a passive layer of PDMS and an active layer comprising of PDMS with reduced graphene oxides (RGOs) and thermally expanding microspheres (TEMs) is created using a versatile and simple fabrication method. The researchers observed that "the two layers exhibited large differences in their coefficients of thermal expansion owing to the large volume expansion of the TEMs." The RGO-TEM-PDMS/PDMS double-layer composites deflected towards the PDMS side upon IR irradiation and exhibited excellent large bending deformation and rapid, responsive properties. Proposed an RGO-TEM-PDMS/PDMS composites with excellent "light/heat-driven bending properties were demonstrated as active hinges for building 3D geometries such as bidirectional folded columns, boxes, pyramids, and cars." Figure 1.10 shows the folding angle (ranging from 0° to 180°), which is well-controlled by tuning the actual hinge length. The presented

approach has potential in biomedical devices, aerospace applications, microfluidic devices, and 4D printing.
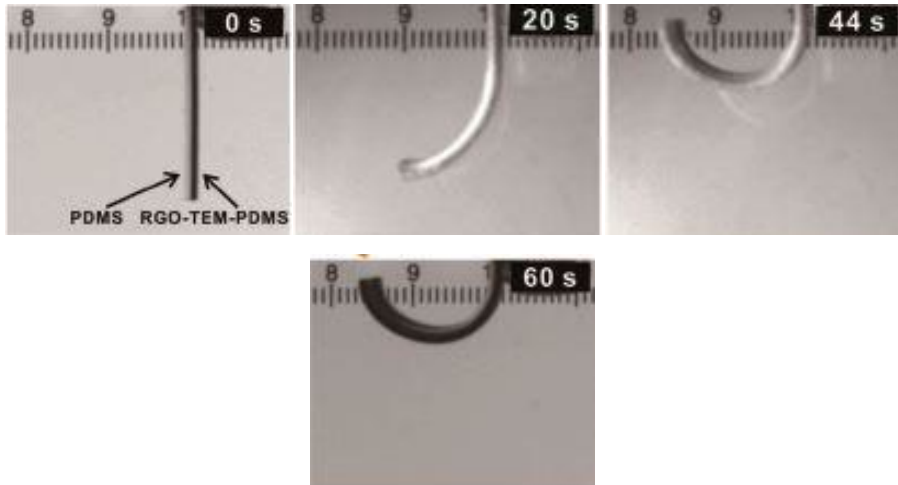
Figure 1.10 Photographs of the dynamic photothermal deflection of the composite element (Tang et al. 2017)

Huang and Zhang (2018) have developed a soft actuator based on molybdenum disulfide and polydimethylsiloxane material. This composite has excellent photothermal bending under UV irradiation. The authors have prepared a bilayer of PDMS and PDMS/MoS_2 composite samples and observed the temperature rise in the sample by exposing under ultraviolet light. Upon irradiation of the UV light, the bending of the bilayer film is tested. The same has extended for prototype testing by fabricating the microgripper. The light-driven and controlled bilayer built samples are shown in Figure 1.11. The design structure uses polyethylene terephthalate (PET) and, isolation layer and photothermal actuator. The microgripper usually opens when there is no light irradiation. When the UV light illuminates the micro-gripper, the gripper closes immediately. This gripper does not require any battery/cable and drive; this non-contact driving of photo thermal soft actuator is significant for miniaturization of the robot and other machines.
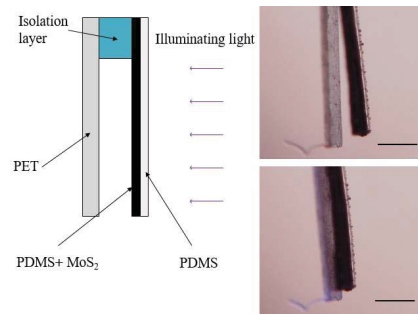
Figure 1.11 UV light-driven microgripper fabricated by MoS$_2$ and PDMS bilayer film. (Huang and Zhang 2018)

Yoon (2019) has reviewed the stimuli-responsive material. In the review, the author has highlighted the material, fabrication method, and the application of soft gripper. The stimulus is used for actuating the gripper is a thermal and light source. The material used is N-isopropyl acrylamide (NIPAM) based stimuli-responsive hydrogels, liquid crystalline material based stimuli-responsive hydrogels, etc. Also shown some the soft actuator utilizing this material. These materials attracted attention because of their promising applications in soft robotics, biomimetic, and biomedical engineering.

Fan et al. (2015) have presented new molybdenum disulfide (MoS$_2$)-based polymer composites and their reversible mechanical responses to light. The authors have suggested, MoS$_2$ is an excellent material for energy conversion. Homogeneous mixtures of MoS$_2$ and polydimethylsiloxane (PDMS) nanocomposites (0.1–5 wt. %) were prepared, and their near-infrared (NIR) mechanical responses were studied with increasing pre-strains. NIR triggering resulted in an extraordinary change in stress levels of the actuators by ~490 times. Actuation responses of MoS$_2$ polymer composites depend on applied pre-strains. At lower levels of pre-strains (3–9%), the actuators showed reversible expansion, while at high levels (15–50%), the actuators exhibited reversible contraction. An optomechanical conversion (η) 0.5-3MPa/W was calculated. MoS$_2$ and PDMS actuators (for 0.1 to 5 wt. % additive) bending is higher than single-layer graphene (188%) and multi-wall nanotubes (172%).

Recently (Cao et al. 2019) have reviewed on soft linear actuator using dielectric elastomer, thermal responsive hydrogels, pneumatic artificial muscle, and conducting polymers. The actuation mechanisms and performances of these soft linear actuators are summarized. Based on the dielectric elastomer, a hybrid system with linear actuation is designed. The electromechanical behaviors of the dielectric elastomer cone have been investigated in both experiments and finite element analysis. The proposed system design and operating methods for this hybrid linear actuator may guide the design of soft robots and smart, flexible devices.

Kim et al. (2018) has introduced the basic theory of light absorption and heat transfer and then summarizes the fundamental understanding of representative light-to-heat conversion agents, including carbon-based, semiconductor-based and plasmonic metal-based materials and structures, and highlights state-of-the-art structural designs towards the development of broadband light absorbers. Also, the practical applications of these materials and designs are discussed. The efficient way of light-to-heat conversion highlights straightforward directions to many biomedical and engineering applications, including photo thermal therapy and imaging, controllable drug delivery systems, solar steam generators, and mechanical actuators are shown in Figure 1.12. Several hurdles associated with light absorbers for light-to-heat conversion should be overcome, for example, simple synthesis process and fabrication of highly efficient light-to-heat conversion materials and use the simple testing system. In the present review, they have summarized the carbon-based material which can be used in the redevelopment of the actuator system.
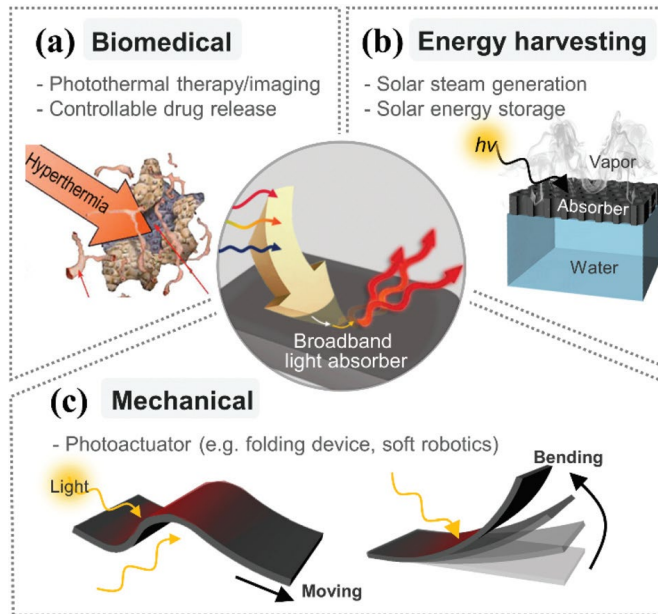
Figure 1.12 Applications of light absorbers including (a) biomedical, (b) energy-harvesting, and (c) mechanical applications (Kim et al. 2018)

1.6.2 Composite materials for a photo actuator

For various applications, it is challenging and essential to obtain a photomechanical actuator in response to environmental stimuli. Thus, developing and producing multiple types of photomechanical actuators using different polymer and nanomaterial is necessary. (Deng et al. 2016) have worked on photomechanical actuators using CNT and polymer material. They have proposed the Ashby chart for comparing maximum deflection of light actuated material concerning time is shown in Figure 1.13. This summary shows the different types of composite material used for the photothermal actuator and their deflection performance. Also, authors have predicted a change in wavelength of light influences the material depending on the application. The essence of photo thermal actuators lies in the development of photo thermal materials that can convert light to heat effectively. Currently, the most popular photo thermal material is graphene, CNT, SWCNT, and CB due to their excellent light absorption property, mechanical strength, lightweight, and excellent stability. To make an overview of photo thermal actuation strategies and their performance are shown in Table 1.2

22
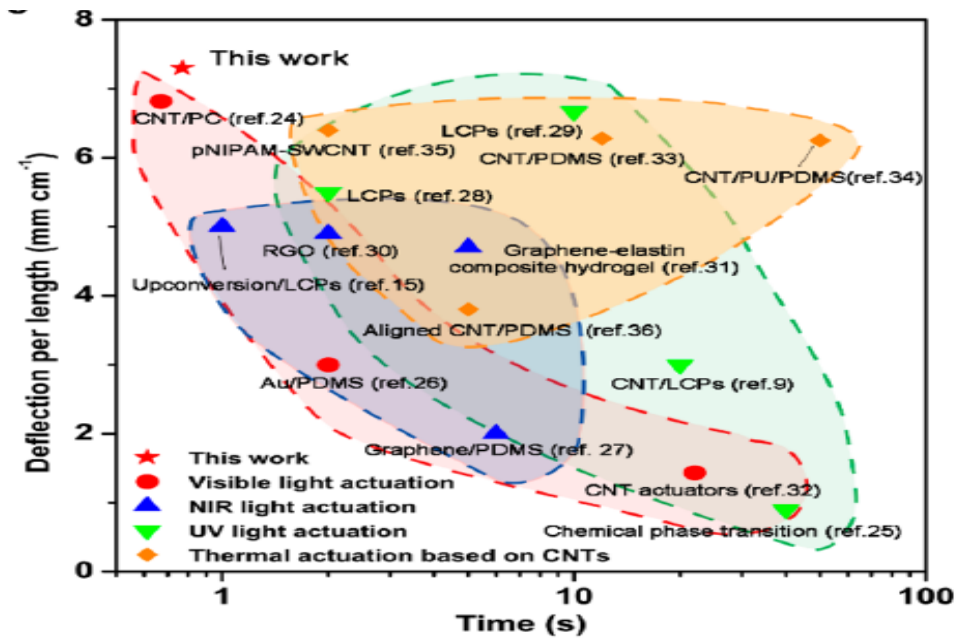
Figure 1.13 Ashby-like plot that compares different light-driven actuation (Deng et al. 2016)

The actuators are produced based on mechanism, material, and structure. The material popularly used for photo actuator is a carbon-based nanomaterial. These material has emerged as the preferred candidates for different actuating systems because of their low cost, ease of processing, mechanical strength, and excellent physical/chemical properties. Mainly, due to their excellent photo thermal activity, which includes both optical absorption and thermal conductivities, carbon-based materials have shown great potential for use in photo thermal actuators.

Han et al. (2018) have summarized photo thermal actuators based on various carbon allotropes, including graphite, carbon nanotubes, amorphous carbon, graphene, and its derivatives, are reviewed. Different photo thermal actuating schemes, including photo thermal effect–induced expansion, desorption, phase change, surface tension gradient creation, and actuation under magnetic levitation, are summarized, and the light-to-heat and heat-to-work conversion mechanisms are discussed. Carbon-based photo thermal actuators that feature high light-to-work conversion efficiency, mechanical robustness, and

noncontact manipulation hold great promise for future autonomous systems. Some of the photo actuation material, structure, and their performances are shown in Table 1.2

In general, light-driven actuators have several advantages, including wireless/remote actuation, displacement control, parallel actuation, the positioning of the arrays and electrical/mechanical decoupling, etc. These can be implemented depending on the stimulus, material, and mechanism.

Table 1.2 Photothermal actuation material and their performance

Mechanism	Materials	Structure	Size of typical devices	Actuation	Performance (bending/angle/curvature)	Light source/ intensity	Response time	Ref.
Thermal expansion	PC/CNT	Bilayer	25mm diameter	Reversible bending	90^0	Simulated sunlight 100 mW cm^{-2}	0.87 s	(Zhang et al. 2014a) (Vassalini and Alessandri 2017)
	Cu/Cu$_2$O/RGO	Multilayer	4 cm × 5 mm	Reversible bending	1.3 cm^{-1}	1000 mW,Infrared light	2 s	(Meng et al. 2017)
	CNT/PDMS	Bilayer	21mm x 14mm	Reversible bending	215^0	Sunlight 250mWcm^{-2}	0.83s 7s,recovery	(Hu et al. 2017)
	RGO-TEM–PDMS	Bilayer	20 mm × 2 mm	Permanent bending	180°	IR lamp 250 W	30 s	(Tang et al. 2017)
	GNP–PDMS/Cr	Bilayer	15 mm × 2.5 mm	Reversible bending	40°	IR 550 mWcm^{-2}	1s,3s,recovery	(Leeladhar et al. 2017)
	PDMS-GNP/PDMS	Bilayer	7mm x 1mm	Reversible bending	1500μm	NIR 29.5 Wmm^{-2}	3.4 s	(Jiang et al. 2014) (Liu et al. 2016)
	ACNT/paraffin wax	Bilayer	20 mm × 4 mm	Reversible bending or twisting	85°	Visible light 100 mW cm^{-2}	0.87 s 1.86 s	(Deng et al. 2016)

Thermal desorption	RGO–CNT/PDMS	Bilayer	24 mm × 5 mm	bending	479°	Simulated sunlight 250 W cm^{-2}	3.6 s 6.8 s	(Hu et al. 2015)
	SWCNT/PVDF	Bilayer	2 cm × 2 cm	Reversible bending or twisting	910°	100 W lamp	1.06 s	(Tai et al. 2016)
	BOPP/graphite/ paper	multilayer	30 mm × 10 mm	Reversible bidirectional bending	1.9 cm^{-1}	NIR light 300 mW cm^{-2}	10s,15s recovery	(Weng et al. 2016)
Shape memory effect	PU and CB	3Dstructure(through printing)	50 mm × 20 mm	Single-shape memory	140°	Sunlight 198 mW cm^{-2}	180 s	(Yang et al. 2017)
	SWNT–LCE/silicone	Bilayer	L=15w= 10 in mm	bending	0.28 cm^{-1}	IR light 1.1 Wcm^{-2}	10s,30s recovery	(Kohlmeyer and Chen 2013)
	LCE/SWCNT	Bilayer	14mmx 3mm	Reversible flat to bent	-	808nm	1.5s ,1.5s ,relaxation	(Loomis et al. 2013)

1.6.3 Modeling of photo actuation

Modeling is the mathematical representation of the physical system. Modeling helps to predict the behavior and optimization of the actual system. An experimental study requires a lot of resources, expensive process, more time, and cost. Whereas modeling reduces the efforts needed for the building of the system. There are several software packages like MATLAB/SIMULINK, COMSOL Multiphysics, ANSYS, etc. available for modeling and analyzing the behaviors of the systems. Few researchers have simulated photo thermal actuators based on input stimulus, material, and depending on the application using commercial software tools. The analysis photo-actuators have tried to model the photo actuators are listed in Table 1.3

Table 1.3 Summary of literature on the modeling of the photo thermal actuator

Author	Software	Shape	Material	Observation
(Li et al. 2014)	COMSOL Multiphysics	Rectangular	Liquid crystal elastomer (LCE)/CNT	Deflection and Temperature change
(Torras et al. 2011)	NA	Cantilever	LCE-CNT	Temperature
(Li and Cai 2016)	MAT LAB	Cantilever	LCE Beam	Bending vibration
(Zhu et al. 2011)	NA	Box-shaped	LCE sample	Bending and Deformation
(Niu et al. 2016)	COMSOL Multiphysics	Bilayer beam	PDMS/GNP	Deflection
(Han et al. 2015)	COMSOL Multiphysics	NA	Black HDPE	Deflection
(Zhang et al. 2017)	ANSYS	Bilayer	CNT/PDMS	Deflection

1.6.4 Prototyping of photo actuator

The researchers have built a prototype and tested it under a light source. The photo actuation of the fabricated sample is applied for soft actuators capable of bending, rolling, walking, helical twisting in a dry environment, and so on (Marina Pilz da Cunha et al. 2019).

Several methods of the sun following have been surveyed and evaluated to keep the solar panels, solar concentrators, telescopes, or other solar trackers perpendicular to the sun rays. Sun-tracking systems are usually classified into three categories: passive (without external source), active (with external source) trackers, and hybrid (combination of both) tracking system. The present work proposed a passive tracking system, which is one of the tracking applications of the photothermal mechanical system. Passive solar trackers are based on thermal expansion of a matter (usually Freon), shape memory alloy, etc. which does not require an external source for tracking a system. The main advantage of the passive tracking system is less cost, simple fabrication, and design, efficiently track the sun and less maintains, even though the consumer has not widely accepted them. The passive system mainly depending on the type of material used to better design of the tracking system. A light source can be used to enable the load or output in where an electric source is unable to trigger external devices.

Clifford and Eastwood (2004) designed a passive tracker using bimetallic material is shown in Figure 1.14 and controlled by a viscous damper. Also, they have modeled and got 23% more efficiency than the fixed solar panel. Hence the passive method is not taking power from the actual solar cell or other power for movement.

Figure 1.14 Prototype of solar tracker using two bimetallic strips. (Clifford and Eastwood 2004)

Ganesh et al. (2011a) have developed an efficient sun tracking mechanism using a shape memory alloy (SMA). The mechanism is made, in such a way that, the position of the solar panel tilt towards the sun. Figure.1.15 shows the design and fabricated setup of the passive solar tracking system. The constructed parts are 1. SMA spring 2. Fixed frames 3. Pulley 4. Wheel 5.Pawl and ratchet 6. Main shaft 7. Stopper arrangement 8. Driving bevel gear 9. Driven bevel gear 10. Mechanism of dead weight 11.Solar receptors 12. Lens 13.Actuator dead weight 14. Solar receptor. This proposed system is the proof concept of the sun-tracking mechanism and requires further improvement.
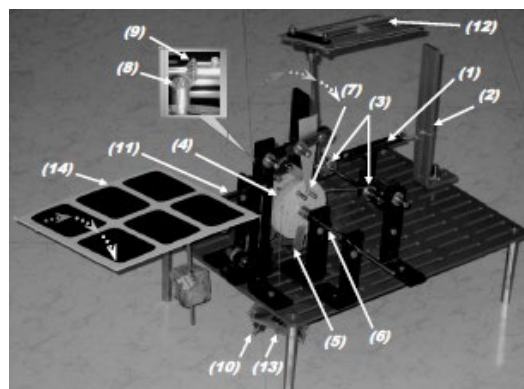
Figure 1.15 Constructed a functional model of solar tracker using SMA(Ganesh et al. 2011)

Li et al. (2012) have developed a prototype of a heliotropic system that can follow the sun throughout the day. They have introduced polymer composite material for tracking, and this material is directly driven by natural sunlight. This is one of the passive energy harvesting methods using a photo thermo mechanism using elastomeric nanocomposite. The prototype of the tracking system shown in Figure 1.16
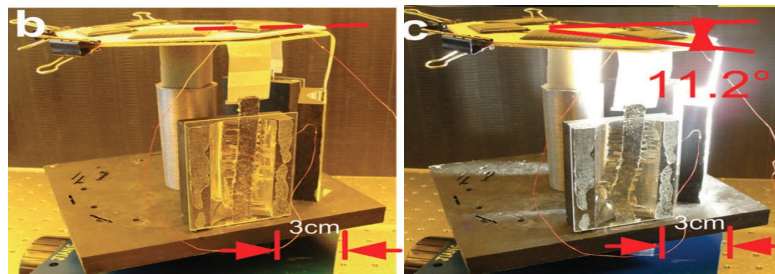
Figure 1.16 The prototype device of artificial heliotropism (Li et al. 2012)

Using polymer composite material, they have achieved 11.20° angles of tilting. The different types of mechanisms of tracking systems motivate to design and develop a passive tracking system using the composite material.

Summary of literature

The photo actuator is an interdisciplinary system having an enormous option for research. The above survey reveals the various manifestation of the photo thermal-mechanical effect leading to the actuation using different materials, methods, and modeling techniques. Hence, there is scope for a research problem in the field of polymer composite material, characterization of the composite material, study the behavior of photo actuation by analytical and numerical modeling method. Finally, testing the photo actuator by developing the appropriate prototype.

Based on the available literature, it appears that a limited investigation is happening in the area of composite-based photo actuation. The composite material can be a significant influence on the development of photo actuators. Proposing the composite material and

investigate the different properties of the composite materials, which are needed for the photo actuator. Also, there is limited work on the numerical modeling of the photo actuator need to be explored. Based on the review, proposed novel material for photo actuators and studied their behavior by varying volume percentage filler and thickness. The different volume percentages of filler and change in the thickness parameters are missing in the literature, which needs to be explored in detail.

1.7 Research Gap

Nature has many parameters to motivate for taking up the research work. In that light-based polymer composite, actuation is one of the areas that is still needed to be explored. Despite the developments in composites for actuators, many issues remain still unresolved like constitute of materials, actuation performance, efficiency, and cost. There is minimal work on photo actuation based on the composite material using a light source. The material processing steps and different characterizations of material need to be addressed for improvement of the actuator performance. Also, there is much work required for an understanding of a photo thermal actuation using numerical (FE) and the analytical methods. These gaps could be addressed in a systematic way for the development of photo actuation.

1.8 Objectives

1. To propose a composite photo actuator and analyze its behaviour using properties from empirical and numerical (FE) methods.
2. To fabricate polymer composite samples and determine their physical, mechanical, thermal, dielectric, and optical properties.
3. To determine the photo thermal deformation by numerical modeling using experimentally determined material properties.
4. To determine the photo thermal deflection of the composite sample experimentally.
5. To construct a prototype of the photo actuator and study its behaviour.

1.9 Scope of the Present Work

The proposed research work is to develop a novel photo actuator using a polymer composite. The actuator is modeled using commercially available software tools. The composite material is proposed and prepared by a solution casting method using a polydimethylsiloxane (PDMS) matrix and carbon black as a filler material and cured at room temperature. The composite sample properties are obtained by conducting physical, mechanical, thermal, dielectric, and optical tests. The analytical and numerical (FE) modeling techniques are used to understand the deflection behaviour by changing the temperature, various volume fraction of filler, and varied thickness of the material. Finally, evaluating the deflection performance of the photo actuator experimentally, and the proof concept is to be tested by constructing the prototype.

Summary

The present chapter has provided an introduction of actuation, composite material, and photo actuation mechanism; An exhaustive review of research work on various aspects of polymer composite used in the actuator. The knowledge from previous researches provides the framing of the present work's objective. The next chapter presents the methods used in composite material development, characterization, and photo actuation testing.

-----------❦❦❦❦❦------------

CHAPTER 2

METHODOLOGY

A research plan that would allow for the best evaluation of predictions and reduction of error would involve separate models and laboratory testing for each sample. With this in mind, the chapter describes the proposed material, study on different models, equipment required for various characteristics, actuator testing method, and finally, constructing of the prototype for deflection study of the composite beam.

The systematic methods followed for the accomplishment of the proposed work are reported in this chapter. Figure 2.1 shows the general steps involved in the current research work.
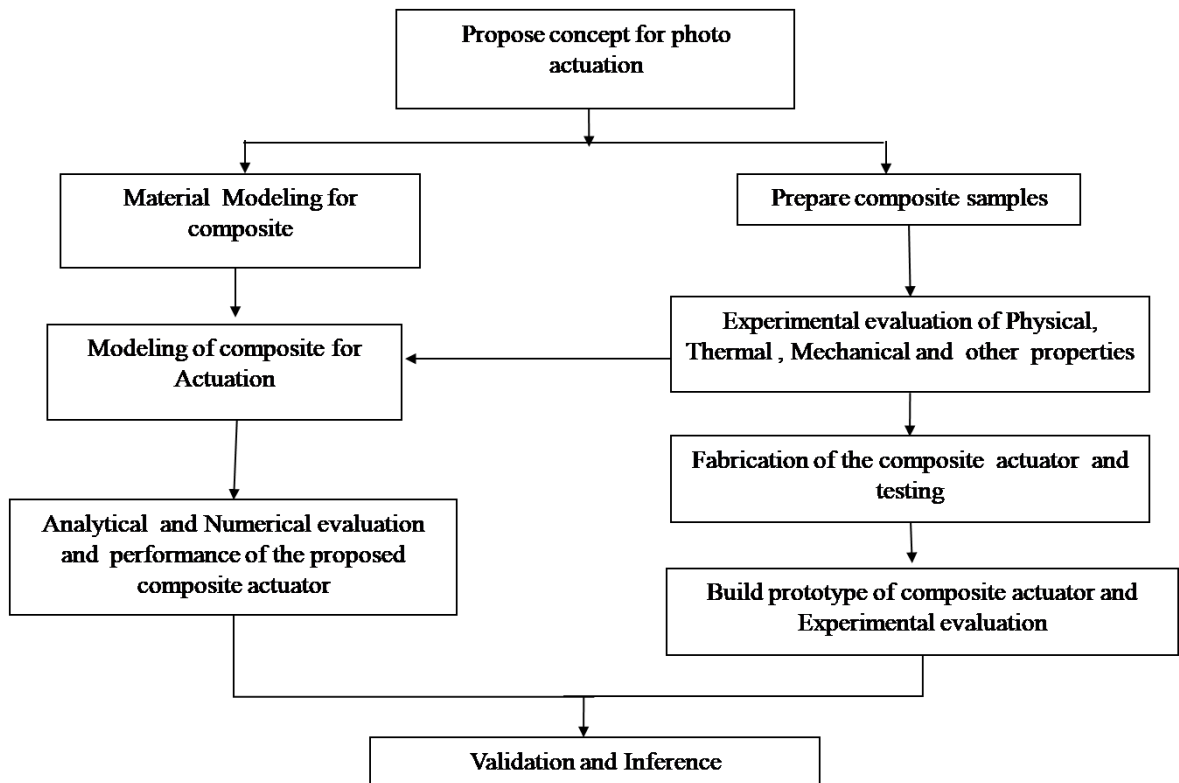
Figure 2. 1 The layout of the proposed research work

2.1 Material and properties

The materials are chosen based on the literature gap, material availability, product ability, and cost. The novel materials selected for the proposed work are PDMS and carbon black. These materials are used in the present study for the development of a composite beam for photo actuation.

Silicone backbone chain structure of PDMS

Through modifying -Si-O- chain sizes, side group's orientation, and molecular chains cross-linking, silicones can be synthesized into an almost infinite variety of materials. Mono-, di-, tri- or tetra-functional siloxane units with Si-O bonds are formed by polycondensation based on the number of primary silane molecule atoms. The various halogenated silane acts as building blocks for synthesizing the specific silicone material forms, such as liquids or resins. Figure 2.2 displays the PDMS material's chain bonding structure after room temperature curing.
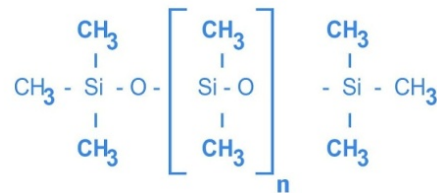
Figure 2.2 Chain bonding structure of PDMS

Recently, polymer-based composites have become more attractive due to their outstanding properties, such as mechanical, thermal, dielectric, electrical, and optical. The polymer is of particular interest due to its lightweight, ease of processing, and low cost. The polymer matrix used in this study is polydimethylsiloxane, which is transparent, superior in mechanical, thermal and electrical properties, excellent performance at high temperatures, non-toxic, strong binding, ease of property adjustment, and easy manufacturing. PDMS polymer has also drawn more to micro and mesoscale applications at the moment.

The filler material used in the present study is the carbon black particle because of its excellent thermal conductivity and mechanical properties. Also, it has a low thermal coefficient, which is suitable for electrical and thermal actuator applications. The procured carbon black particle size varied from 230 to 400 nm in size. The carbon black material has advantages, such as synthesizability (productibility), availability, and less cost compared to graphene, carbon nanotube material. Thus, the pictorial view of PDMS and corresponding cross-linker and filler material is shown in Figure 2.3.

Polydimethylsiloxane   Carbon black powder

Figure 2.3 Procured polymer and filler materials

Particle size analysis

The procured carbon black material particle size is analysed using a dynamic light scattering (DLS) particle size analyser, and a transmission electron micrograph (TEM). The DLS particle size analysis was carried out in standard analysis time, and the size of carbon black is found to vary between 184 nm, and 416 nm is shown in Figure 2.4.
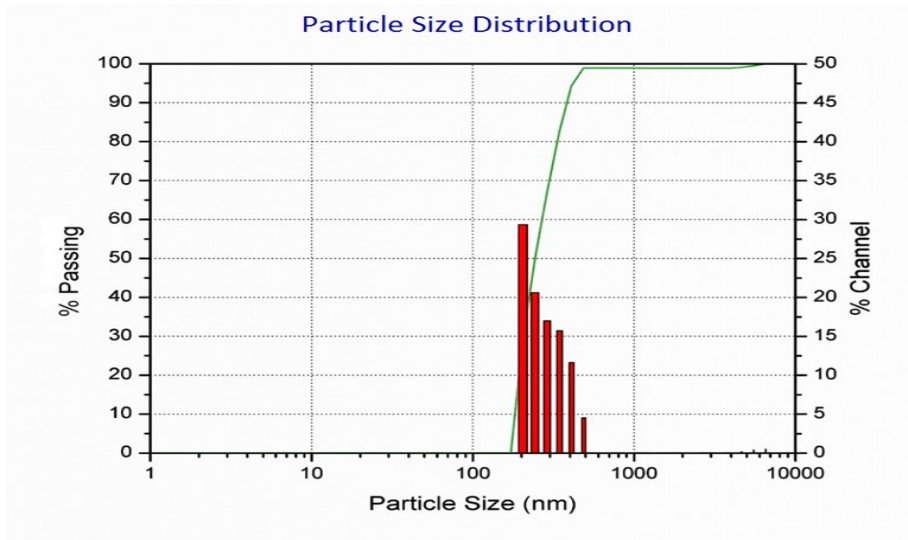
Figure 2.4 Particle size study of carbon black nanoparticles

The transmission electron micrograph (TEM) images of the carbon black powder shown in Figure 2.5. The carbon black powder particle has an average size between 180 nm to 400 nm. It shows that the particle size of carbon black from both methods is between 180 to 400 nm.
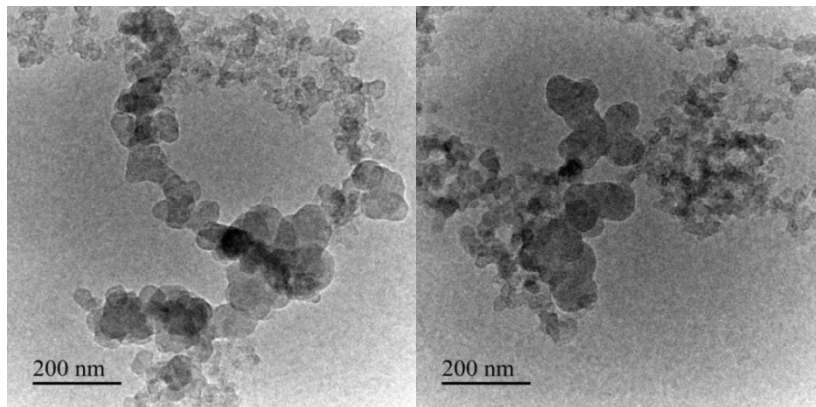
Figure 2.5 TEM images of carbon black powder taken at 200,000x

The procured material properties are taken from the literature, datasheets, and experimental method. Some of the vital features of the matrix and filler are listed in Table.2.1

Table 2.1 Properties of PDMS and CB material

Materials / Properties	PDMS	Carbon black (CB)
Material procured from	Ellsworth Adhesives India Pvt. Ltd. Mumbai (Dow Corning India Ltd)	Gautama dyes and Chemical Inc. Chennai (Cabot India Ltd)
Young modulus (E) MPa	0.75-1.96	10.04 -14
Density (ρ) kg/m^3	1030	1890
Poison's ratio (v)	0.45-0.50	0.27-0.33
Thermal conductivity (k) W/(m.K)	0.15-0.27	24-176
Specific Heat capacity (Cp) J/(kg.K)	1460	690.82
The coefficient of thermal expansion (α) (1/K)	310×10^{-6}	9×10^{-6}
Particle size	NA	230 to 400 nm
Dielectric constant (ε)	2.3-2.8	4
Electrical conductivity (σ)	10^{-12}	10^{-1} to 10^2

2.2 Material modeling

The material model is necessary to eliminate trial and error loops during the development of material, manufacturing process, and to make reliable predictions of the behaviour of existing material. In the present study, empirical and numerical (FE) models are used to estimate the properties of polymer composites filled with carbon black particulate filler. These models give an overview of the principle used for the correlation of particulate filled polymer composite.

2.2.1 Empirical models for material properties

Empirical models are used to analyze, and the findings are used in developing actuator models. Empirical modeling can be seen as a framework for a wider computing view, and such models are constructed from material elements. In the present study, more influencing empirical models are studied and correlated with experimental results.

2.2.1.1 Empirical model for the density of the material

The density model is based on the weight and volume of the material. Density (ρ) is the proportion of mass (m) to the volume of the material. The density of the composites of pure PDMS and CB/PDMS is calculated by the rule of mixtures (ROM) using the following Equation 2.1.

$$\rho_c = \rho_f V_f + \rho_m V_m \tag{2.1}$$

Where, ρ_c is the calculated density of the composite, ρ_f is the density of the reinforcement (CB= 1890 kg/m^3); ρ_m Is the density of the matrix (PDMS = 1030 kg/m^3) and V_f and V_m the volume fractions of the reinforcement and matrix, respectively.

Void Content:

The incorporation of filler into the matrix or during the manufacturing of composite, air bubbles and other volatiles may be trapped in the material. The trapped air or volatiles exist in the composite as microvoids, which may significantly affect some of its mechanical properties. The void content in a composite can be estimated by comparing the empirical density with its actual density can be calculated using Equation 2.2 (Sharma and Sharma 2016).

$$V_{void} = \frac{\rho_{ct} - \rho_{ce}}{\rho_{ct}} x100 \tag{2.2}$$

Where ρ_{ct} is the empirical density of the composite material, ρ_{ce} is the experimental density of the composite material.

2.2.1.2 Empirical model for Young's modulus

The mechanical properties of the composite material are predicted empirically. In that, Young's modulus is the ratio of the stress applied to the material strain associated with applied stress. The Young's modulus of the composite material is estimated using different empirical models. These models are easy to determine the relationship between the components of the composite material and elastic modulus. The study can predict a

composite material value, which is a basis for the characterization of new composite material. However, these models depend on their constituents. In the present study, the elastic modulus of the PDMS/CB composite with variations of CB content obtained experimentally and predicted using some of the popular empirical models and those models are shown in Table 2.2 (Duc and Minh 2012, Athimoolam et al. 2016).

The empirical model formulation of particle-filled polymer composite for Young's modulus is represented as E_c. Where, V_m and V_f are the volume fraction of the equivalent matrix and filler material, and E_m and E_f are Young's modulus of the matrix and filler material, respectively.

Table 2.2 Young's Modulus of the composite is predicted using a different empirical model

Models	Equations	Remarks
Rule of Mixture	$E_c = V_f E_f + V_m E_m$	
Einstein Guth	$E_c = E_m(1 + 1.25V_f)$	
Guth	$E_c = E_m(1 + 1.25V_f + 14.10V_f^2)$	
Kerner	$E_c = E_m\left[1 + \dfrac{15V_f(1 - \nu_m)}{(1 - V_f)(8 - 10\nu_m)}\right]$	ν_m is Poisson's ratio of matrix material
Thomas	$E_c = E_m(1 + 2.5V_f + 10.05V_f^2 + 0.00273\exp(16.6V_f))$	
Quemada	$E_c = E_m\dfrac{1}{(1 - 0.5kV_f^2)}$	k=0.25 has chosen for the fitting reason

2.2.1.3 Empirical models for a coefficient of thermal expansion

Usually, solid-state materials expand to heating and contract to cool. This response to changes in temperature is expressed as its CTE or only coefficient of thermal expansion. The linear CTE is defined as

$$\alpha = \frac{1}{L}\left(\frac{\Delta L}{\Delta T}\right) \tag{2.3}$$

Where L is the original length, then ΔL and ΔT are the change in original length, and temperature, respectively, is given in Equation 2.3.

The thermal expansion coefficient of the PDMS/CB composite is predicted using empirical models, as shown in Table 2.3 (Dey and Tripathi 2010, Tani et al. 2007).

Table 2.3 CTE composite is predicted using different empirical models

Models	Equations	Remarks
ROM	$\propto_c = V_f \propto_f + V_m \propto_m$	
Turner	$\propto_c = \dfrac{V_f \propto_f K_f + V_m \propto_m K_m}{V_f K_f + V_m K_m}$	
Kerner	$\propto_c = V_f \propto_f + V_m \propto_m$ $+ [V_f V_m (\propto_f - \propto_m)]\ \dfrac{K_f - K_m}{V_f K_f + V_m K_m + (^{3K_m K_f}/_{4G_m})}$	
Thomas	$\alpha_c^a = \alpha_m^a V_f + \alpha_f^a V_m$	Where exponent 'a' may vary from +1 to -1
Chen et. al.	$\propto_c = a \propto_m \exp(-\frac{V_f}{b}) + (1-a) \propto_m$	Where 'a' and 'b' are constants
Vo et. al.	$\propto_c = \dfrac{1}{1+V_f V_m a_1}\ \ \ [\ \ \ \ \ V_f \propto_f + V_m \propto_m +$ $a_1 V_f V_m (\propto_f + \propto_m) + a_1 V_f V_m a_2]$	a_1 and a_2 are the matrix and filler interaction strength a_2, is the measure of the temperature dependence of a_1
Schapery lower	$\propto_c = \propto_m + \frac{K_f}{K_c^l}\frac{(K_f - K_c^l)(\propto_f - \propto_m)}{K_m - K_f}$	$K_c^l = K_m + \dfrac{V_f}{\frac{1}{K_f - K_m} + \frac{3V_m}{3K_m + 4G_f}}$

| Schapery upper | $\propto_c = \propto_m + \dfrac{K_f}{K_c^u}\dfrac{(K_f - K_c^u)(\propto_f - \propto_m)}{K_m - K_f}$ | $K_c^u = K_f + \dfrac{V_m}{\frac{1}{K_m - K_f} + \frac{3V_f}{3K_m + 4G_m}}$ |

According to the models, the CTE of composites (α_c) can be calculated, Where, α_f and V_f are the CTE of the filler and equivalent volume fraction, respectively. α_m and V_m are the CTE of the matrix material and equivalent volume fraction, respectively. Where K_m and K_f represents the matrix and filler bulk module. G_m and G_f, represent the shear modulus of the matrix and filler of the material.

2.2.1.4 Empirical models for thermal conductivity

Thermal conductivity is the transfer of energy in a conductive medium between adjacent molecules and electrons; it is a material property that defines heat flow within a body for a given difference in temperature per unit area.

$$Q = kA\frac{T_1 - T_2}{t} \tag{2.4}$$

Where Q is the heat flux (W), A is the cross-sectional area (m^2), k is thermal conductivity (W/mK), t is the thickness (m) of the sample, and T_1-T_2 (ΔT) is the difference in temperature between surfaces ($^\circ$C or K).

Effective thermal conductivities are empirically tested for PDMS composites filled with carbon black fillers. For composites with similar amounts of filler, the interpretation and comparison of results obtained from different methods are provided. The plain PDMS and PDMS/CB thermal conductivity are obtained from the empirical models and FE modeling and then compared to experimental results. Some of the empirical models used in present analysis as shown in Table 2.4 (Agari and Uno 1985, Dey and Tripathi 2010).

Table 2.4 Different empirical models for thermal conductivity

Models	Equations	Remarks
Maxwell	$$k_c = k_m \frac{k_f + 2k_m + 2V_f\,(k_f - k_m)}{k_f + 2k_m - V_f(k_f - k_m)}$$	
Hamilton and crosser	$$k_c = k_m \frac{k_f + (n-1)k_m + (n-1)V_f\,(k_f - k_m)}{k_f + (n-1)k_m - (k_f - k_m)V_f}$$	n is the shape of the filler particle (sphere n=3)
Meredith and Tobias	$$a = \frac{2\left(2+\frac{k_f}{k_m}\right) - 2(1 - k_f/k_m)V_f}{2\left(2+\frac{k_f}{k_m}\right) + (1 - k_f/k_m)V_f} \qquad b = \frac{(2-V_f)\left(2+\frac{k_f}{k_m}\right) - 2(1 - k_f/k_m)V_f}{(2-V_f)\left(2+\frac{k_f}{k_m}\right) + (1 - k_f/k_m)V_f}$$ $$k_c = abk_m$$	
Cheng and Vashon	$$\frac{1}{k_c}$$ $$= \frac{1}{\sqrt{A(k_f - k_m)(B(k_f - k_m))}} \ln \frac{\sqrt{k_m + B(k_f - k_m)} + B/2\sqrt{A(k_f - k_m)}}{\sqrt{k_m + B(k_f - k_m)} - B/2\sqrt{A(k_f - k_m)}}$$ $$+ \frac{1-B}{k_m}$$ Where $A = -4\sqrt{\dfrac{2}{3V_f}} \qquad B = \sqrt{\dfrac{3V_f}{2}}$	Where "a' and "b' are constants
Lewis and Nielsen	$$k_c = k_m \frac{1 + ABv_f}{1 - Bv_f C}$$ Where B= $$B = \frac{k_f/k_m - 1}{\frac{k_f}{k_m} + A} \qquad \text{also, } C = 1 + \frac{1-m}{m^2}v_f$$	A is the constant, which depends on the shape and orientation of the dispersed particles.
Agri and Uno	$$\log k_c = V_f A_2 \log k_f + V_m \log A_1 k_m$$	A_1 is the factor influencing the effect of crystalline nature of the polymer and A_2 is the formation of the conductive chains of the filler particle

According to the models, the thermal conductivity of the composites (k_c) can be calculated using the empirical equations. Where, k_f and V_f are the thermal conductivity and volume fraction of the equivalent filler material, respectively. Where, k_m and V_m are the thermal conductivity, equivalent volume fraction, matrix material, respectively.

2.2.1.5 Empirical models for dielectric constant

The dielectric material can be used to store the electric charge when an external electric field polarizes the electron distributions around the constituent atom. As an alternating current passes through the material, it oscillates at the same frequency as that of the applied electric field. The capacitance and the tangent loss are monitored as a function of frequency at given signal strength using an impedance analyser. These experimental parameters are used to calculate the dielectric permittivity and dielectric loss of the material are mentioned using Equation 2.5 and 2.6 (Dang et al. 2012, Panahi-Sarmad et al. 2019).

$$\varepsilon' = \frac{C_m t}{\varepsilon_o A} \qquad (2.5)$$

Where, C_m is the measured capacitance, t is the thickness of the sample, ε_o is the dielectric permittivity of the free space (8.854 x 10^{-12} F/m), and 'A' is the active area of the electrode. The ability of the material to store the energy from the applied electric field is indicated as magnitude or dielectric permittivity (ε'). The dielectric loss results from the inability to polarization process in an atom to follow the rate of change of the oscillation due to the applied electric field. The ratio of the energy loss to the energy stored indicates the relative loss factor of the material.

$$\tan \delta = \frac{\varepsilon''}{\varepsilon'} \qquad (2.6)$$

Here, the loss tangent $(\tan \delta)$ is also represented as dissipation factor (D) or dielectric loss factor. The complex permittivity of the material can be expressed using Equation 2.7.

$$\varepsilon^* = \varepsilon' - i\varepsilon'' \qquad (2.7)$$

Where, ε' is the magnitude of the real component, is referred to as the dielectric permittivity and ε'' is the magnitude of the imaginary part, which is also called dielectric

loss. The polarization of the material under an applied electric field depends on the frequency. The AC conductivity of the polymer composite is the function of frequency. Thus, the AC conductivity (σ) is calculated from the relation of the real part of the complex conductivity and angular frequency (ω). Where $\omega = 2\pi f$ and f is the frequency at which the dielectric constant is measured, it can be expressed as in Equation 2.8.

$$\sigma = \omega \varepsilon_o \varepsilon'' \tag{2.8}$$

Empirical approaches can predict the effective dielectric permittivity of the composite materials. The empirical equations have been used based on a mean-field approximation for determining the effective permittivity of polymer nanocomposites (Tsai et al. 2017, Rao et al. .2000, Namitha et al. 2013).

Predicting the effect of the second phase of the dielectric properties of the composite is discussed using the mixing rules. Considering the homogenous and isotropic matrix material of dielectric permittivity ε_m is filled with nanopowder of dielectric permittivity ε_f. The volume fraction of the filler particle is defined as v_f , and the resulting volume fraction of the matrix is $v_m = 1 - v_f$. It is assumed that the composite component has no dielectric loss in the interested region of frequency. Thus, the effective dielectric permittivity of the composite mixture is ε_c .The approximately modified empirical equation for the interactions between the inclusions and polymer are given in Table. 2.5.

Table 2.5 Effective dielectric mixing rules for composite material

Dielectric Models	Equations	Remarks
Maxwell-Garnett rule	$\varepsilon_c = \varepsilon_m \left[1 + \dfrac{3v_f(\varepsilon_f - \varepsilon_m)}{(1 - v_f)\,(\varepsilon_f - \varepsilon_m) + 3\varepsilon_m} \right]$	
Bruggeman rule	$\varepsilon_c = \varepsilon_f \dfrac{3\varepsilon_m + 2v_f(\varepsilon_f - \varepsilon_m)}{3\varepsilon_f - v_f\,(\varepsilon_f - \varepsilon_m)}$	
Lichtenecker rule	$\varepsilon_c^\alpha = v_f \varepsilon_f^\alpha + v_m \varepsilon_m^\alpha$	where α varies (-1 to 1)

Jaysundere–Smith rule	$a = \varepsilon_m v_f + \varepsilon_f v_f \dfrac{3\varepsilon_m}{2\varepsilon_m + \varepsilon_f}\left[1 + \dfrac{3v_f(\varepsilon_f - \varepsilon_m)}{2\varepsilon_m + \varepsilon_f}\right]$
	$b = v_m + v_f \dfrac{3\varepsilon_m}{2\varepsilon_m + \varepsilon_f}\left[1 + \dfrac{3v_f(\varepsilon_f - \varepsilon_m)}{2\varepsilon_m + \varepsilon_f}\right] \qquad \varepsilon_c = \dfrac{a}{b}$
Weiner rule	$\varepsilon_c = \left[\dfrac{v_m}{\varepsilon_m} + \dfrac{v_f}{\varepsilon_f}\right]^{-1}$
Hashin-Strickmann (HS) rule	$\varepsilon_c = \varepsilon_m\left[1 + \dfrac{v_f}{\dfrac{1}{\varepsilon_f - \varepsilon_m} + \dfrac{v_f}{3\varepsilon_m}}\right]$

2.2.2 Numerical (FE) modeling of material properties

For decades, numerical simulations were used to investigate the process of composite thermal conduction. The finite element method is a numerical technique that can be used to acquire solutions to a great elegance of engineering problems related to pressure assessment, heat switch, fluid glide, etc. FE method generally requires an exploration of the generation of a new model for each specific composite system. The finite element software package is used to evaluate the composite's new properties. FEM is considered one of the most promising methods to research the enhancement/reduction of composite materials by thermal expansion coefficient (CTE) and thermal conductivity (TC). This approach has already been used to predict a wide range of two-phase composites, including plastic, polymer, ceramics, and nanocomposites, for CTE and TC.

FEM's basis is based on discretizing the solution domains into finite elements for which approximate systematic solution is developed by applying weighted residual method variation. In turn, FEM reduces the trouble to that of many unknowns by dividing the domain names into factors and expressing the unknown discipline variable within each component in phrases of the assumed approximating capabilities. Such interpolation capabilities are represented at accurate points called nodes in terms of the values of the sector variables. Nodes are usually located along the borders of the elements and meet the nearest elements. The ability to discretize the irregular domains with finite elements makes

the method a useful and functional tool for analysing the problems of the boundary, initial, and unique meaning arising in different engineering disciplines.

The estimation of the useful properties of composite materials is of vital importance for the proper design and development of composite-based applications. The microstructure of the composite characterization is an important criterion that affects the active properties of the composite. The composite modeling is changing parameters, including the shape, volume, spatial distribution, and embedding orientation in the matrix. Although most composite structures have inclusions of random allocation and path, the study of composites with periodic structure can provide a great insight into the impact of microstructure on the useful properties. A system with a high degree of symmetry is chosen because it can be evaluated easily (Nguyen and Duc 2016, Qian et al. 2017, Nayak et al. 2010).

2.2.2.1 Numerical (FE) modeling of the coefficient of thermal expansion

The FE modeling of the PDMS and CB/PDMS composite is created for a different volume percentage of CB content. A three-dimensional model has been created with spherical shapes of the filler and square box as a matrix material. The configuration of volume fraction evaluated and the number of inclusion model is developed as per Table 2.6.

Table 2.6 Model developed based varied percentage of filler and inclusion

Materials	No. of filler inclusions (4x4x4 mm^3)
PDMS	0
05% CB	25
10% CB	25
15% CB	25
20% CB	25
25% CB	25

Three-dimensional models with length, width, and height of 4 mm^3 are created. The filler is added to the block (polymer) in the shape of the sphere. The spheres filler model consists of twenty-five with radii depending on the number of inclusions. Then Equation 2.9 is used to determine the radius of the spheres based on the volume fraction and number of particles.

$$v_f = \frac{nV_f}{V_c} = \frac{n\left(\frac{4}{3}\pi r_{sph}^3\right)}{lwh} \rightarrow r_{sph} = \sqrt[3]{\frac{lwhv_f}{n\pi}} \qquad (2.9)$$

The geometry of the model with the initial condition is shown in Figure 2.6. The model contains a spherical filler particle. Models are made using spherical inclusion arranged in equal distance within the matrix. In this account, different simulation is run, and the results are obtained for each specific case. The geometry and mesh models of these models are shown in Figure 2.7.

The COMSOL multiphysics tool is used to create a composite structure and then assigned material properties independently to each particle and matrix element. The only load applied to this block is the temperature of 70K. In the end, create a mesh model as the free tetrahedral of the finer size element created for both filler and matrix. The x=0, y=0, and z=0 faces are added to the selection block and other side rolls.

Micro-sized carbon black particles are used in the present investigation as the filler material embedded in the PDMS matrix, the almost spherical filler form. The FE models considered for this analysis include the spherical inclusions of the cubic shaped matrix. Schematic representation of carbon particles embedded in a PDMS body with a periodic structure and the prescribed boundary conditions appeared in Figure 2.6. The temperature is applied on the surface of the square block. The temperature at the left surface is T_1 (applied), and other surfaces are fixed to room temperature. The method is believed to evaluate the discrepancy that could be due to the matrix and filler product between the experimental and FE model. The main objective of the analysis of the FE model for CTE is to create and validate experimental data by building a model with no void and a perfect connection between the matrix and the filler.
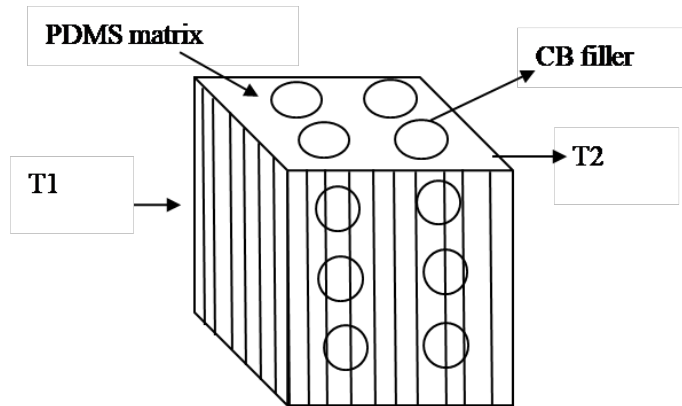
Figure 2.6 Schematic representations of particulate polymer composite of CTE
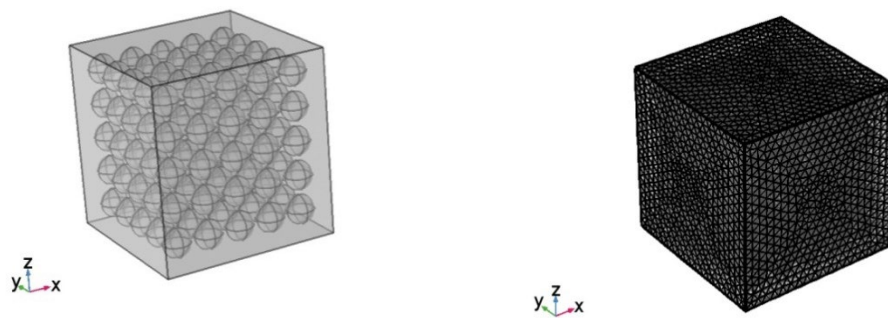
Figure 2.7 The geometry and mesh model PDMS/CB composites of CTE

2.2.2.2 Numerical (FE) modeling of the thermal conductivity

Micro-sized carbon black particles are used in the present investigation as the filler material contained in the PDMS matrix, and it shows the almost spherical filler shape. For this analysis, therefore, the FE models considered include the cubic form matrix with spherical inclusions. Figure 2.8 shows a schematic representation of carbon black particles embedded in a PDMS body with a normal arrangement and the specified boundary conditions with heat flow direction for the conductive problem. The temperature is estimated to be 2.5 W/m^2 K at the left surface T_1, the ambient convective heat transfer coefficient, and the problem is analysed at 27 °C room temperature. It is assumed that the similar surfaces perpendicular to the heat flow are adiabatic. The internal and other

boundary temperatures are not detected. In this study, a few presumptions are implemented when modeling.
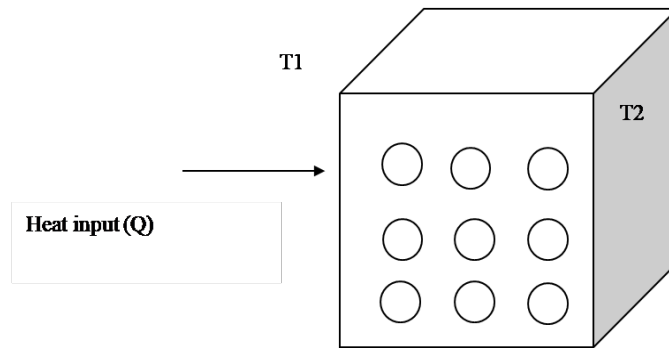
Figure 2.8 The direction of heat flow and boundary conditions for the thermal conductivity

The FE model includes sphere-in-cube, then the thermal conductivities of the PDMS and CB composites are calculated. Typical 3-D physical models are shown in Figure 2.9 and Table 2.7, showing the arrangement of CB microspheres inside cube-shaped composites with filler concentrations of 5 Vol percent to 25 Vol percent.

Table 2.7 Thermal conductivity configuration of PDMS/CB composite

Materials	No. of filler inclusions (4x4x4 mm^3)
PDMS	0
05% CB	25
10% CB	25
15% CB	25
20% CB	25
25% CB	25

The FE modeling is carried out by developing an independent model for different filler content of the PDMS/CB composite. The thermal conductivity of plain PDMS and PDMS/CB is determined by the simulation method.

Figure 2.9 FE model arrangement of PDMS/CB composite of thermal conductivity

2.3 Processing of the composite material

Fabrication of composite

A polymer material Slygard 184 silicone elastomer was procured from Dow Corning Ltd. It was chosen as the matrix material. An industrial standard nano-sized carbon black powder Vulcan XC72 Cabot Corporation was selected as the filler material. The silicone elastomer was provided as two parts of a liquid component kit, composed of a monomer material (part A) and a curing agent (part B). These were mixed in a weight ratio of 10:1 to make a silicon matrix for the composites. The PDMS polymer sample was prepared by adding a cross-linker with the monomer as specified by the supplier. A shear mixing of 8 to 10 minutes was done using a mechanical stirrer to uniformly blend the cross-linker with the monomer, followed by degassing for 20 to 25 minutes, and the sample was kept in a vacuum chamber to clear it of any entrapped air bubbles. The degasified mixture was then poured into an aluminum mould. It was then allowed to cure for 48 hr at room temperature. Then the cured sample was unclamped from the mould (Pimentel-Domínguez et al. 2016, Kong et al. 2014). The same technique is used for the preparation of PDMS composite samples for tensile, compression, and tear testing. The preparation process was continued by incorporating a different percentage of CB particles into the PDMS. The schematic steps involved in the fabrication composites are shown in Figure 2.10. The experimental equipment used for the preparation of composites for the present investigation appears in Figure 2.11.

50
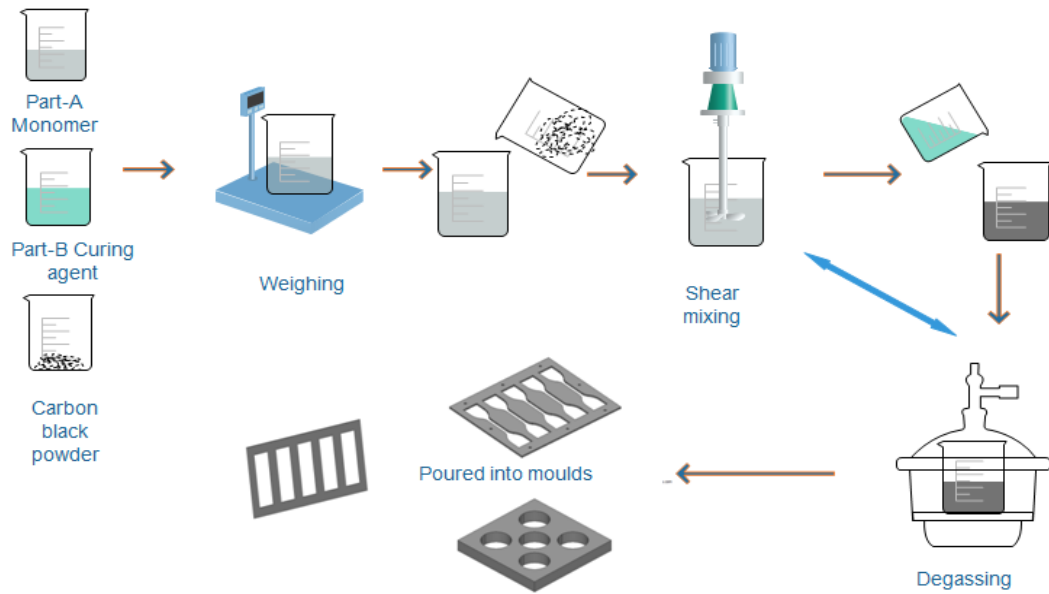
Figure 2.10 Schematic steps for preparation composite materials

| Part-A (Monomer) | Part-B (Curing agent) | Carbon black Powder | Weighing a matrix and filler |

Vacuum chamber for degassing

Mechanical stirrer for mixing
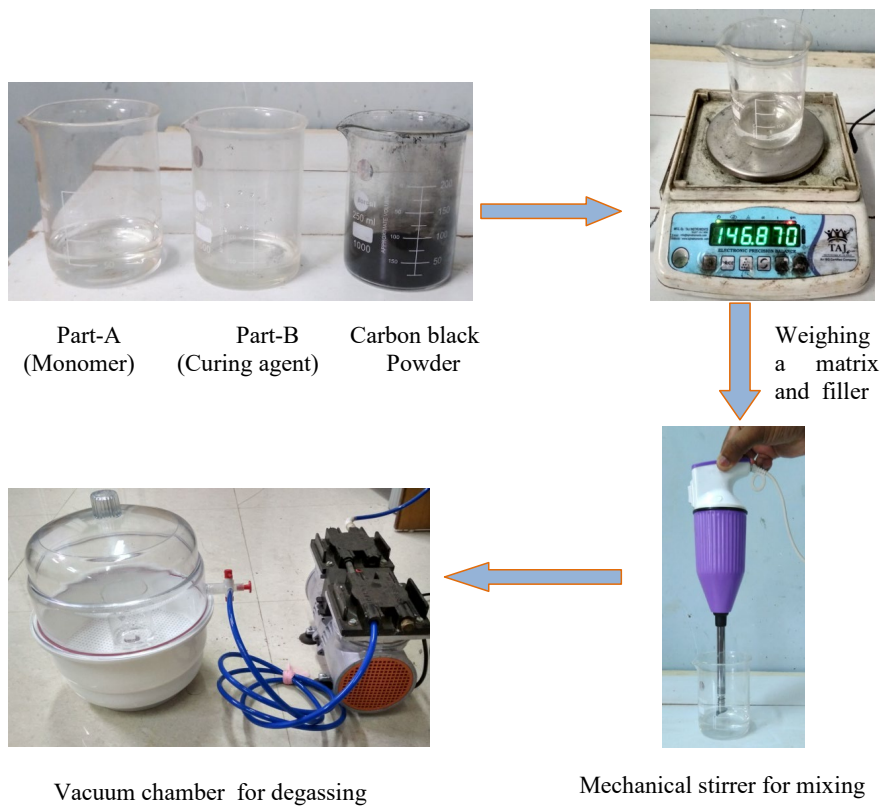
Figure 2.11 Experimental equipment used for the preparation of composites

2.4 Composite material testing

Once the polymer composites sample were prepared and then performed the physical, mechanical, thermal, optical, and dielectric tests. These test results were used for developing actuator models as well as comparing empirical and numerical (FE) materials model results. Finally, the experimental results of these properties give confidence in the justification and validation of developed composite material.

2.4.1 Physical test

Density is one of the crucial parameters in evaluating product behavior for specific applications in engineering. The density of the composite material and its components is typically measured using one of three methods, the Archimedes, the method of sink-float, and the method of gradient density. The real or apparent density of the composite is calculated in the present work by using kerosene as the medium is shown in Figure 2.12.
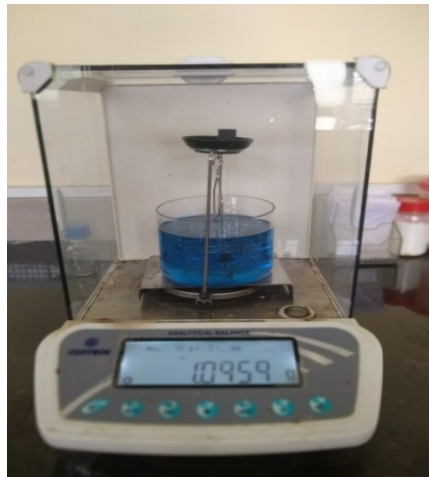
Figure 2.12 Density measurement kit

Density calculation is carried out in compliance with the D 792 ASTM standard. According to this theory, when a sample is immersed in a liquid, the apparent weight loss is proportional to the upthrust, and the weight of the displaced fluid is equivalent. The composite's estimated density is calculated using Equation 2.10.

$$\rho_m = \frac{\rho_k W_a}{W_a - W_k} \tag{2.10}$$

where, ρ_m is the measured density of the composite, ρ_k is the density of the kerosene (810 kg/m³),$'W_a'$ is the weight of the composite sample in air and $'W_k'$ is the weight of the sample in kerosene.

2.4.2 Mechanical testing

In order to examine the material characteristics of the PDMS and PDMS/CB composite moulds are manufactured. The moulds are designed as per the ASTM guidelines for tensile and compressive testing of polymer composite materials. Similarly, the compression test mould samples fulfill the ASTM standard for polymer composites hardness testing.

2.4.2.1 Tensile test

The tensile test is performed in line with the ASTM D412, TYPE C standard. The standard of mould dimensions and fabricated mould are shown in Figure 2.13 (a) and Figure 2.13 (b). The plain PDMS and PDMS/CB composites are fabricated for the tensile test, as shown in Figure 2.13 (c) and Figure 2.13 (d). Tensile testing of the sample is performed using a universal testing machine (Zwick Roell Z020 Loadcell-20kN) crosshead velocity is 500 mm/min tensometer date recorded using inbuilt data monitoring software. To ensure the uniform pressure distributions over the composite sample by adding proper gripping mechanism on both sides of the test sample by avoiding slippages. As per the ASTM standard, the elastic test is conducted by feeding the appropriate dimensions of the test samples into the machine. The composite material test is accompanied using a tensile machine is shown in Figure 2.14.

The elastomer material can show the elastic behaviour up to extremely high strain level. At the strain levels underneath of 40 to 45 percentage, the linear behaviours are allowed to obtain Young's modulus using Hooke's law ($E = \frac{\sigma}{\varepsilon}$). Whereas the applied stress is the force per unit area, and the resultant strain is nothing but change in elongation length (Johnston et al. 2014). The influence of filler contents on the tensile strength of PDMS is determined

by averaging the data from each of five test samples for every volume percentage of filler. The specimens are tested for the maximum tensile stress and percentage strain of varied filler content of CB.
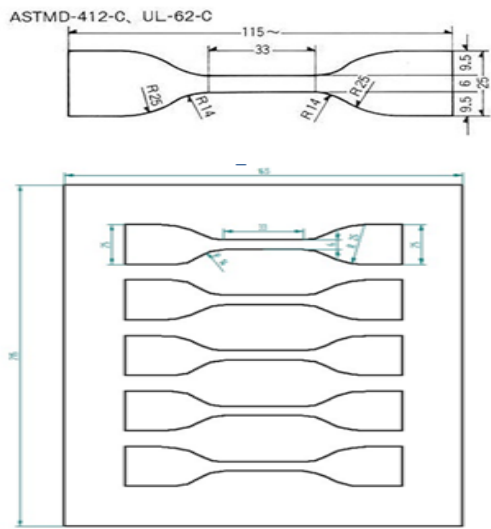
(a)

(b)

(c)

(d)

Figure 2.13 (a) Dimensions (Dog-bone) of tensile as per ASTM standard (b) Prepared aluminum mould (c) Fabricated pure PDMS samples (d) Sample of PDMS/CB composite

Figure 2.14 Experimental test setup for tensile test

2.4.2.2 Compression test

The compressive test mould is manufactured as per the ASTM D575-91. The mould is fabricated with a multi-part comprising of the well-polished aluminum plate on top and base constraining the central mould. The mould dimensions and prepared mould is shown in Figure 2.15 (a) and Figure 2.15 (b) for the compressive test. The compressive strength is evaluated using prepared plain PDMS and PDMS/CB composites samples, as shown in Figure 2.15 (c) and Figure 2.15 (d). Compressive testing of the sample is performed using a universal testing machine (Zwick Roell Z020 Loadcell-20kN). The crosshead speed is to be set at a maximum of 20mm/min. Compression testing systems are known to incorporate a few inaccuracies because of the diversity of the cross-sectional area and the barrelling of the test sample as the load increases (pre-load 1N). At the first stage, high friction between the test plates and sample exists, which results in a deviation from uniform axial compression stress states.
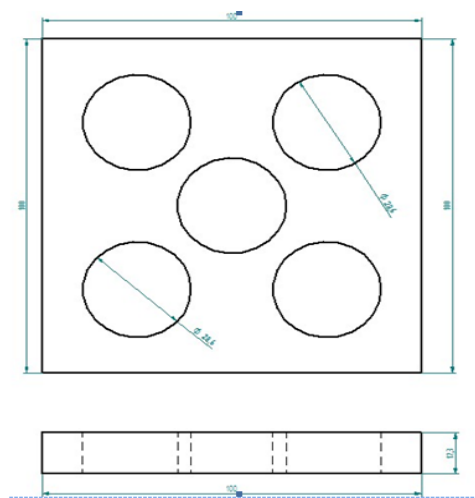
(a)   (b)

(c)   (d)

Figure 2.15 (a) Dimensions (Circular) of compression as per ASTM standard (b) Prepared aluminum mould (c) Fabricated pure PDMS samples, (d) Sample of PDMS/CB composite.

In all samples, the following tests over friction and resultant barrelling are prevented promptly before the testing. During operation, the data is recorded with a maximum load condition. The samples are tested consequently at the ambient temperature using a compressive UTM setup, as shown in Figure 2.16.

56

Figure 2.16 Experimental setups for the compressive test of composites

2.4.2.3 Hardness testing

The hardness test is conducted using a handheld Durometer (Shore-A hardness tester) as per the latest German standard DIN 5350 and American standard ASTM D 2240. Hardness estimations are recorded, when complete indentation had occurred on the surface of the test sample. The relaxation of the polymer composite material can happen between 8 sec to 12 sec after indentation. This procedure is repeated and found the average value over the sample surface to guarantee homogenous hardness estimation. The setup and procedure of experimental hardness measurement appear in Figure 2.17.

Figure 2.17 Measurement setup of the shore-hardness

2.4.2.4 Tear testing

For tear strength, the specimens were prepared in a rectangular shape with dimensions of 75 mm length, 25 mm width, and 1.5 to 2 mm thickness as per the ASTM standard. Five samples of each composite were prepared for tear testing. A low inertia instrument is required for a continuous recording of force throughout the tearing process of the T-type sample. Hence, the tear strength test was carried out as per the ASTM D 624 standard on a universal testing machine (Zwick Roell Z020 Loadcell-20 kN). For the T-type, the crosshead speed rate of jaw separation was maintained at 50mm/min.

The tear strength specimens of the plain PDMS and CB/PDMS composites are shown in Figure 2.18 (a) and Figure 2.18 (b), respectively. A specimen was pre-cut along the axis of the sample measuring about 30mm with a razor blade just before testing. The sample was loaded in the tension direction, along the scissor arms of the specimen, as shown in Figure 2.19. The test was carried out until a tear propagated through the unslit region. The results were recorded in the computerized UTM machine, and the reported average values were obtained with five test specimens. The tear strength of the polymer composite sample was calculated using a well-known analysis of the Rivlin and Thomas crack growth behavior (Rivlin and Thomas 1953). The tearing strength of the composites was computed using Equation 2.11.

$$T_s = \frac{2F}{b} \qquad (2.11)$$

Where T_s is the tear strength in force per unit thickness (per unit length torn), F is the force applied to each specimen end, and 'b' is the thickness of the sample. The force required to disseminate the tear was averaged as described in ASTM D624, to give average tear force for each sample.
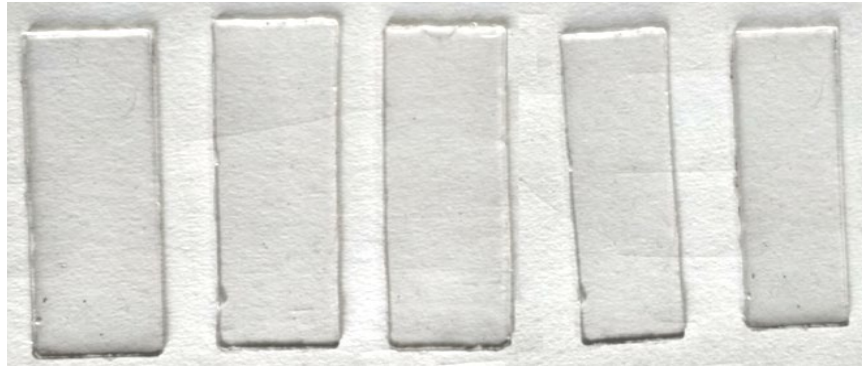
(a)
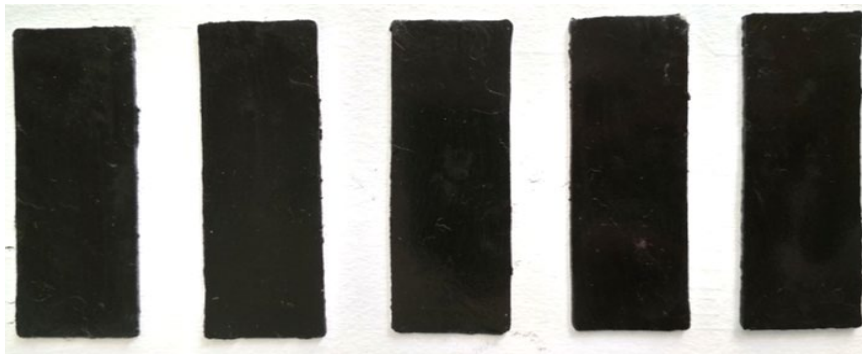
(b)

Figure 2.18 A fabricated tear test sample of (a) Plain PDMS, and (b) PDMS/CB composite

Figure 2.19 Experimental setups for tear test specimen

2.4.3 Thermal testing

Thermal properties are very crucial in the development of photo actuators. Thus, the coefficient of thermal expansion, thermal conductivity, and specific heat capacitances are used to measure the heat flow through the material. The composite test sample was prepared for varied volume percentage of filler, which includes a low conductive polymer material and high conductivity filler material for obtaining the thermal properties polymer composite.

2.4.3.1 Experimental testing of the coefficient of thermal expansion

Solid-state materials typically expand on heating and contract on cooling. This response to temperature change is expressed as the thermal expansion coefficient. CTE is a vital property for actuator applications because it induces the stresses in the material. A sample was prepared as per the ASTM standard E831-14 and tested under a thermal-mechanical analyser (TMA). The test sample is prepared by various (5 Vol% to 25 Vol %) volume percentage of CB filler content in PDMS material. The sample was cured at room temperature in a pre-prepaid mould with the dimension (10x10x3 mm), and the fabricated samples are shown in Figure 2.20. The dimension change with an increase in temperature is measured to obtain a coefficient of thermal expansion of the polymer composite. The temperature increments are in steps of 10 $^{\circ}$C per 10 minutes from room temperature to 200 $^{\circ}$C. The temperature of the specimen and dimensions are measured and stored using a data logger and computer. From these raw data, a linear section is selected from the plot and calculated the effective thermal expansion of the material. Three samples are considered for the measurement of CTE calculation. The CTE is then averaged and normalized for the baseline material. Coefficients of thermal expansion of the composites are experimentally examined and acquired the consequences of the use of thermal-mechanical analyser is shown in Figure 2.21.
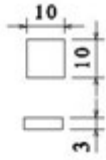
(a)
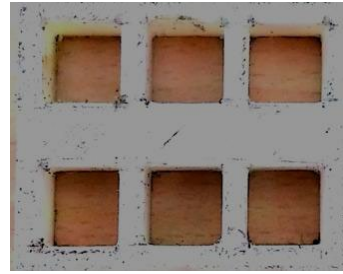
(b)
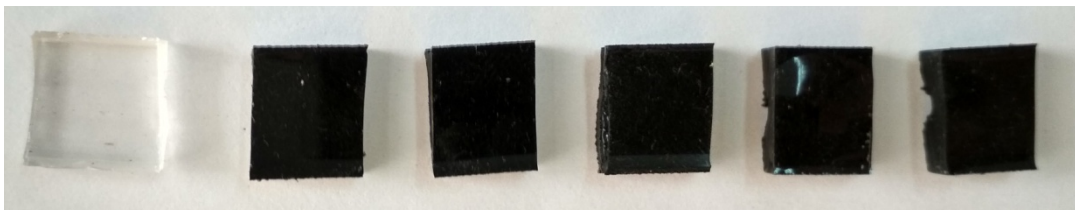
(c)

Figure 2.20 (a) CTE Sample dimension (b) Mould is used for the preparation of the
sample, and (c) Fabricated composite sample for CTE test
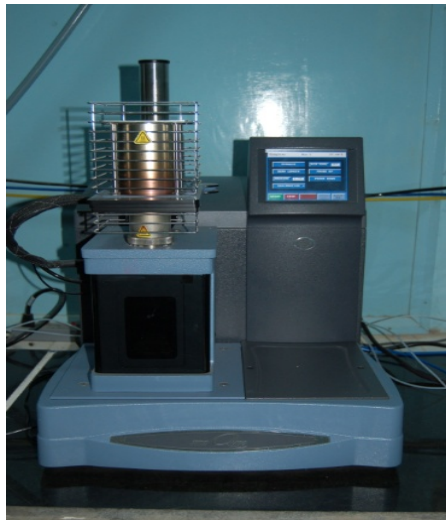
Figure 2.191 Experimental setup of TMA for CTE measurement

2.4.3.2 Experimental testing of thermal conductivity

Thermal conductivity is the transfer of energy in a conductive medium between adjacent molecules and electrons; it is a material property that defines heat flow within a body for a given difference in temperature per unit area. Thermal conductivity values are used to measure the heat flow through the composite material. As the conductivity of the material increases, the heat flow in the material is also increased. Thus, to obtain the thermal conductivity of PDMS and carbon black composite, a different volume percentage of the CB sample is prepared. The specimen of a diameter of 12 mm and a thickness of 3.2 mm is made as per the ASTM E1530 standard. The prefabricated mould for thermal conductivity is shown in Figure 2.22(a). The test sample of plain PDMS and PDMS/CB composite samples are fabricated, as shown in Figure 2.22 (b). For each formulation, typically, three different sets of a total of 18 samples are tested. Finally, the average of each sample thermal conductivity is taken for the analysis.

(a)

(b)

(c)
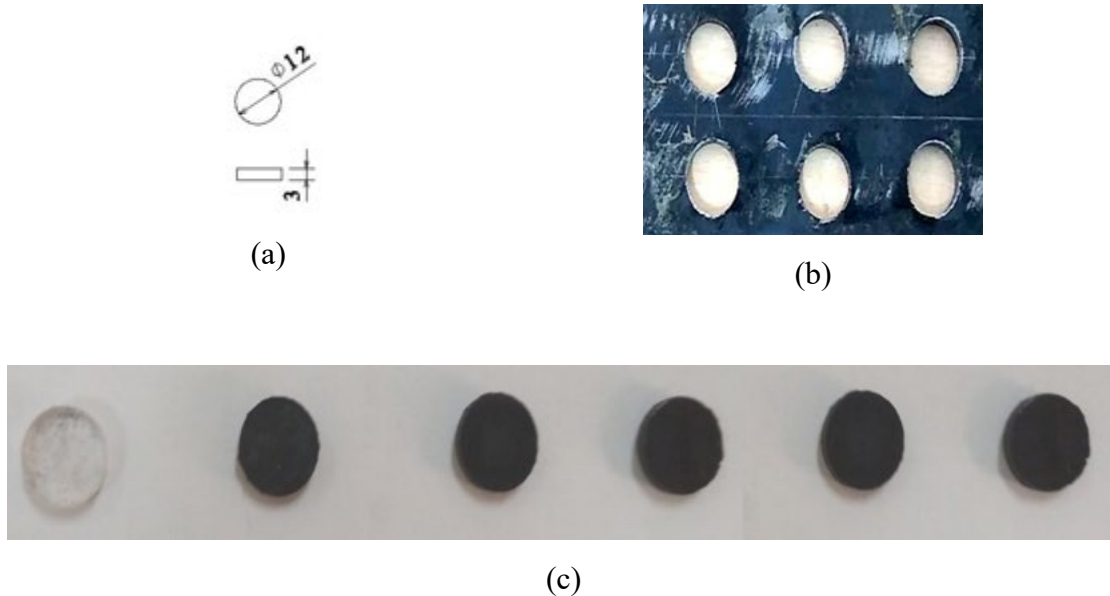
Figure 2.22 (a) Thermal conductivity test sample dimension (b) Samples are prepared in circular mould (c) Plain PDMS and varied Vol % of CB composite sample for a conductivity test.

The well-established Hot Disk Transient Plane Source (TPS) method allows rapid, accurate, and non-destructive testing of thermal conductivity. The Hot Disk TPS method

uses the transient plane source technique to measure the in-plane and through-plane thermal conductivity of isotropic and anisotropic material in the same test. The sensors used in this take a look at the approach consisted of a 10µm thick nickel foil embedded among 25.40 µm thick layers of Kapton polyimide films. The Hot disk transient experimental setup is used for determining the thermal conductivity of the polymer composite, as shown in Figure 2.23.

Figure 2.20 Hot Disk TPS thermal constants analyzer setup

2.4.3.3 Specific heat capacity

The specific heat capacity at constant pressure can be determined using the thermal conductivity technique. Specific heat is the quantity of heat required with the help of one Kelvin to increase the temperature of one kilogram of mass. If the thermal diffusion (σ) and thermal conductivity of the material is known, then the specific heat capacity can be calculated ($Cp = k/\rho\sigma$). Where σ is the density of the material. In the present work, the specific heat capacity of the plain PDMS and various PDMS/CB composites is calculated from the measured data of the thermal diffusivity and thermal conductivity using a Hot Disk instrument.

2.4.4 Optical testing

In the development of the photo actuators, optical properties are also significant (Kim et al. 2018, Wang et al. 2017). The material light absorbance, transmittance, and radiation could lead to an increase in the temperature of the composite material. Thus, the composite samples are used to study some of the optical properties.

2.4.4.1 Light absorbance test

The material is identified as photoresponsive by conducting a UV-Vis-IR light absorption test. The experimental analysis is performed for carbon black, PDMS, and the combination of both (CB and PDMS) samples. The sample was fit with a 20 mm path length of the quartz substrate, which was used for light absorbance study. The light absorbance of the composite was carried out using UV-Vis-IR Spectrophotometer (Shimadzu-3600 plus), as shown in Figure 2.24.
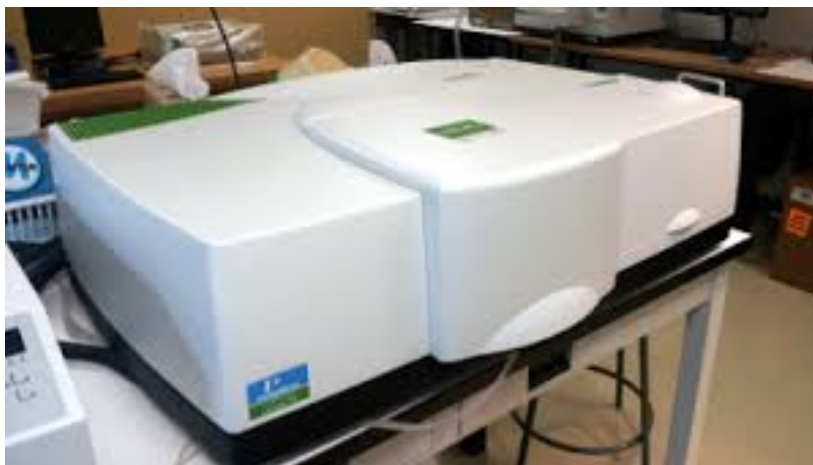
Figure 2.21 UV-Vis-IR Spectrophotometer instrument

2.4.4.2 X-Ray Diffractometer (XRD) studies

The composite of plain PDMS and PDMS/CB was analysed using X-ray diffraction (XRD) technique. The composite samples were taken for XRD measurement, broadening in size

of the peaks in the XRD pattern was recorded in the angular range 10-55 degrees. XRD analysed the crystal structure and thermal stability of the polymer composite (Pimentel-Domínguez et al. 2016) with JEOL XRD -Diffractometer operated at 30 kV and 20 amp using Ni-filtered Cu-kα radiations with a scan speed 100 min^{-1} for 2θ as shown in Figure 2.25.

Figure 2.22 X-ray diffractometer measuring instrument (JDx8P, JOEL model)

2.4.5 Dielectric testing

The dielectric material is nothing but an electrical insulator that can be polarized by applying the electric field. The imbalance in material position is causing the dielectric polarization. The dielectric material used to store the energy can be used for capacitance and actuation applications. In the present investigation, the dielectric properties of the composites are determined to understand the electrical behavior of the material. This can be adopted in the development of the polymer composite based capacitive pressure sensor/actuators. The dielectric constant of the material is also known as dielectric permittivity, which can be determined using the impedance analyser technique.

2.4.5.1 Impedance analyser

The polymer is procured as two parts of a liquid component kit composes of a base material and a curing agent. The sample preparation procedure is the same as followed in the above for the preparation of polymer nanocomposite by incorporating carbon black particle into the PDMS. The different volume percentage of carbon black is mixed with plain PDMS material.

The impedance analyser technique obtains the dielectric characterization of the polymer nanocomposites. The fabricated samples of pure PDMS and nanocomposites with the different volume fraction of carbon black (5% 15% and 25%) are as shown in Figure 2.26. The samples are prepared in a cylindrical shape with 3mm thick and 12 mm diameter in size. The circular surface of both sides are polished and then pasted with a thin layer of silver to act as an electrode.

The capacitance and tangent factor are measured using an E4980A impedance analyser (Agilent technologies) and recorded in the computer. The measurement is carried out by constructing a lab-made set up according to the ASTM-D150 standard, and the schematic of the configuration is shown in Figure 2.27. The analysis is accomplished in the range of frequency 100Hz to 100 kHz, under room temperature conditions. While measuring, the instrument error, the test sample, and lost impedance of cable are normalized by the corresponding average distance between the electrode and the matched capacitance method.

| Pure PDMS | 05% CB | 15% CB | 25% CB |
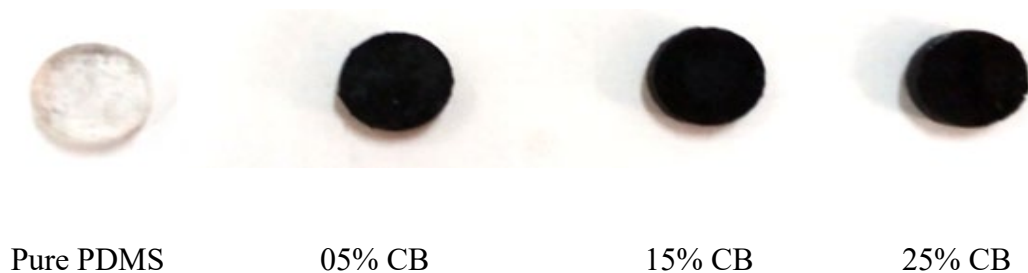
Figure 2.23 Fabricated samples of pure PDMS and PDMS/CB composites

Agilent Technologies,E4980A
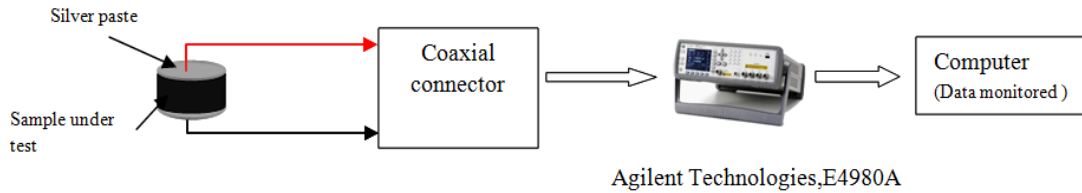
Figure 2.24 Schematic test setup of a dielectric measurement

2.4.6 Microstructure analysis

Research of microstructure or morphology is well known to strongly influence the properties of the composite by the compatibility between the phrases of matrix and filler. To determine the matrix and filler interaction, various experiments are used to observe the size of the filler particle and its dispersion in the matrix structure.

2.4.6.1 Scanning Electron Microscope (SEM)

The morphologies study of prepared base material and PDMS/CB composite was conducted using a scanning electron microscope (SEM) technique. This test shows the distribution of matrix and filler content in the composite. The analysis is performed using a JEOL make Scanning Electron Microscope, as shown in Figure 2.28.

Figure 2.25 JEOL made scanning electron microscope instrument

2.5 Modeling of the Actuator

The analytical and numerical approach is used to model the actuator. In the case of an analytical model, the equations are derived and used for understanding and studying the behavior of the actuator system. While the simulation approach used as a numerical model is almost identical to experimental work by assuming or restricting some of the parameters (initial conditions and boundaries). In the present study, both analytical and numerical methods are being used to study the behavior and performance of the composite actuator.

2.5.1 Analytical modeling of the actuator

Analytical models are nothing but mathematical equations with a closed-form solution, and a mathematical function can be the answer to the equation to describe the process parameter. The cantilever beams of single and bilayer equations from the previous work are used in the present study, and these equations are implemented using commercially available MATLAB tools. The beams are assigned the composite material properties, and the deflection behavior is studied by varying the thickness of the beam and volume percentage of the filler.

2.5.1.1   Analytical model for a single layer actuator

The analytical study on a single layer beam is carried out using composite material by stimulating thermal input. It is essential to understand the bending movements of the composite beam. Figure 2.29 illustrates the proposed schematic for the bending response of the single-layer actuator.

Single layer
composite

T_0 T_1

α_c

E_c

Fixed edge

δ
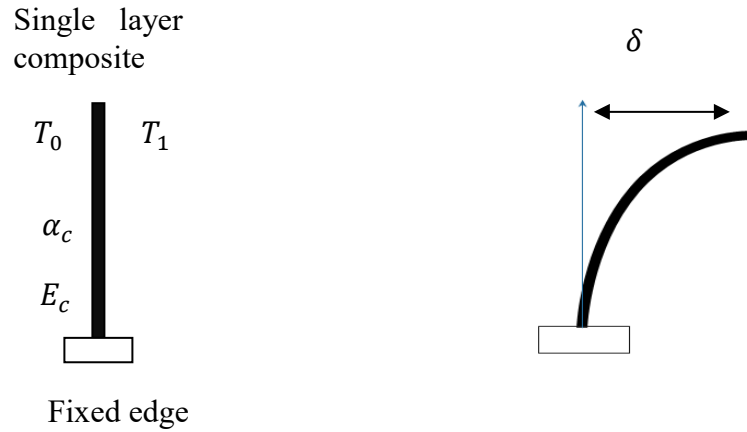
Figure 2.26 Schematic diagrams of a single layer bending

The deflection of single layer composites is calculated using Equation 2.12. $'\alpha_c'$ is the thermal coefficient expansion of the composite. L and 'b' are the length and thickness of the composite beam. The composite sample is fixed at the bottom and free to move on the other end. Then, T_0 is the applied temperature on the surface of the beam and T_1 is the ambient temperature of the composite beam.

$$\delta = \frac{\alpha_c(T_1-T_0)L^2}{2b}$$ (2.12)

2.5.1.2 Analytical model for bilayer layer actuator

The bilayer polymer composite's analytical study is implemented, and its bending movement is derived from the bilayer geometry. Figure 2.30 (a) provides an image of the proposed schematic for the curvature arc and the bilayer actuator's bending response.

The curvature (R) equation radius is derived from inertia's bending moment. The curvature is obtained along the direction of thickness and has been seen in Equation 2.13 (Lim et al. 2017).

(a)   (b)
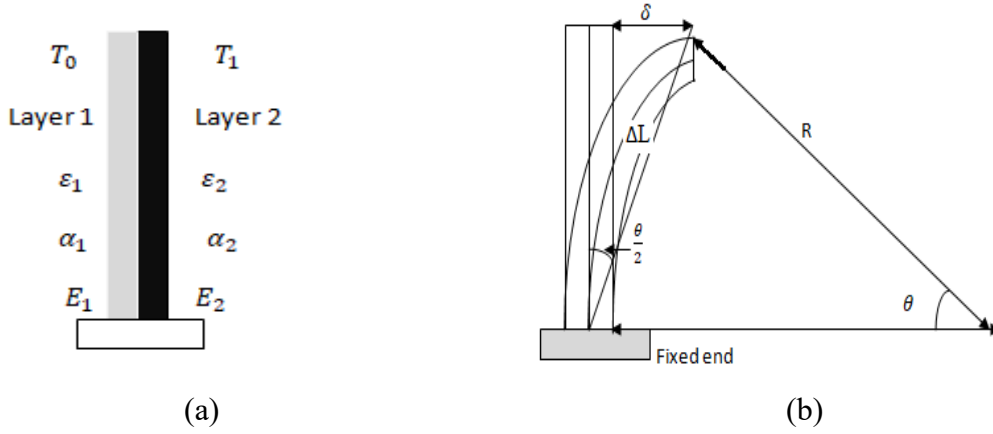
Figure 2.27 Schematic diagrams of a bilayer bending cantilever

$$\frac{1}{R} = \frac{6\frac{t_2 w_2 E_2}{t_1 w_1 E_1}(1+\frac{t_2}{t_1})^2(\alpha_2-\alpha_1)(T_1-T_0)}{\left(\left(\frac{t_2}{t_1}\right)^4\left(\frac{w_2}{w_1}\right)^2\left(\frac{E_2}{E_1}\right)^2+4\left(\frac{t_2}{t_1}\right)^3\frac{w_2 E_2}{w_1 E_1}+6\left(\frac{t_2}{t_1}\right)^2\frac{w_2 E_2}{w_1 E_1}+4\frac{t_2 w_2 E_2}{t_1 w_1 E_1}+1\right)+(t_1+t_2)} \tag{2.13}$$

Where, $\frac{t_2}{t_1}$; $\frac{w_2}{w_1}$; $\frac{E_2}{E_1}$; $w_1 w_2$, $t_1 t_2$, $E_1 E_2$ are the width, thickness, and Young's modulus of

layer one and layer two of the polymer composite beam. α_1 , α_2 $(\Delta\alpha)$ are the coefficient

of thermal expansion of their respective layers. The initial and final temperature of the

bilayer is represented as T_1 and T_0. Hence the radius of curvature is proportional to the

change in the coefficient of thermal expansion and change in temperature (ΔT) and

inversely proportional to the thickness of the material.

The tip deflection of the bilayer cantilever is shown in Figure 2.30 (b). The radius of

curvature is found; the deviation of the free end of the beam can be determined by

trigonometrically. The deflection at the free end of the bilayer cantilever is obtained using

Equation 2.14.

$$\delta = \frac{3\frac{t_2 w_2 E_2}{t_1 w_1 E_1}(1+\frac{t_2}{t_1})^2(\Delta\alpha)(\Delta T)}{\left(\left(\frac{t_2}{t_1}\right)^4\left(\frac{w_2}{w_1}\right)^2\left(\frac{E_2}{E_1}\right)^2+4\left(\frac{t_2}{t_1}\right)^3\frac{w_2 E_2}{w_1 E_1}+6\left(\frac{t_2}{t_1}\right)^2\frac{w_2 E_2}{w_1 E_1}+4\frac{t_2 w_2 E_2}{t_1 w_1 E_1}+1\right)+(t_1+t_2)} \tag{2.14}$$

2.5.1.3   Cyclic mode of the actuator

Photo-thermal analysis

The focused light causes a heating of the beam resulting in a bending of the free end. The change in temperature of the beam could be obtained by assuming a relation between optical intensity and power. (a) Intensity follows exponential decay inside the layer of the beam, along with the direction of their thickness. (b) Assumed that, all transmitted light energy is absorbed by the beam, and then converted into heat.

The thermal power generated along the thickness (x) from the surface of the incident is given by (Baglio et al. 2002). The heat generated can be formulated using Beer-lamberts' law (Tjahjono and Bayazitoglu 2008), (Cerretti et al. 2016). Figure 2.31 shows the intensity of light through the thickness of the sample. The range of light intensity passes through the material. There is a decay of light intensity along the thickness direction. The heat generated on the surface and through the material mainly depends on the thickness (5 mm) and an absorption coefficient of the material. Thus, it can be predicted that as depth increases, the intensity of light through the material decrease and generates the heat is given by Equation 2.15.
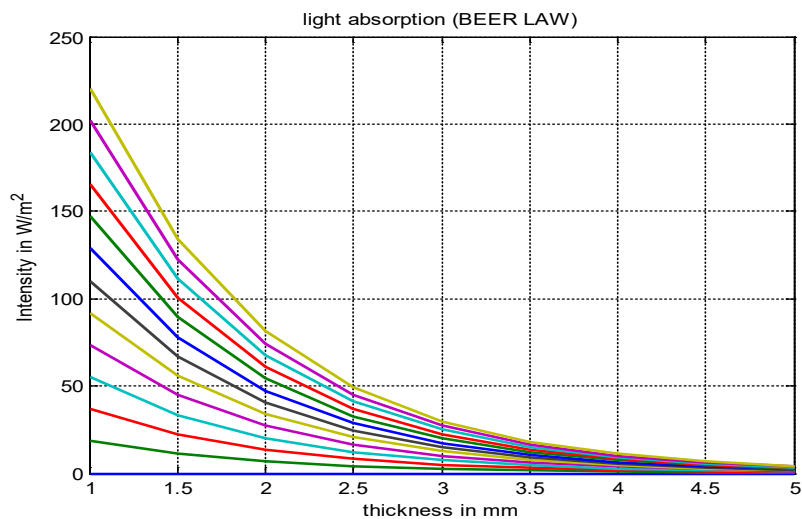
Figure 2.28 The intensity of light through the thickness of the beam

$$P_h(x) = A\, I_{in}(1 - \exp^{-ax}) \qquad (2.15)$$

Where, $P_h(x)$ is generated heat power, light flowing through an area A, and I_{in} is the intensity of light. It is essential to relate heat power and with the temperature difference because this will help to determine the deflection of the beam.

Thermo-mechanical analysis

The relationship between the thermal power and the temperature is expressed as

$$\frac{dQ}{dt} = mCp\frac{dT}{dt} \qquad (2.16)$$

Where 'm' is the mass of the beam obtained from the density and volume of the sample, and Cp is the specific heat capacitance at constant pressure. Thus, in this relation, the workings steps can be divided into two phases (a) in phase one heating takes place, where heat flux is constant (i.e., the light source is on). (b) In phase two, cooling takes place, during which the light source is off, and the system cools down by exchanging heat with its surrounding area.

These steps can express mathematically as.

$$mCp\frac{dT}{dt} = \begin{cases} P_h & 0 \le t_0 \le t_{on} \\ -hA(T_m - T_a) & t_{on} \le t \le t_{off} \end{cases} \qquad (2.17)$$

Where the power that reaches the beam during heating steps' is the coefficient of heat exchange, T_m is the maximum temperature of the beam at the end of the heating step, and then T_a is the ambient temperature. The initial conditions are assumed for the above two steps T (0) $=T_a$ and T (ton) $=T_m$. Thus the final temperature of the structure can be expressed as a function of time. The working period for on and off-cycle is expressed in Equation 2.18.

$$T(t) = \begin{cases} \dfrac{P_h}{mCp}t + T_a & 0 \le t_0 \le t_{on} \\ \dfrac{P_h t_{on}}{mCp}\exp\left(-\dfrac{hA}{mCp}(t - t_{on})\right) + T_a & t_{on} \le t \le t_{off} \end{cases} \qquad (2.18)$$

Hence, the change in temperature causes the deflection of the beam. Thus, the difference in temperature is obtained as $\Delta T = T_m - T_a$. From a qualitative point of view, the differential heating of the structure obtained by concentrating heat source on the beam with respect to uniform heating. It can be predicted that the area is at the higher stress of the beam and its heating will be more effective than the other region. Also, non-differential heat is taken into account; the entire beam is subjected to deformation. The deformation of the composite beam can be proved using the coupled analytical equation. The deflection (δ) of the composite beam with varying temperatures is given in Equation 2.19.

$$\delta = \frac{\alpha_c A I_{in}(1 - \exp^{-ax})(\Delta T)L^2}{2mC_p x} \qquad (2.19)$$

Where, α_c is the thermal coefficient of the composite, ΔT is a difference in temperature, L, and x is the length and thickness of the beam. Light flowing through an area A, I_{in} Is the intensity of light, and 'a' is the absorption coefficient. Finally, 'm' is the mass of the beam obtained from the density and volume of the sample. Cp is the specific heat capacitance at constant pressure is also depends on the thermal conductivity of the material.

2.5.2 Numerical (FE) modeling of the actuator

The numerical approach uses the finite element analysis method to understand the polymer composite actuator's behaviour. Until moving to experimental work, FE can achieve the numerical result for the complicated system and give insight into the model.

The parameters of the actuator are chosen depending on the application, as for now, based on literature, the size of the actuator is considered as 90mmx14mmx10mm with variable thickness. Considering it in terms of temperature on an average of 60-70 °C reached the earth depends on day and time of place. The proposed mesoscale composite beam is

modeled and simulated using commercially available COMSOL multi-physics software. For the solution of the model, structural mechanics, and heat, transfer modules were selected. These models are used to couple the physics to determine the deformation at a different temperature of the actuator. The meshing is used for the analysis of free triangulation techniques.

2.5.2.1 Modeling of single-layer composite beam

The modeling of the single-layer beam is created in the modeling software. The deflections of the beam are studied for varied volume percentage of the filler and thickness. The single layer is fixed at one end and free to move at the other end. All other initial and boundary conditions are applied and simulated for the deflection beam. Figure 2.32 shows the simulation steps such as geometry, boundary condition, and meshing the composite beam.

| Single Geometry | Boundary conditions | Meshing |
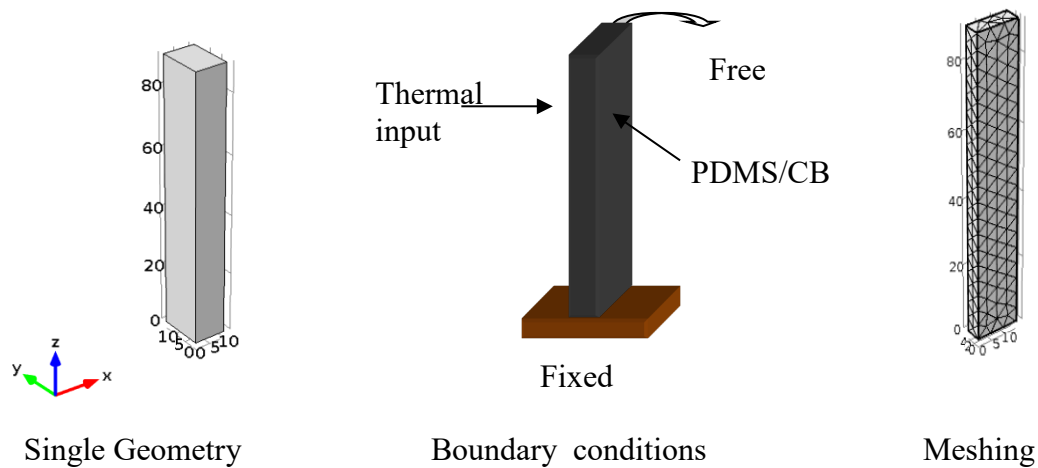
Figure 2.29 Single layer beam model for FE simulation

2.5.2.2 Modeling of bilayer composite beam

The bilayer actuator modeled structure is as shown in Figure 2.33, COMSOL multiphysics simulation tool is used to analyze the behavior of the bilayer beam on thermal stimulus. Investigate the bilayer displacement performance by varying the filler concentration of CB and thickness of the layers.

74
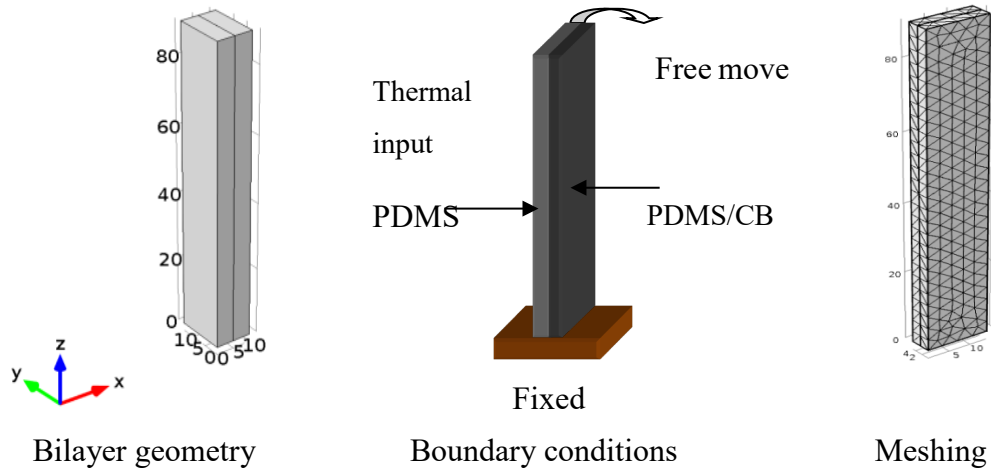
Figure 2.30 Meshed and boundary condition model of the bilayer beam

FE analysis of a stacked composite beam requires a coupled-field or multiphysics approach for solving the problems. This involves the coupled interaction between thermal and structural engineering. The geometry of the bilayer is created with fixed boundary conditions and simulated for bilayer actuation.

2.6   Testing of the actuator

The photo actuation testing is carried out for prepared single and bilayer composite samples. The photo actuation test was conducted for optimum thickness and volume percentages of PDMS and CB composite samples. The deflections of the composite's beam were noticed by stimulating the light source. Also, the actuation prototype is constructed for the proposed conceptual model. The prototype of the photoactive switch and a heliotropic tracking system using the PDMS/CB composite beams are built.

Measurement of photo actuator deflection

The sample obtained from the fabrication process with the dimensions of 90mm (length) x 14mm (width) x5mm (thickness) is used for photo deflection measurement. The schematic setup used for photo actuation is shown in Figure 2.34. The IR light incident on composite beam with a light intensity of 1000 W, and it is predicted that temperature change attributed

to the carbon black and PDMS composite and gives rise to the photomechanical deflection of the actuator.

The Micro-epsilon laser displacement sensor records the photomechanical tip deflection of the composite beam actuator. In the case of a static model of testing a graph, a sheet is used to note down the deflection. It is assumed that the transmitted intensity follows an exponential decay inside the layer of the beam, along with the direction of their thickness. Also, it is believed that all the transmitted light is absorbed in the composite beam, and other parameters are neglected. The specification of equipment used in the experimental setup is provided in Table 2.8.

Table 2.8 Specification of equipment's used in the experimental setup

Equipment's	Specifications
IR Light source	1000Watt. 230 VAC
Solar power meter	Intensity meter Measuring Range : 0 ~ 2000 W/m^2
IR thermometer	HTC thermometer : -30 to 550 ^{0}C
Laser displacement sensor	Model: Opto NCDT-1402; measurement range : 0-10 mm; Resolution : 1µm: Voltage output: 1-5 V
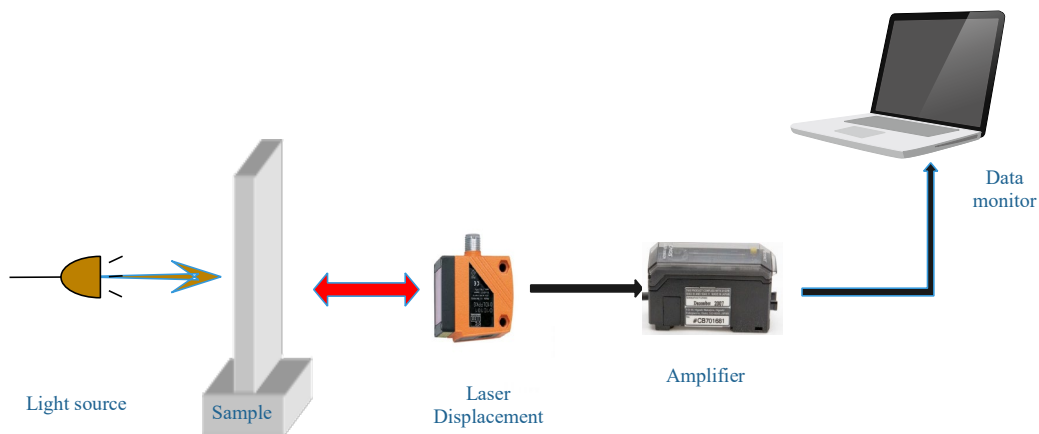
Figure 2.31 The schematic setup of the photo actuator

2.7 Construction and testing of the prototype

Build a prototype model of an idea using the composite material. Thus, the proposed concept of photo actuation using a polymer composite was built and tested. The prototype test was conducted in the laboratory environment to evaluate its performance. In the present study, PDMS/CB composite beams were used for testing of the conceptual model.

2.7.1 Conceptual model of the proposed photoactive switch

The PDMS/CB based composite beams of dimension 45x 14 x 2 mm^3 are prepared using the fabrication procedure. The copper strip is pasted on the surface of the beam, and light source illuminated on to it. The two copper wires are used and connected to the load. Figure 2.35 shows the schematic construction of the photoswitch using a composite beam.
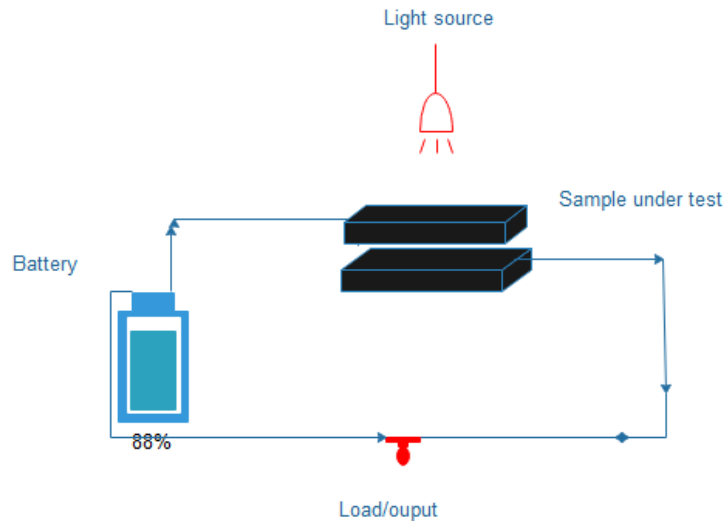
Figure 2.32 Prototype test setup for photoswitch

2.7.2 Conceptual model of the proposed heliotropic system

An effort was produced to use polymer composite material to create a straightforward sun tracking mechanism. The composite-based material beam does the dual-sensing and actuating tasks in such a manner to place the tilted solar receptor to face the sun straight

throughout the day. The mechanism has been created to activate the beam by the sunlight stimulus and to focus on the solar receptor, the incident rays.

The core function of the proposed smart sun tracking mechanism would be to keep the solar receptor always facing the sun directly from sunrise to sunset. A tilting device consisting of a polymer-based actuator would be fitted into two sides of the solar receptor. The sun's heat would trigger this scheme, causing the tilt of the solar receptor to face the sun. Once the composite beam receives the heat of the sun, it deflects towards sunray and solar receptor face at the sun.

The first step towards realizing this goal is the fabrication and assemblage of a table-top functional model that could be scaled up later to an actual working device on the site. The open-loop functional model must be designed based on the composite beams. Figure 2.36 shows the arrangements of the functional model of the sun-tracking solar energy receptor.

Solar cell
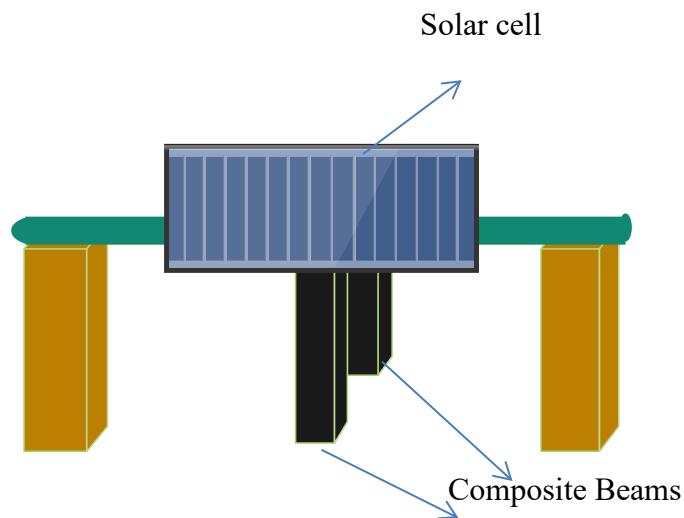
Composite Beams

Figure 2.33 Functional models of the proposed sun tracking mechanism

In this model, a solar receptor (cell) tilted by a composite beam due to the sun's heat. Its fixed legs are holding solar cells, and rod support rotates the solar cell when the composite

beam deflects. This proposed concept is tested at a laboratory level, and this could be extended for a larger scale in the outside environment using composite beams.

Summary of methodology

The above section offers descriptions and techniques used for the processing of material for photo actuator study. Detailed studies are outlined as empirical, and numerical (FE) material modeling, Testing methods for material characterization such as physical, mechanical, thermal, optical, and dielectric properties of PDMS and carbon black composite are discussed in detail. The analytical and numerical (FE) modeling concepts for single and bilayer actuators are mentioned. Also, in this section, briefs on photo actuation testing and the proposed conceptual prototyping methods. In further sections, discusses the outcomes of all the techniques described in the methodology section.

-----------֍֍֍֍֍------------

CHAPTER 3

RESULTS AND DISCUSSION

In the present chapter, results and discussions on the development of polymer composite for photo actuators are discussed. Starting with these results and discussion, reports on material modeling and experimental test results, presentation of the analytical and numerical (FE) modeling of the actuator were followed. Finally, the deflection behavior of the photo actuator and the test result of the proposed model are highlighted.

3.1 Results of the empirical model

The empirical analysis of polymer composite is implemented using available predictive models. The Young's modulus, coefficient of thermal expansion, and thermal conductivity are the more influencing parameters in the development of photo actuator. Hence, the empirical models of PDMS/CB composite were implemented and compared with experimentally obtained results.

The empirical results for Young's modulus with the different volume fraction of carbon black content are shown in Figure 3.1(a). Comparisons between the experimental results and the results calculated from for different empirical models of Young's modulus of polydimethylsiloxane reinforce carbon black particle can be validated confidently. Because the test results of composite material follow very near to the empirical results, it is also noticed that all models were not fit the experimental result; the reason could be that the equation is derived based approximation method.

Figure 3.1 (b) shows the measured coefficient of thermal expansion of the PDMS/CB composite along with that calculated using the expression derived from the different empirical models. It is evident from Figure 3.1 (b) that the empirical equation derived by (Chen et al. 2007) is an excellent agreement with experimental results. It confirms the

important role of the interphase volume and strength of the matrix and filler interactions for the successful prediction of CTE of the polymer composite.

The measured thermal conductivity of the PDMS/CB composite and those predicted by the various empirical models are plotted in Figure 3.1 (c) over a wide range of filler content between 0 to 25%. Most of the model fails to predict the experimental thermal conductivity of the PDMS/CB composite used in the present study. Because these models are derived from the approximate method and which are overestimated for an entire range of filler concentration. Lewis Nielsen model predicts reasonably well thermal conductivity of the carbon black in PDMS. The predicted conductivity of the composite is high conductivity with high filler content.
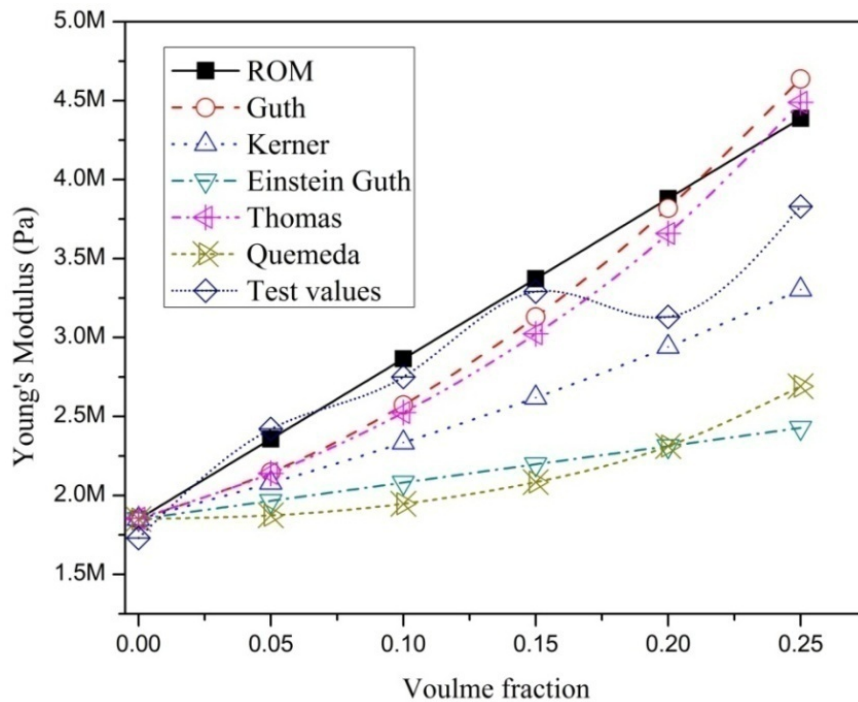
(a)
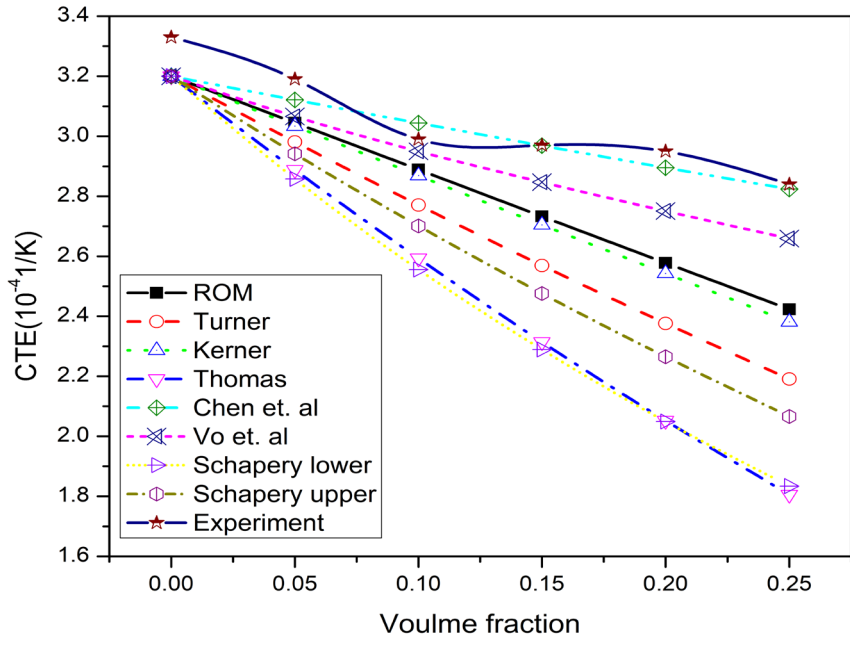
(b)
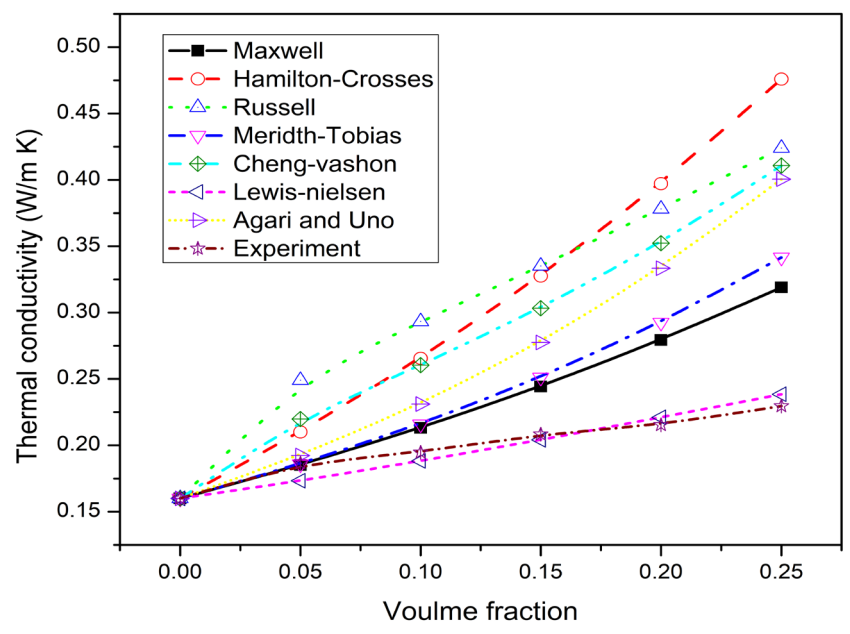
(c)

Figure 3.1 Empirical model results of (a) Young's modulus (b) Coefficient of thermal expansion, and (c) Thermal conductivity of the polymer composite

82

Further study on empirical models, which are proposed in predicting the dielectric permittivity of the polymer composites. These models predict the composite dielectric constant based on the respective dielectric permittivity of the material. Each model depends on a different assumption, like the distribution of particle and interaction among the fillers and the matrix. Hence, this may lead to a slight discrepancy in these models and which do not fit most of the composite systems. Also, there may be reasons due to inconsistency in processing and interaction between the molecules. The typical plot of composite dielectric permittivity with respect to the volume fraction of the filler is presented in Figure 3.2.

The experimental data fit better into the Wiener model compared to other approximation models. The Wiener model corresponds to capacitors that are arranged in parallel in the circuit and provide the maximum fit value. In the case of other models, follow the same trend; do not precisely fit the present experimental values. The reason could be the absence of interaction between the different constituents. This interaction depends on filler sizes; the particular volume fraction of filler, smaller particle size has a larger fraction of interface between the filler and matrix, granting more polarization. Thus, they may lead to a relatively marginal increase in dielectric permittivity.
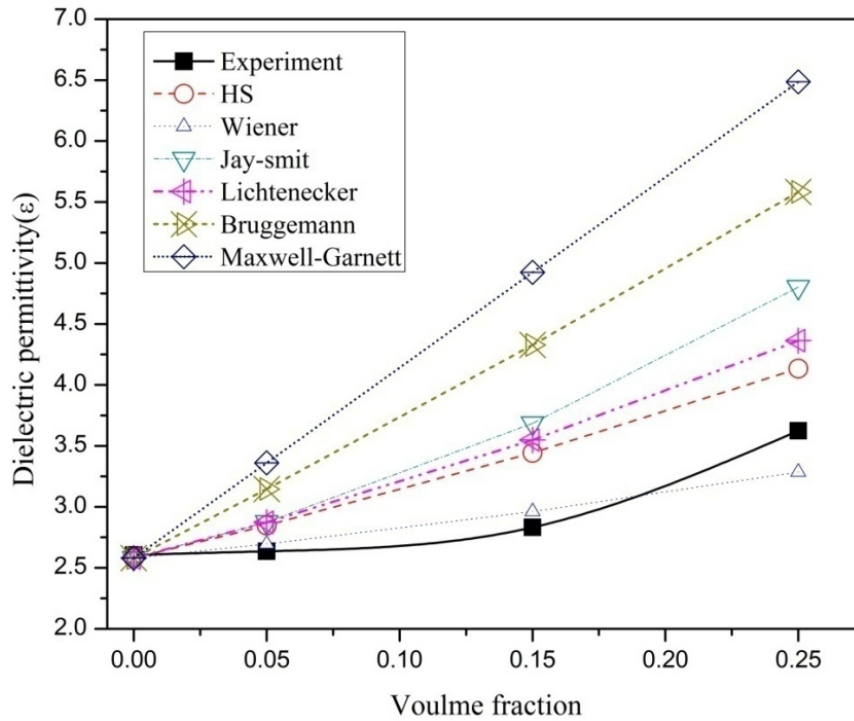
Figure 3.2 The prediction of the dielectric permittivity with varied volume fraction filler

3.2   Results of numerical (FE) modeling

The development of a composite-based actuator mainly depends on material properties. In that, more influencing material properties for the photo actuator are the coefficient of thermal expansion and thermal conductivity. These material properties are obtained by numerical (FE) modeling of the composite using commercially available FE software.

3.2.1 Coefficient of thermal expansion

The numerical (FE) analysis is carried out with a different volume percentage CB and several inclusion particles in a cube structure. Figure 3.3 shows the displacement of the cube model with a CB particle inclusion. The CTE for the varying percentages of CB is calculated $\alpha = \frac{\Delta v}{3v*\Delta T}$ where; v is the original volume, Δv change in volume, ΔT changes in temperature, and volumetric coefficient of thermal expansion (α). The model results of

the CTE are shown in Table 3.1. It shows that modeling results are near to the experimental result with a small discrepancy. The difference in results may be due to many parameters, either neglected or approximated.
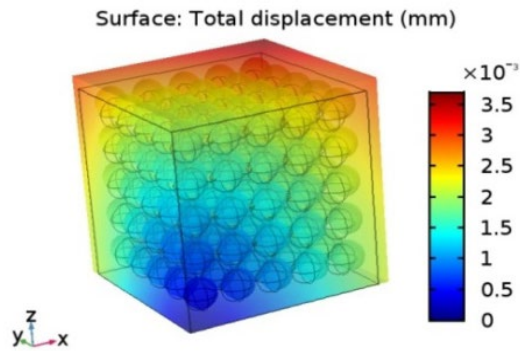
Figure 3.3 Displacement of the cube with the inclusion of the CB particle

Table 3.1 Comparison of modeling and experimental results of CTE

Composition	Numerical (FE) (3-D)model (ppm/K)	Experimental Avg. CTE (ppm/K)
PDMS	340	333
CB (05 Vol %)	328	319
CB (10 Vol %)	319	299
CB (15 Vol %)	308	297
CB (20 Vol %)	302	295
CB (25 Vol %)	296	284

3.2.2 Thermal conductivity

Thermal conductivity is also one of the essential influencing parameters for the thermal actuator. The conductivity of the composite can be improved by adding conductive material. This phenomenon is studied using FE analysis by creating a matrix and filler model. "One-dimensional heat flow, the equation is given as $Q = kA\frac{\Delta T}{t}$, where Q is the

heat flux (W), A is the cross-sectional area (m²), k is thermal conductivity (W/m.K), t is the sample thickness (m), ΔT is the temperature difference between surfaces (°C or K)". The thermal conductivity of the composite has obtained the ratio of the total heat flux to the temperature gradient. Figure 3.4 shows the total heat flux of the varied inclusion of CB particles. The model is simulated for different volume percentages of CB filler and compared with the experimental result is shown in Table 3.2.

$$k = \frac{\text{Total heat flux}}{\text{Temperature gradient}}$$
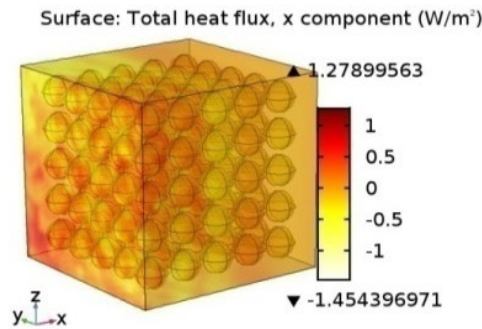
Figure 3.4 Total heat flux of the composites with CB particle inclusion

Table 3.2 Comparison of modeling and experimental results of TC

Composition	Numerical (FE) (3D) model (W/m.K)	Experimental (W/m.K)
PDMS	0.1499	0.1698
CB (05 Vol %)	0.1711	0.1868
CB (10 Vol %)	0.1831	0.1949
CB (15 Vol %)	0.1901	0.2077
CB (20 Vol %)	0.2025	0.2101
CB (25 Vol %)	0.2192	0.2285

3.3 Results of experimental testing of composites material

The properties of polymer composite for varied volume percentage of filler content is obtained by conducting physical, mechanical, thermal, and optical tests. These results are compared with empirically and numerically (FE). The results of density, mechanical, thermal, dielectric, and optical properties are discussed in detail.

3.3.1 Results of density

The density of pure PDMS and PDMS/ CB polymer composite is obtained experimentally. Whereas the empirical densities of polymer composite are calculated using the rule of a mixture shown in Table 3.3. The density of the polymer composite is increasing with the addition of carbon black (CB) from 5 Vol% to 15 Vol %. There is a disturbance in experimental data at 20 Vol% filler content. The reason could be an agglomeration effect for decreasing properties in 20 Vol% of the CB filler sample. It is challenging to achieve the 100% relative density provided by experimentally. Also, the elastic response of the PDMS tangles or agglomerates at higher CB contents increases the polymer composite void content.

Table 3.3 Density of composites samples

Composition	Empirical density (kg/m^3)	Measured density (kg/m^3)	Void content (%)
PDMS	1030	1033.40	0.33
CB (05 Vol %)	1054	1046.85	0.67
CB (10 Vol %)	1079	1057.50	1.99
CB (15 Vol %)	1105	1067.95	3.35
CB (20 Vol %)	1133	1062.00	6.26
CB (25 Vol %)	1162	1085.35	6.59

3.3.2 Results of mechanical properties

The mechanical properties of the PDMS/CB composites with 5 Vol % to 25, Vol% samples were prepared, and mechanical tests were carried out according to ASTM standard. The details of each composite property are discussed for tensile, compression, hardness, and tear tests.

87

3.3.2.1 Tensile testing

The effect of carbon black on the tensile strength of the plain PDMS was determined. The data averaged from each of the five samples for every filler concentrations is displayed in Figure 3.5 (a). The stress versus strain plot manifested a linear elastic region up to a strain value of 40%, as seen in Figure 3.5 (b). The data reveals that the maximum strain of the sample directly corresponded to the percentage filler of the CB composites.

The Young's modulus of the neat PDMS and PDMS/CB composite sample of the different percentage fillers, as determined in the linear elastic area using Hooke's law, is exhibited in Table 3.4. It also shows elongation at failure, failure load, and ultimate tensile strength of the composites. It is observed that the tensile strength of the composites increases with an increase in CB content. However, the ultimate tensile strength was highest for maximum loading of 15% CB. The Young's modulus of the tested sample was observed to be directly reliant on its filler concentration of CB.

| (a) | (b) |
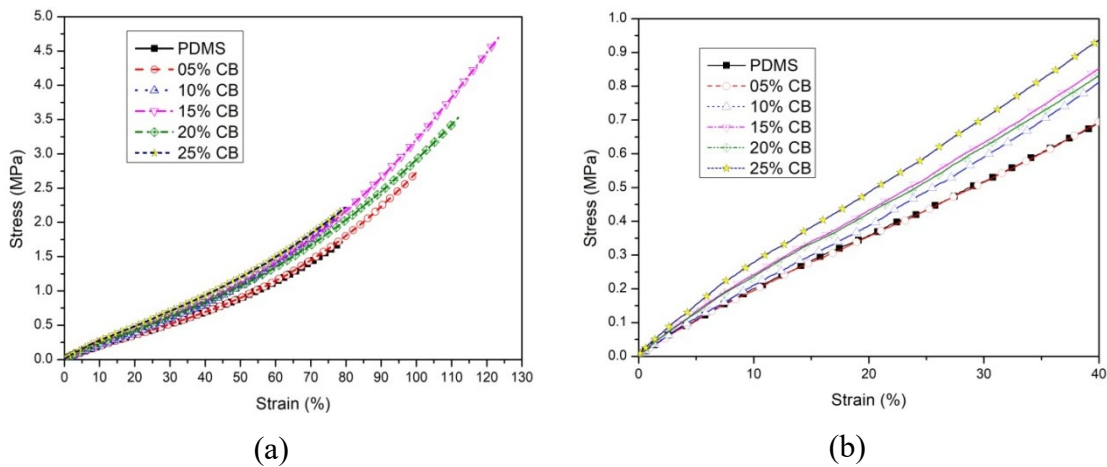
Figure 3.5 Average tensile stress/strain plot-(a) for PDMS and varied percentage filler of CB, and (b) up to 40 % strain for plain PDMS, and PDMS/CB composite
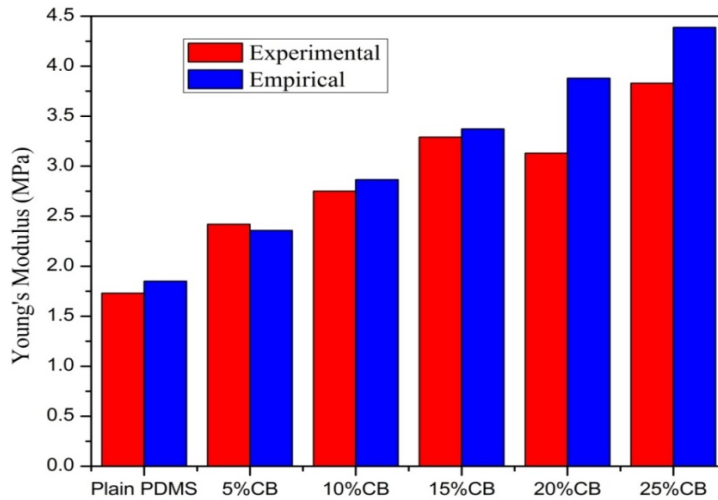
Figure 3.6 The comparison of Young's modulus with empirical results of PDMS/CB composite

It is noticed that Young's modulus of the PDMS 1.73MPa, and it increases to 3.83 MPa, it is almost double of the plain material with the incorporation of 25 Vol% of CB. Figure 3.6 shows a column graph of comparative results of the experimental and empirical values of Young's modulus of the composites. The average error in experimental results compared to empirical values are approximately 5%.

Table 3.4 Tensile test data of different volume percentages of carbon black

Material	Average Failure Load (N)	Elongation Break (mm)	Young's Modulus (MPa)	Ultimate Tensile Strength (MPa)
PDMS	34.900	065.80	1.73	1.86 ±0.397
CB (5 Vol %)	50.723	100.00	2.42	2.77 ±0.947
CB (10 Vol %)	63.695	108.80	2.75	3.69 ±1.268
CB (15 Vol %)	88.617	123.70	3.29	4.71 ±1.398
CB (20 Vol %)	69.735	112.10	3.13	3.53 ±0.724
CB (25 Vol %)	41.704	079.90	3.83	2.22 ±0.116

3.3.2.2 Compression testing

The stress/strain curve of the plain PDMS and PDMS/CB composites is shown in Figure 3.7 (a). The modulus is usually acquired in the linear elastic region up to strain estimations of around 40%, as shown in Figure 3.7 (b). The non-linear part before the failure of stress

shows almost the same compressive strength as of the different percentages of the CB filler. The compressive modulus of the sample increases linearly with an increase in the proportion of CB filler concentration, as shown in Figure 3.8. However, the ultimate compressive strength of the CB filler composites is almost equal to the plain PDMS, as presented in Table 3.5.

(a) (b)
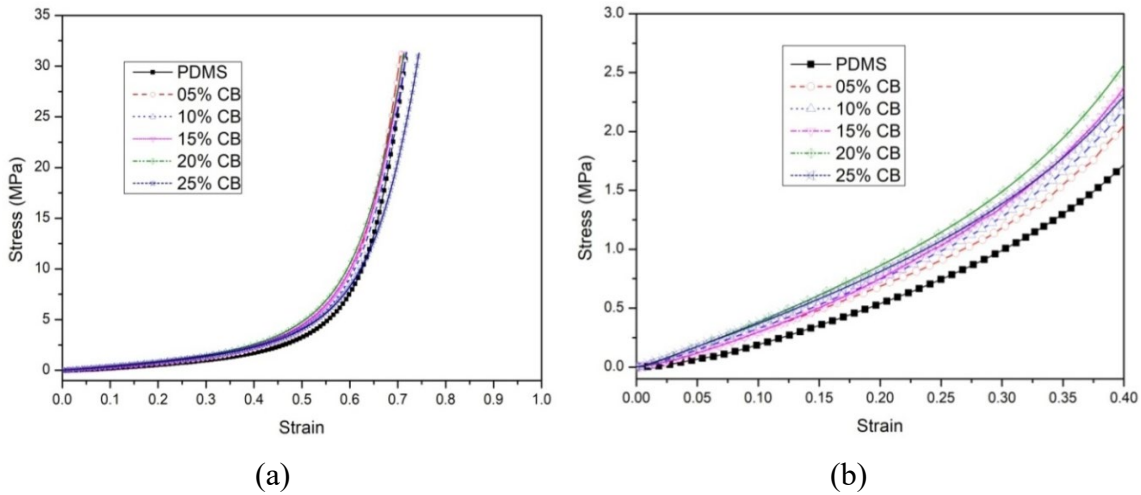
Figure 3.7 Average compression stress and strain curves of (a) plain PDMS and PDMS/CB composite, and (b) up to 40% strain for plain PDMS and PDMS/CB composites.
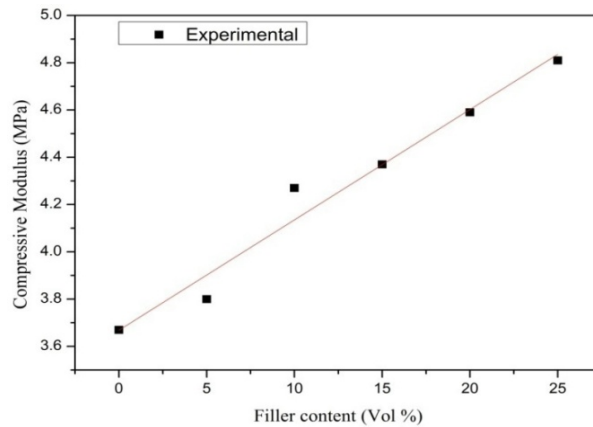
Figure 3.8 The relation between filler content and compressive modulus

Table 3.5 Compressive Properties of Plain PDMS and PDMS/CB Composite

Material	Compressive Modulus (MPa)	Ultimate Compressive Strength (MPa)
PDMS	3.67	31.28 $\pm$0.06
CB (5 Vol %)	3.80	31.36 $\pm$0.05
CB (10 Vol %)	4.27	31.28 $\pm$0.10
CB (15 Vol %)	4.37	31.23 $\pm$0.09
CB (20 Vol %)	4.59	31.28 $\pm$0.07
CB (25 Vol %)	4.81	31.27 $\pm$0.06

3.3.2.3 Hardness testing

The hardness of the fabricated sample was investigated as per the ASTM standard. Six sets of five samples each were tested for different percentages of the CB filler content. The hardness of each sample was recorded in eight distinctive positions, and the average data were considered. The hardness of the sample changed linearly with the increasing CB concentration, with an error bar of 3% to 5 % hardness is shown in Figure 3.9. There was a 30% enhancement in hardness compared with plain PDMS.
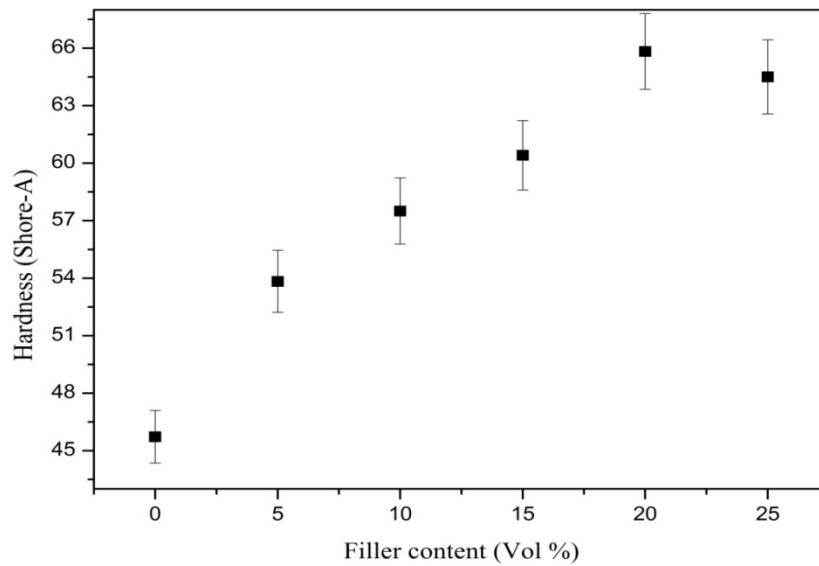
Figure 3.9 The average hardness of the PDMS/CB composite

3.3.2.4 Shear and bulk modulus

Also, properties such as shear modulus and bulk modulus for plain PDMS and PDMS/CB composite were evaluated. The determination of shear and bulk modulus depends on Young's modulus via the Poisson ratio, as mention in Equation 3.1 and Equation 3.2 (Kaw 2005).

$$G = \frac{E}{2(1+v)} \tag{3.1}$$

$$K = \frac{E}{3(1-2v)} \tag{3.2}$$

Where E is Young's modulus, v is the Poisson ratio, K is the bulk modulus, and G is the shear modulus.

The exact Poisson ratio of the PDMS and CB material is not available in the reports, whereas it ranges from 0.40-0.50 (Dogru et al. 2018, Liu et al. 2017, and Pritchard et al. 2013) and 0.23-0.35 (Ahmedzade and Geckil 2007, Holownia 1975). However, there are a few reports which recommend an estimated Poisson ratio of the PDMS and CB, which is employed to avoid the mistake in the computation of the modulus. The Poisson ratio of the PDMS/CB composites with different volume in percentage filler was resolved from the law of mixture. However, small changes in the Poisson ratio can result in a significant difference in shear and bulk modulus. Thus, in the present calculation, the commonly acceptable approximation values were used for the determination of the shear and bulk modulus, as presented in Table 3.6.

Table 3.6 Shear and bulk modulus of the plain PDMS and PDMS/CB composite

Material	Shear Modulus (MPa)	Bulk Modulus (MPa)
PDMS	0.56	5.46
CB (5 Vol %)	0.84	6.25
CB (10 Vol %)	0.96	5.86
CB (15 Vol %)	1.16	6.03
CB (20 Vol %)	1.12	5.06
CB (25 Vol %)	1.38	5.58

3.3.2.5 Tear strength

The knotty tear curves of the plain PDMS and PDMS/CB composite samples are shown in Figure 3.10 (a). It displays the relation between the applied load and the displacement, which traces the load through the tearing process and forms a saw-toothed curve consisting of peaks and valleys. For each sample, the increasing load produces a rapid tear rupture, which relieves the concentrated stress and increases the torn length. In the present analysis, only peak forces were considered. The sum of the peak force values divided by the number (more than 4 to 6) of peaks gives the average force. If the peak deviates, more than 20% is discarded and corrected for abnormal value. The thickness of every sample became measured at 3 locations throughout the period, and its mean value was recorded. The tear strength of the composites was calculated using Equation 2.11. The tear strength of the plain PDMS and CB content of the composites increased with increasing filler concentration. The tear strength of the plain PDMS also matched with the available literature, (Keller et al. 2007, and Huang et al. 2017). There was a sudden jump in tear strength at 25% filler content, which may be because the composite becomes harder. The inclusion of CB particles increases the plain PDMS tear strength by approximately 111%, as shown in Figure 3.10 (b).

(a)   (b)
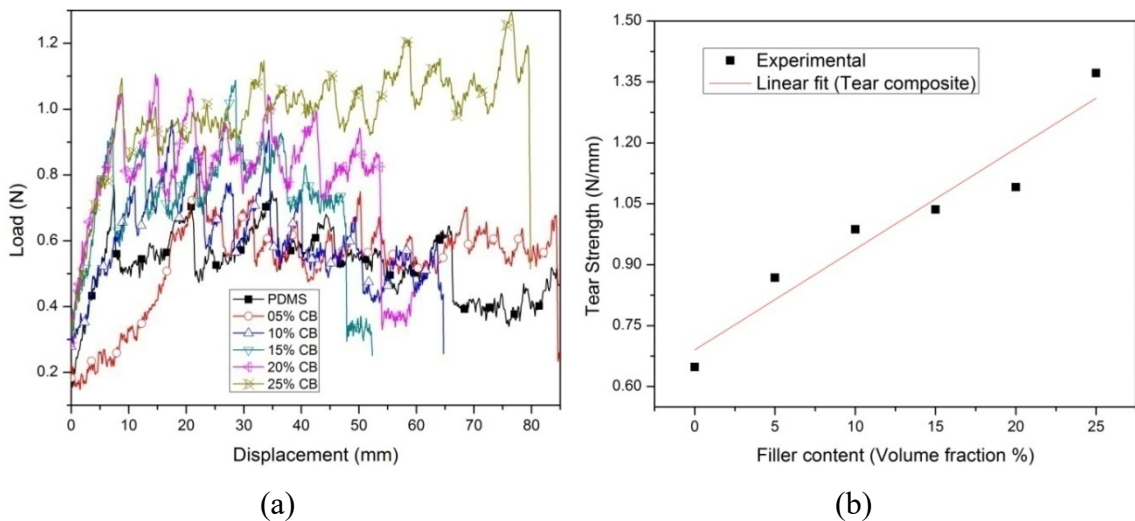
Figure 3.10 (a) Average tear test results of plain PDMS and PDMS/CB, and (b) Tear strength of the composites

3.3.3 Results of thermal properties

Thermal properties are more influencing properties in the development of the photo actuator. In the present study, the coefficient of thermal expansion, thermal conductivity, and specific heat capacity are experimentally obtained. The detailed results of the thermal properties are discussed.

3.3.3.1 Coefficient of thermal expansion

The CTE of polymer composite is obtained from the thermomechanical analyzer test. Figure 3.11 shows the CTE value of plain PDMS and PDMS/CB composite (5% to 25%) with error bars. The comparisons of the empirical, numerical (FE) modeling and experimental value of composites are shown in Table 3.7. It can be observed that there is a reduction in CTE with an increase in carbon black percentage in PDMS. There is a 17.25% decrease in CTE of composite with 25% CB when compared to plain PDMS.
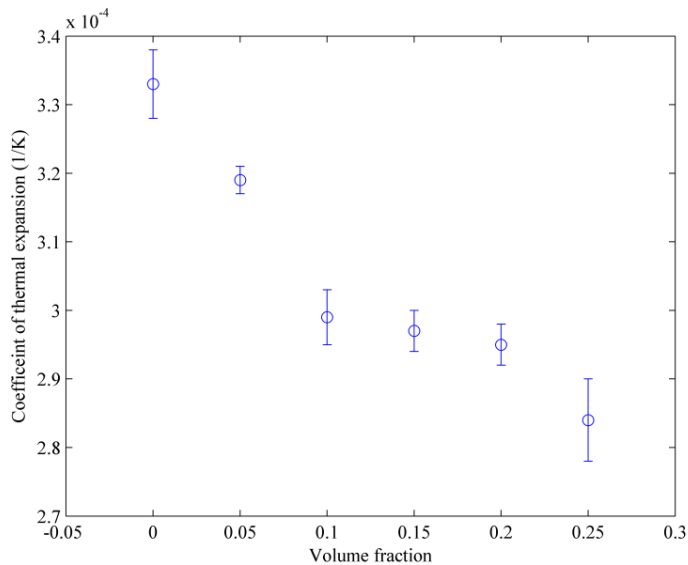
Figure 3.11 Coefficient of thermal expansion with a varied filler content of CB

Table 3.7 Comparison of empirical, FE-model and experimental results of CTE

Material composition	Empirical Model (ppm/K) (Chen model)	Numerical (FE) model (ppm/K)	Experimental Avg.　CTE (ppm/K)
PDMS	333	340	335
CB (5 Vol %)	324	328	319
CB (10 Vol %)	316	319	299
CB (15 Vol %)	308	308	297
CB (20 Vol %)	295	302	295
CB (25 Vol %)	284	296	284

3.3.3.2 Thermal conductivity

The thermal conductivity of the composite specimens are obtained experimentally with varied CB content is shown in Figure 3.12. Also, evaluated empirically and numerical (FE) modeling for the PDMS/Carbon black composites are presented in Table 3.8. It is noticed that with the addition of carbon black particles, the conductivity of the composite increases, and this increment is a function of the filler content. The composite with 25 Vol % filler is observed to have 29.6 % higher conductivity compared to plain PDMS.
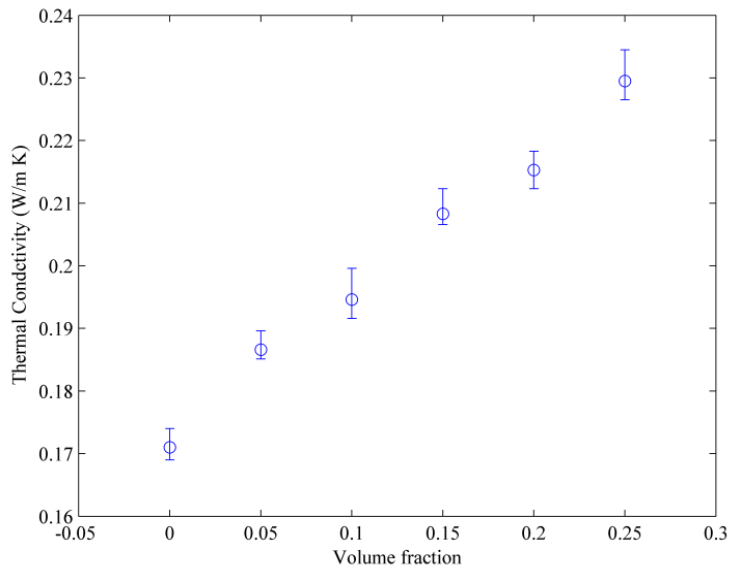
Figure 3.12 Thermal conductivity of varied filler content of CB

Table 3.8 Comparison of empirical, FE-model and experimental results of TC

Material composition	Empirical Model (W/m.K) (Lewis-Nielsen model)	Numerical (FE) model (W/m.K)	Experimental Avg. TC (W/m.K)
PDMS	0.1600	0.1499	0.1698
CB (5 Vol %)	0.1734	0.1711	0.1868
CB (10 Vol %)	0.1881	0.1831	0.1949
CB (15 Vol %)	0.2041	0.1901	0.2077
CB (20 Vol %)	0.2210	0.2025	0.2101
CB (25 Vol %)	0.2384	0.2192	0.2285

3.3.3.3 Specific heat capacity

The experimental and empirical values specific heat capacity (Cp) at constant pressure for the PDMS and its composites are shown in Table 3.9. It can be observed that the experimental and empirical values are matching with an average error of 19 %. Also, the specific heat capacity of the composites is decreasing with an increase in the filler content. Composite with 25 Vol % CB shows to have 27.8% less Cp compared to plain PDMS.

Table 3.9 Experimental and empirical results of the specific heat capacity

Material composition	Empirical Model (J/kg.K)	Experimental Avg. (Cp) (J/kg.K)
PDMS	1460	2034.95
CB (5 Vol %)	1383	1945.9
CB (10 Vol %)	1313.7	1780.3
CB (15 Vol %)	1251.1	1729.4
CB (20 Vol %)	1194.1	1503.1
CB (25 Vol %)	1147.16	1142.1

3.3.4 Results of optical properties

The carbon black composite absorbs IR light, which requires photo actuation to allow the sample temperature to rise. The absorbance and transmittance of the composite material of CB and PDMS have been discussed in detail. Also, the study of X-ray diffraction reveals the composite's crystal structure, which guides the path to heat absorbance.

3.3.4.1 Light absorbance

The analysis of light absorption is checked for plain PDMS and various percentages of CB composite material. For all these specimens, the measurement of the UV-Vis-NIR spectrophotometer was carried out in absorbance mode, and the absorbance value was plotted against the wavelength, as shown in Figure 3.13 (a). From the graph, it is visible that the absorbance value rises from 0 to about 1.05, with a variance of the CB from 5% to 25%. It shows increases in IR absorption with an increase in the volume percentage of CB, which helps for the sample temperature increase required for photo actuation (Li et al. 2013, Han et al. 2011).

The spectrum of absorption and transmittance may provide some insight into the samples ' optical behaviour. Figure 3.13(b) indicates the spectrum of transmittance for plain PDMS and PDMS/CB composite samples. It can be noticed that when carbon black is added, the transmittance is decreased. This type of behavior suggests the sample's crystalline existence and no dependence on the incident light's wavelength. The less light is transmitted through the material when more carbon black incorporated into the composite (Wang et al. 2019).
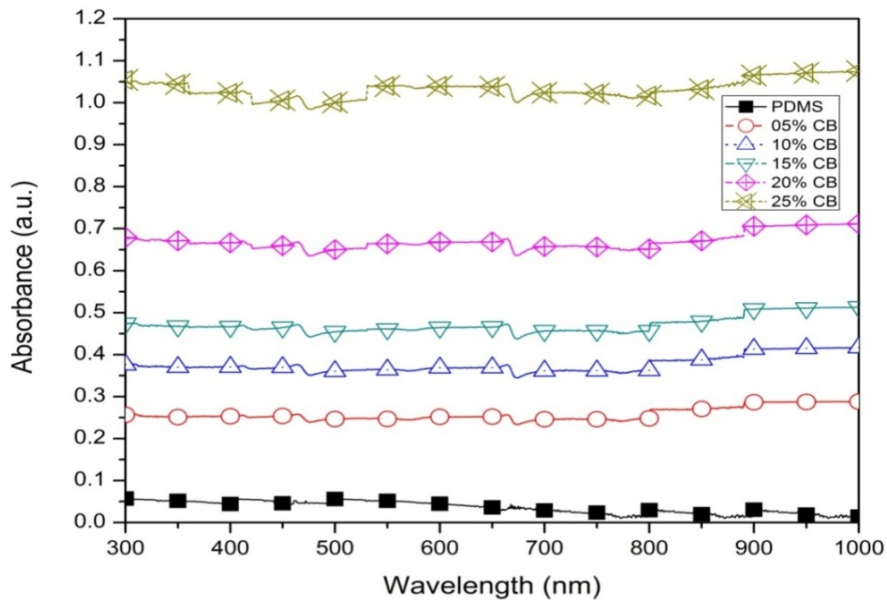
(a)
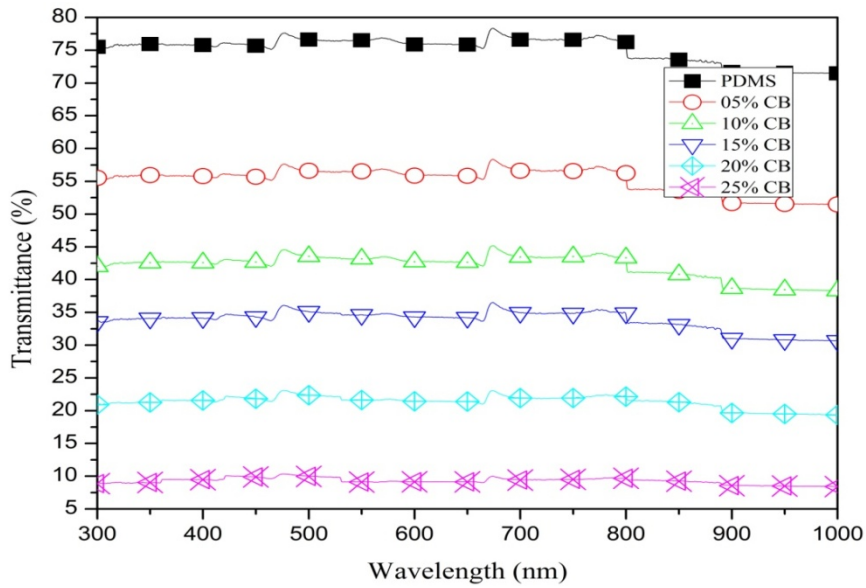
(b)

Figure 3.13 UV-Vis-NIR spectrophotometer results of PDMS and PDMS/CB composites
(a) Absorbance versus wavelength (b) Transmittance versus wavelength

3.3.4.2 X-ray diffraction

X-ray diffraction analysis shows the crystalline and amorphous phases of the material. The characteristic peaks of the PDMS were easily detected, with the most intense peak located at 12.5° corresponding to its tetragonal phases is shown in Figure 3.14 (a). The PDMS has wide diffraction peaks indicates that it was almost an amorphous polymer. Whereas the inclusion of carbon black, the diffraction pattern is observed for the composite, occurring at 17.5°, 22.5° and 26.5° for 25 Vol% of CB is a significant change in crystallinity, as shown in Figure 3.14 (b). The addition of the CB filler, the diffraction peaks were much sharper than the plain material, which also meant that the crystallinity of the composite was increased. The percentage of crystallinity for the sample is found to be more at 25 Vol % CB compared to plain PDMS (Pimentel-Domínguez et al. 2016).

The increase in crystallinity found in the composite sample can refer to an arrangement of the polymeric chains favoured by the CB acting as the crystalline zone yielding. The improvement in crystallinity would boost the composite material's thermal stability. The polymer's crystallinity would also influence the behaviour of thermal responsive deformation. Both the contraction speed and the degrees of the polymer layer were improved with the enhancement of the crystallization, which resulted in the composite beam becoming larger and more quickly deformed. Thus, the increased crystallinity of the polymer layer was also helpful in increasing the thermal responsiveness of the composite beams (Zhou et al. 2019).
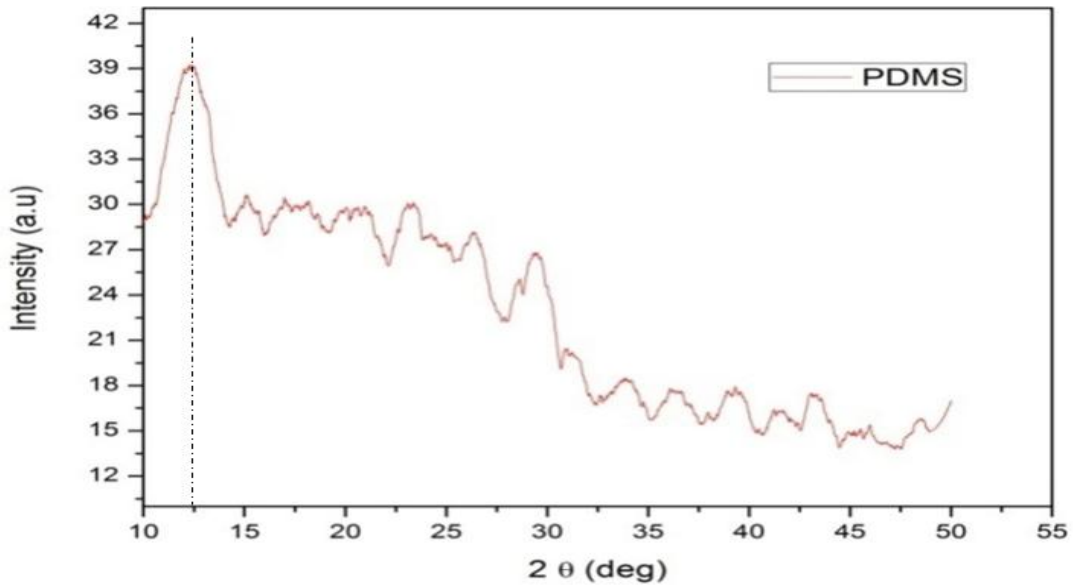
(a)
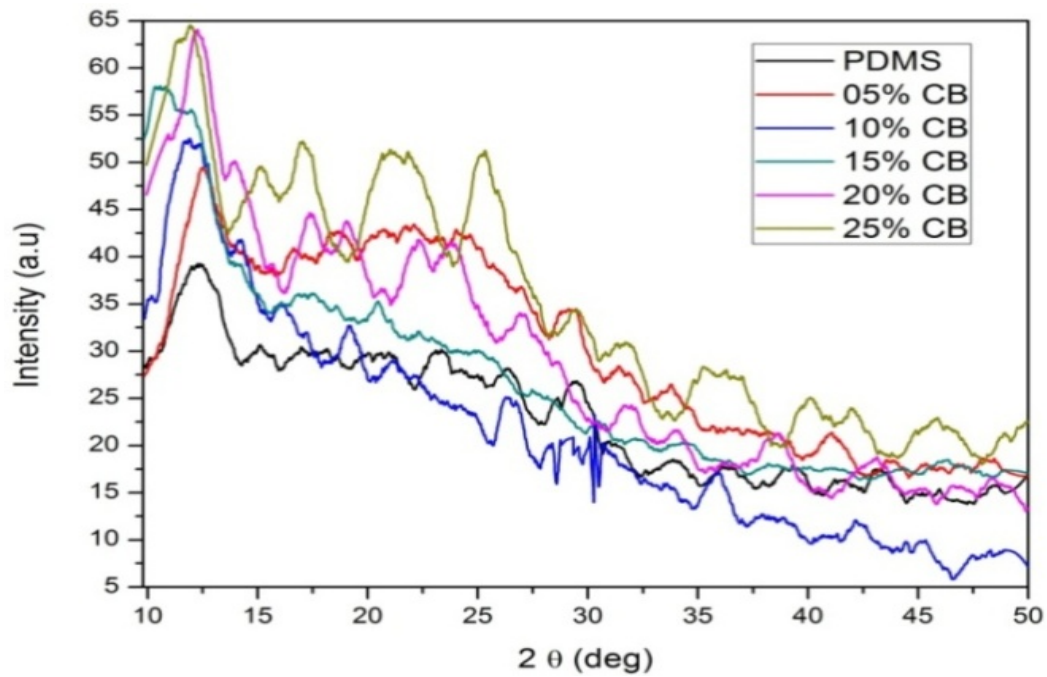
(b)

Figure 3.14 X-ray diffraction spectra are showing the crystallinity features of the (a) PDMS matrix material (b) PDMS/CB composites

3.3.5 Results of dielectric properties

The preliminary investigation of impedance measurement of pure PDMS and nanocomposite with 5, 15, and 25 Vol% of carbon black is accomplished. The real part of the complex dielectric permittivity (ε') of pure PDMS and different volume fraction of CB composite with sweep frequency is shown in Figure.3.15 (a). The impedance measurement gives the near detection range of the composite, and the noise with large scattering data is eliminated in the present work. The dielectric permittivity of the pure PDMS is predicted in the range of 2.58 to 2.70, which satisfies the values available from the literature (Du et al. 2011, Tripathy et al. 2018). The increase in dielectric value due to the rise in conductive reinforcement is observed. There is a surprising soar in dielectric consistent at higher filler awareness is also noticed. This could be more interaction/bonding of nanocomposite may occur.

The dielectric loss (ε'') for pure PDMS and PDMS/CB nanocomposite with varying filler concentrations at different frequencies is shown in Figure 3.15 (b). This plot shows the frequency at which the dipole polarization is completely out of phase for the applied electric field. It can be observed that the dielectric loss shifts towards higher frequency, where losses are minimum. Also, it does not form any peak in the frequency window of the measurement. Hence, there is a slight existence of dielectric loss with the different volume percentages of filler. However, the losses related to this relaxation are much smaller than the dielectric permittivity.
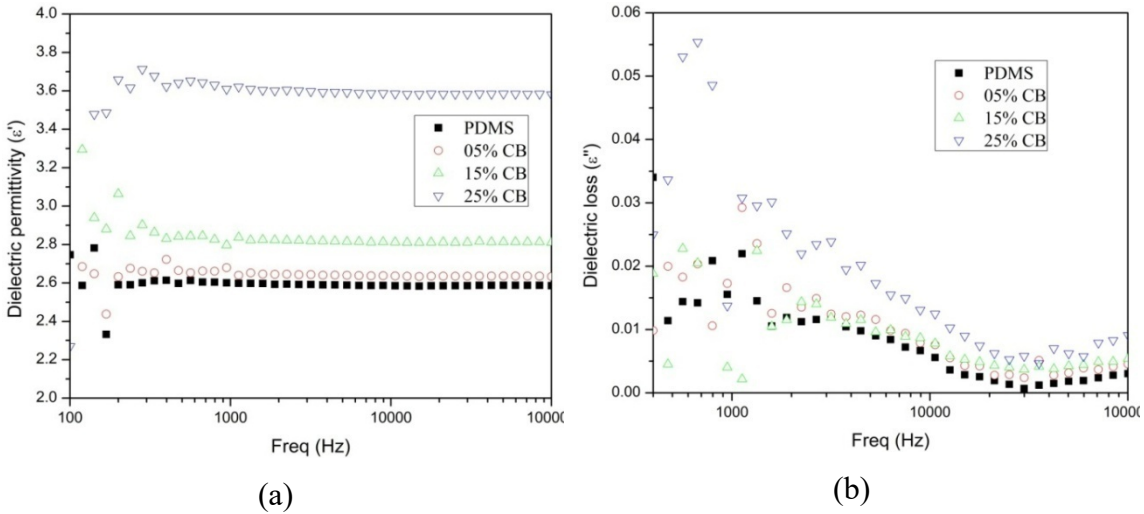
Figure 3.15 (a) The real part of dielectric permittivity, and (b) The imaginary part of the dielectric loss for a variation of volume fraction of CB at a frequency range of 100Hz to 100kHz

The AC conductivity of the composites material with varying concentrations of carbon black filler is shown in Figure 3.16 (a). It is calculated from the imaginary part of the complex permittivity (ε'') and angular frequency (ω). The AC conductivity of PDMS/CB composite is relatively low because the charge flows through the nanocomposite, which depends on the electric conductivity of the composites. The conductivity is almost independent of the change in frequency at a low frequencies range, and it starts to increase approximately linear at a higher frequency range. This may occur due to the transition of the insulation state to the conduction state. Also, it follows the power law, which is seen in the literature on these types of composites (Pradhan et al. 2008, Dang et al. 2004). The power-law may occur due to charge transport in the conductive nanocomposite, which leads to an increase in mobility carriers.

The point in which conductivity starts increasing is represented as a critical frequency. The critical frequency which follows the power law is described as $\sigma_{ac} \sim \omega^k$ with $0 \leq k \leq 1$. Figure 3.16 (b) shows the logarithmic plot of the AC conductivity versus the angular frequency, which can be used to obtain the critical exponent (k). The exponent value of plain PDMS and PDMS/CB nanocomposites are in the range of 0.48 to 0.57. According to

102

the power law, the exponent varying between 0 and 1 implies that the conduction mechanism is frequency-dependent. The conductivity of these types of polymer nanocomposites follows the same as other composite systems (Pradhan et al. 2008).

(a)   (b)
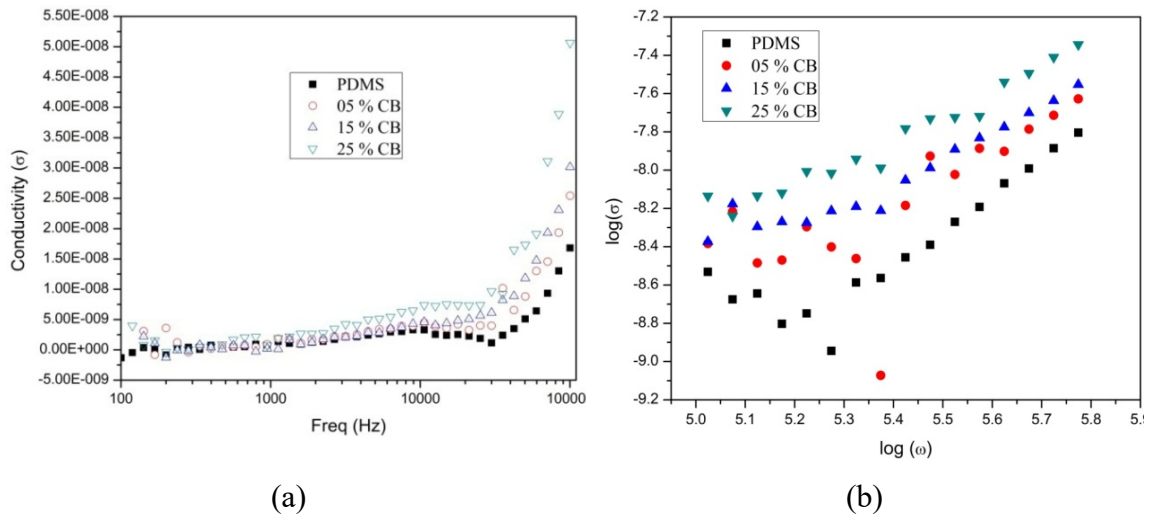
Figure 3.16 The conductivity of polymer composite with (a) Varying frequency and (b) Power-law with angular frequency

3.4 Results of microstructure

The scanning electron microscopy technique is employed to observe the morphology and bonding structure of the pure PDMS and PDMS/CB composite. The tensile sample was used for microstructure analysis. The part of the sample taken from the breaking region of the composite and gold plated prior to the microscopy observation.

3.4.1 SEM analysis

The filler material makes either large irregular or smaller aggregate as the concentration of the reinforcement is increased. These aggregates are derived from the process of manufacturing, and it can be examined using a scanning electron microscope (SEM). The SEM images were taken from the fractured surfaces of the plain PDMS and PDMS/CB composites. From the SEM analysis, the distribution of the particles, mode of fracture, and interfacial bonding on the composite can be observed, as shown in Figure 3.17. The plain

PDMS material is a smooth surface at a 50 μm scale (Figure 3.17 (a). As the percentage of filler increased in the matrix, the tensile strength of the composites enhanced until 15% reinforcement, the increment of carbon content in PDMS could be seen. Also, the strength obtained in the case of 15 % carbon black superior may be due to the proper interfacial bonding between the CB and the PDMS, as shown in Figure 3.17 (d) compared to higher filler content. After that, particle distribution and bonding are not so uniform, which may lead to a reduction in the strength of the composite. Improper bonding of higher percentage composite can be seen in Figure 3.17 (e) and Figure 3.17 (f). Also, the agglomeration of the particles occurs on further addition of reinforcement, which may cause a reduction in the mechanical properties. Further, observation showed that the river band pattern of failure occurred, leading to ductile dominated failure.
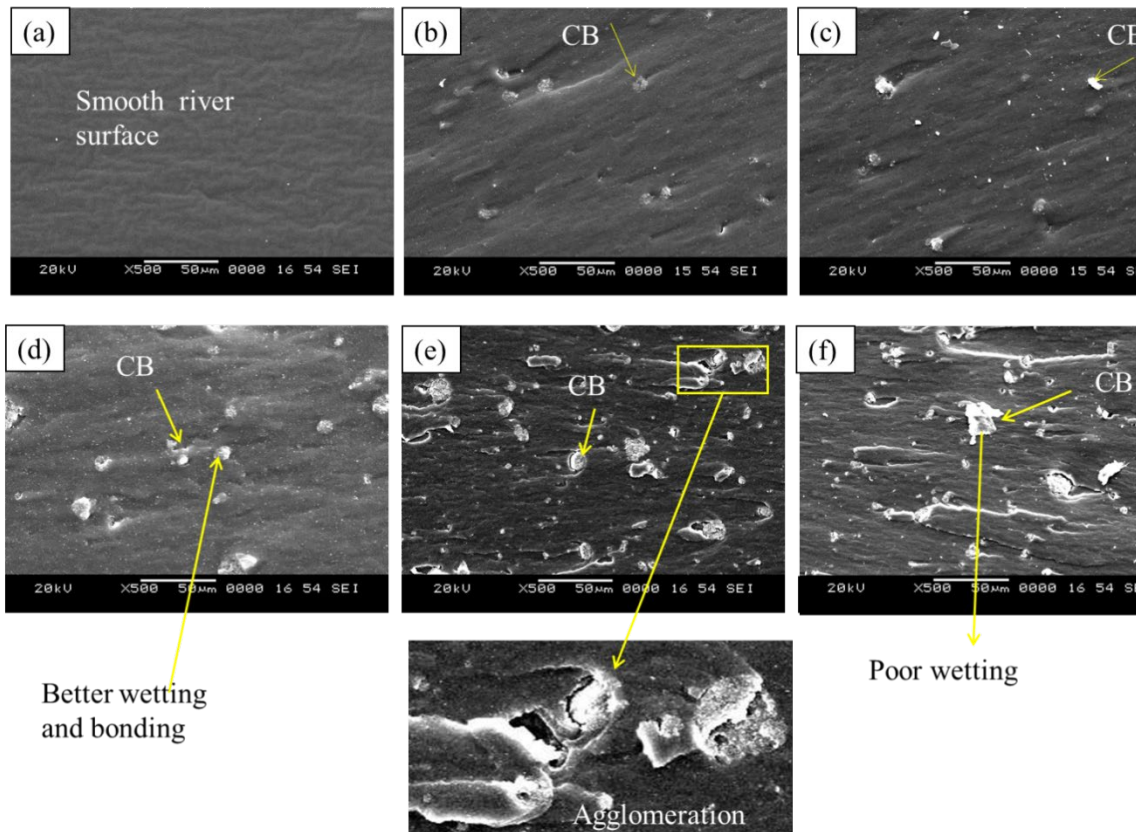
Figure 3.17 SEM images of composite- a) Plain PDMS, b) 5 %CB, c) 10 %CB, d) 15 %CB, e) 20 %CB, and f) 25 %CB

3.5 Results of actuator model

The actuation of composite material evaluated using analytical and numerical methods. In the analytical study, the equation is used to determine the deflection of the single and bilayer beams. The analytical result is compared with the numerical model by varying the thickness and volume percentage of composite material. It also highlighted the comparison results of the single and bilayer actuator beam.

3.5.1 Results of single layer modeling

The deflection of the single layer model is developed as the mentioned steps in the modeling section. The model is analysed for 5 to 25 Vol% CB and thickness ranging from 1mm to 5mm. Figure 3.18 (a) and Figure 3.18 (b) shows the numerical (FE) model of deflection for the single layer of 5 Vol % and 25 Vol % CB content at a fixed thickness of 3mm. As the percentage of the CB increases, the deflection of the single layer decreases. The reason could be, increase in the CB content stiffens or hardens the composite beam. Also, it reduces the CTE of the composite. In the same way, the various thickness of 1mm and 3mm at fixed CB content (15 Vol %) for single layer appears in Figure 3.19 (a) and Figure 3.19 (b). It shows that as thickness increases, deflection is reduced. This proves the phenomenon that, increase in temperature covers a thin layer immediately rather than the thick layer.

(a)   (b)

Figure 3.18 Deflection of a single layer model for varied volume percentage of CB (a) 5 Vol% (b) 25 Vol%

(a)   (b)

Figure 3.19 Deflection of a single layer model for the varied thickness of the layers (a) 1mm (b) 5mm

Figure 3.20 (a) and Figure 3.20 (b) shows the deflection of the single layer for different Vol % CB content and various thicknesses with a change in temperature, respectively. In both cases, as the temperature increases, the deflection of the single layer also increases. There is a 71.6 % reduction in deflection of the single layer as the CB content change from 5 Vol % to 25 Vol %. Also, as the thickness of the single layer change from 5 mm to 1 mm, the deflection result increase to 81.91 %.

(a)   (b)
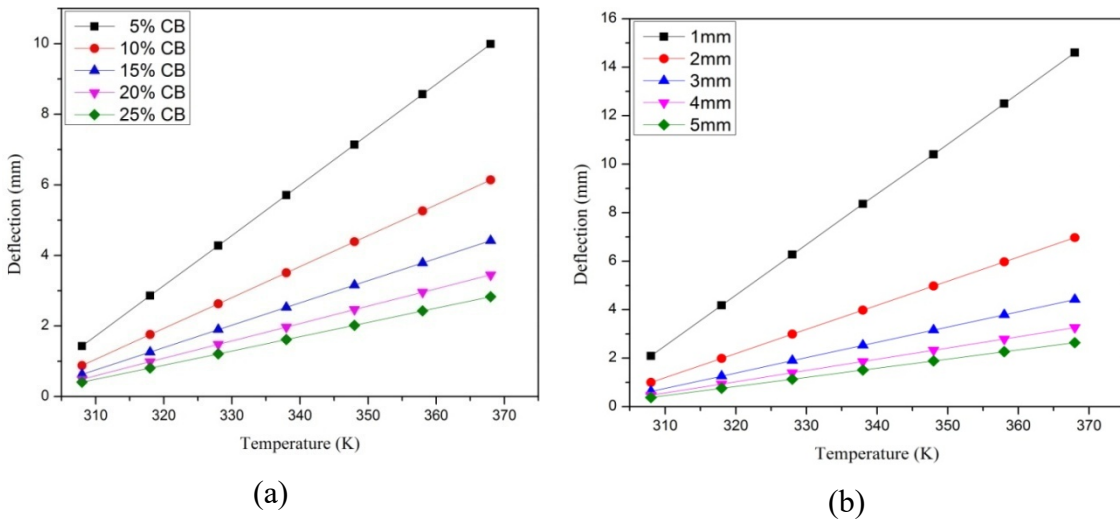
Figure 3.20 Deflection of the single layer beam with a change in (a) Vol% of CB content, (b) Thicknesses of the beam for temperature change

106

The numerical (FE) model is compared with analytical results for varied filler content of CB, and an increase in thickness is shown in Figure 3.21(a) and Figure 3.21(b). The comparative prediction shows that both the analysis is very near to each other. Hence, this proves that the assumptions were made for analysis of numerical models, and analyses are appropriate. It is noticed that results obtained from the analytical method are higher than that of numerical (FE) modeling. This may be due to; few assumptions that are either neglected or unable to set during analysis.

(a)   (b)
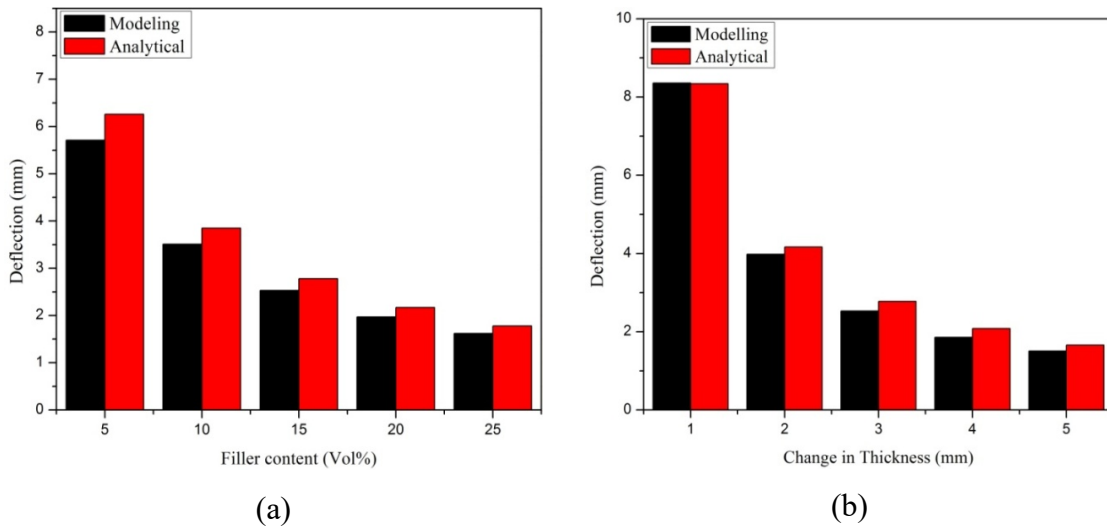
Figure 3.21 Comparison of single layer models with a change in (a) Vol % CB content, and (b) Thickness of the beam

3.5.2 Results of bilayer modeling

The numerical (FE) modeling of the bilayer is carried out for varied Vol % of CB and different thicknesses. Figure 3.22 (a) and Figure 3.22 (b) shows the fixed thickness of the bilayer 3 mm (PDMS=1.5mm and PDMS/CB=1.5mm) with different CB content (5 Vol % and 25 Vol %). The deflection of the bilayer increases with increases in the percentage of CB content. This enhancement may be due to, stacking of dissimilar coefficient of thermal expansion material.

Similarly, the varied thickness of the bilayer (1mm and 5mm) with the arrest of 15 Vol % CB is shown in Figure 3.23 (a) and Figure 3.23 (b). As the thickness of the bilayer

increases, a reduction in deflection is observed. This is a similar phenomenon like a single layer, but a more significant deflection compared to a single layer is noticed.
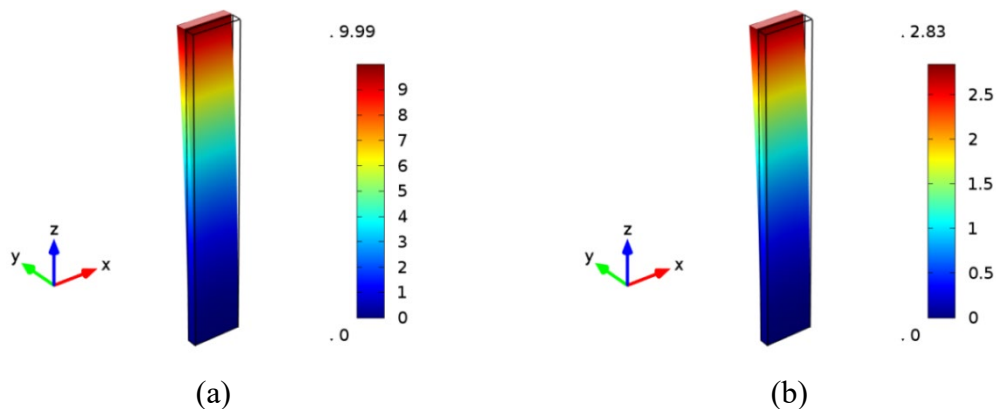

(a) (b)

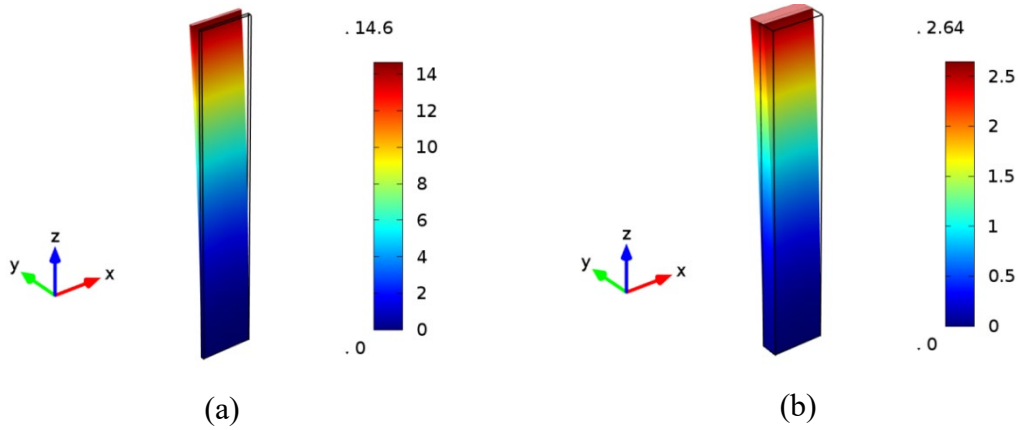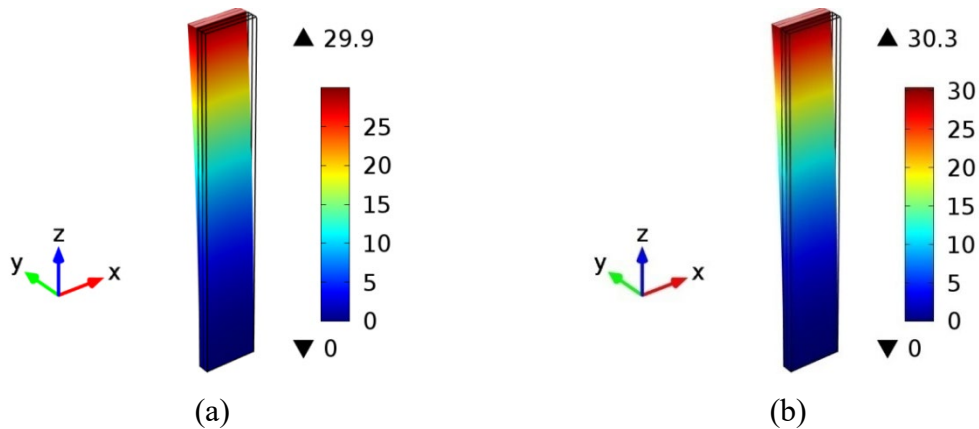Figure 3.22 Deflection of bilayer model for varied volume percentage of CB (a) 5 Vol% (b) 25 Vol%

(a) (b)
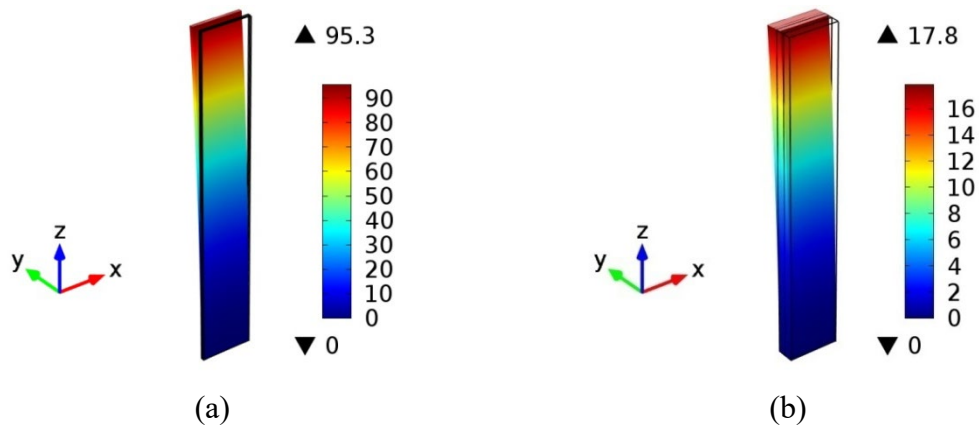
Figure 3.23 Deflection of bilayer model for the varied thickness of the layers (a) 1mm (b) 5mm

Figure 3.24(a) and Figure 3.24(b) shows the deflection of a bilayer beam for different percentage of CB and thickness. Similar to the behavior of the single layer beams, the deflection of the bilayer beams increases with temperature input. The plot shows that a 1.32 % increase in deflection as CB content increases from 5 Vol% to 25 Vol%. Likewise, as the thickness changes from 1mm to 5mm, the deflection is reduced to 81.32%.

108

(a)   (b)
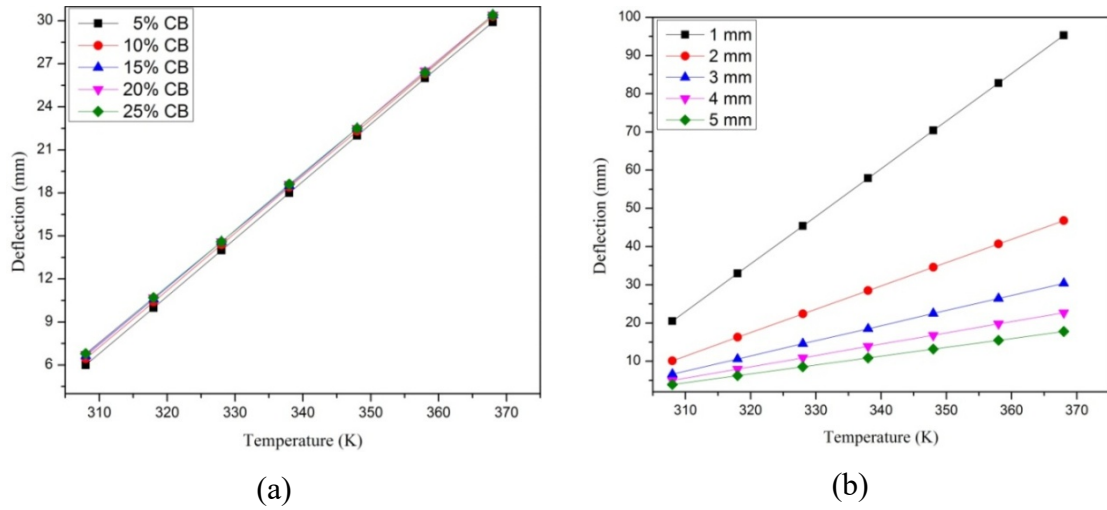
Figure 3.24 Deflection of the bilayer beam with a change in (a) Volume percentage of
CB content, (b) Thickness of the beam concerning temperature change

The analytical and numerical (FE) analysis of bilayer deflection with different filler content
and thickness change are shown in Figure 3.25 (a) and Figure 3.25 (b). It proved that
analytical results are closely following the numerical (FE) model in both cases (change in
filler content and thickness). It is also observed that modeling results are lower than the
analytical results. Maybe due to assumption and boundary conditions were made, need to
be considered carefully. Also, Even it may same as explained previously.

(a)   (b)
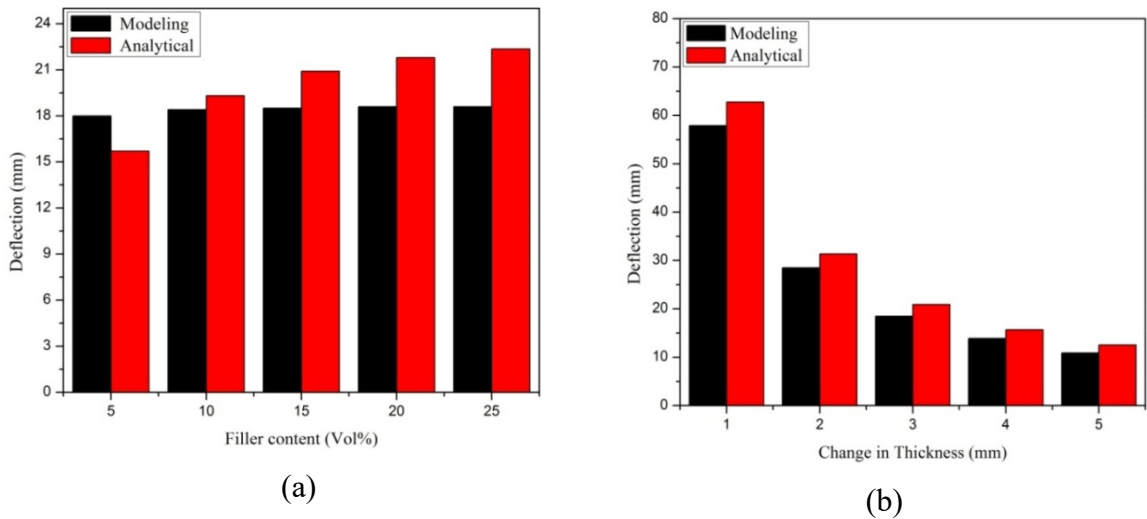
Figure 3.25 Comparison of Bilayer models with a change in (a) Vol% CB content (b)
Thickness of the beam

3.5.3 Comparison results of single and bilayer beam

The further study continues for comparison of single layer and bilayer thermal actuators. Figure 3.26 (a), Figure 3.26 (b) and Figure 3.26 (c) show the deflection for varying filler content, thickness, and temperature of the single layer and bilayer beam.

(a)

(b)

(c)
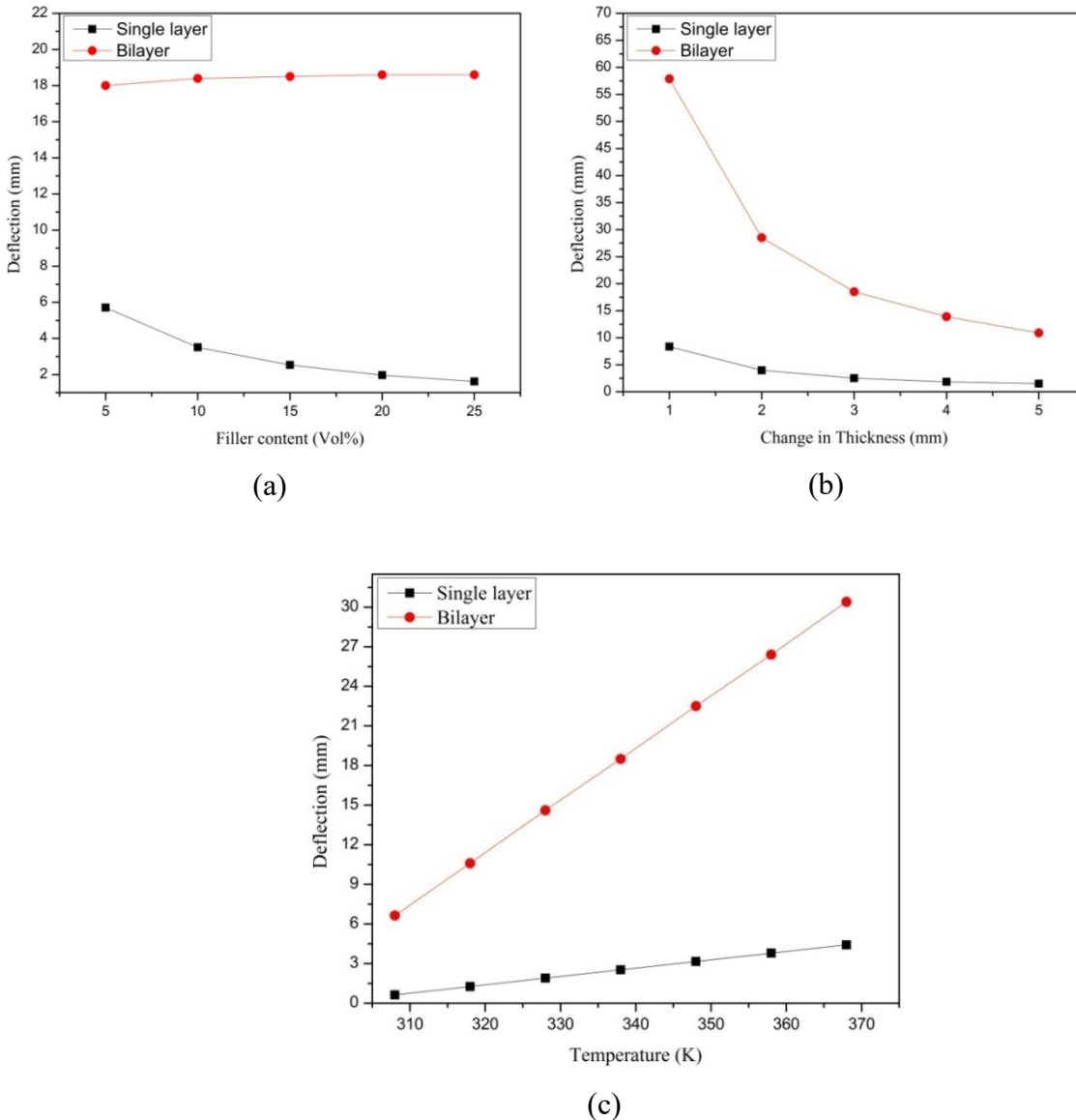
Figure 3.26 Comparison of single layer and bilayer with a change in (a) Vol % CB content (b) Thickness of the beam (c) Temperature of the surface

As the percentage of filler content increases, a 91.29 % increment in bilayer deflection is observed when compared to a single layer. For particular thickness, the bilayer beam deflects higher than the single layer. Also, it noted that the thickness of the single layer and bilayer influence more compared to the percentage of the CB content. The deflection of the single layer and bilayer beam increases linearly with a temperature input range of 308 K to 368 K. In the same contrast, the bilayer beam deflection is 85.46 % more than the single layer.

3.6 Experimentation on a photo actuator

The research work aims to carry out experimental studies; therefore, the single and bilayer beam studies have been carried out. The light source is applied to the prepared layered specimens, and the deflection of the actuator is observed. The single-layer composite beam is tested for the cyclic mode of light stimulation, and the conceptual prototype model is also examined. The description of the experimental test results is addressed in the following section.

3.6.1 Fabricated single and bilayer actuator

The plain PDMS and different percentage of carbon black incorporated PDMS samples are prepared for a single layer, and bilayer is shown in Figure 3.27 and Figure 3.28. This sample was used for testing of the photo actuator.
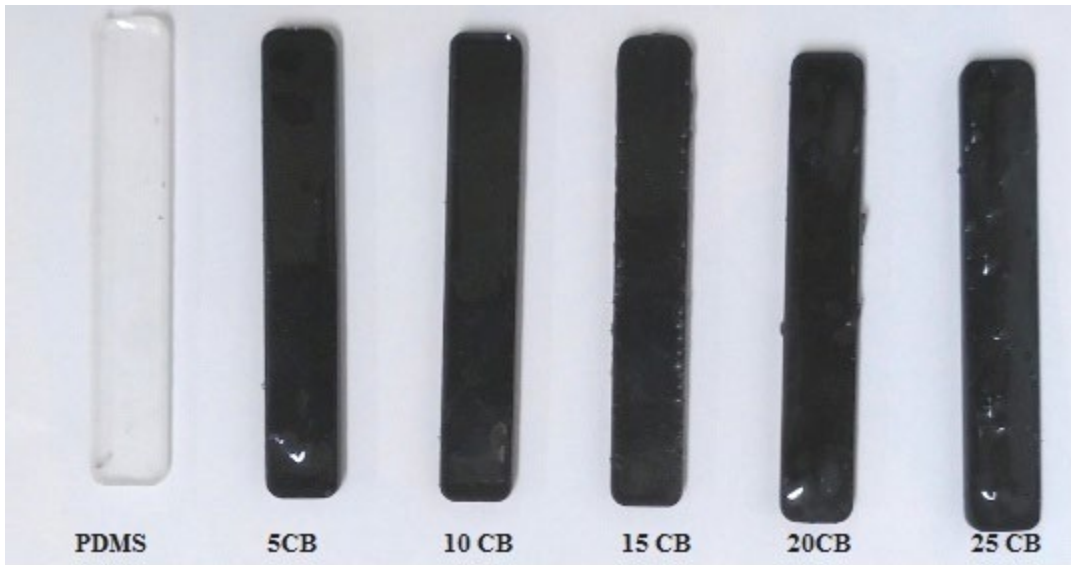
Figure 3.27 Prepared single layer samples of plain PDMS and PDMS/CB composites
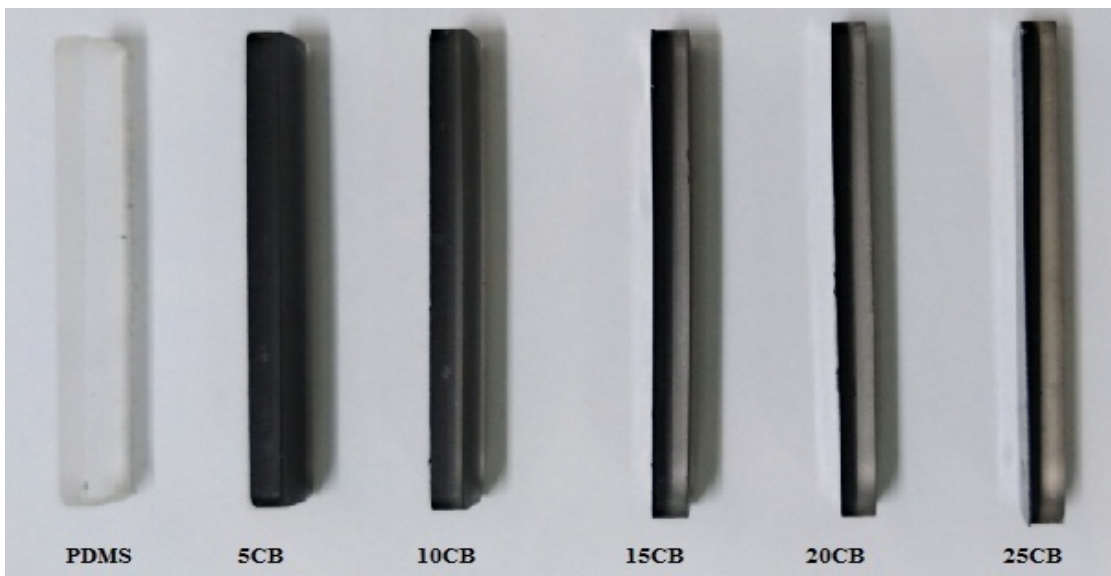
Figure 3.28 Prepared bilayer samples of plain PDMS and PDMS/CB composites

3.6.2 Results of the single layer actuator

The single-layer sample of a composite beam is fixed at one end of the sample holder, and a light source of 1000 W is focused. The deflection of a different volume percentage of CB is shown in Figure 3.29. The result was noted for a 2 mm thick sample at a temperature of

45 °C to 50 °C. Table 3.10 shows the summary of the deflection with varied percentage filler and compared with numerical (FE) modeling results of the composite beam.

| 5 Vol% | 10 Vol% | 15 Vol% | 20 Vol% | 25 Vol% |
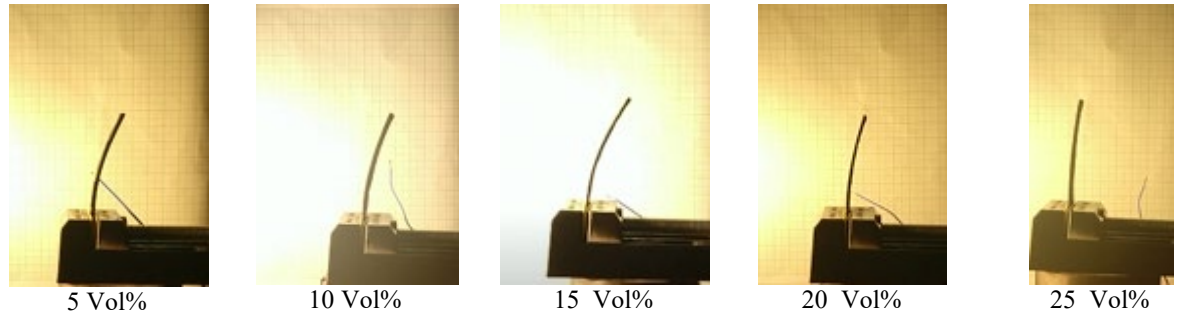
Figure 3.29 Deflection of the single layer   PDMS/CB composite beam with a different volume percentage of the beam

The experimental and Numerical (FE) modeling results were compared. It shows that for varied volume percentage of carbon black and PDMS composite beam is much closer to each. Thus, the proposed material can be used for photo actuation.

Table 3.10 Single layer deflection results of the varied volume percentage of CB

Single layer Composite beam	Numerical (FE) modeling Deflection (mm)	Experimental Deflection (mm)
CB (5 Vol %)	11	12-14
CB (10 Vol %)	09	09-11
CB (15 Vol %)	06	07-09
CB (20 Vol %)	03	04-06
CB (25 Vol %)	02	02-03

3.6.3 Results of the bilayer actuator

A similar test is conducted for the bilayer composite photo actuator. The bilayer of 3 mm (1.5 mm plain PDMS and 1.5 mm PDMS/CB composite) composite beam is prepared, tested under IR light source, and observed the deflection of the beam. The test results of the bilayer deflection of the composite beam shown in Figure 3.30. The deflection results

compared with numerical (FE) and experimental, it indicates almost near to each other. As a result, the developed composite beam provides the potential for the implementation of different stimulus-based actuators.

| 5 Vol% | 10 Vol% |
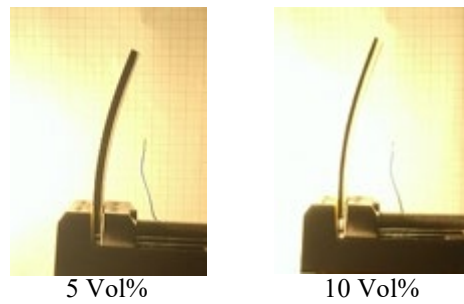
Figure 3.30 Deflection of the bilayer composite beam with a varied volume percentage of CB beam

Table 3.11 Shows the bilayer deflection of the varied percentage of CB

Bilayer Composite beam	Numerical (FE) modeling Deflection (mm)	Experimental Deflection (mm)
CB (5 Vol %)	18	17-18
CB (10 Vol %)	18.4	15 -17
CB (15 Vol %)	18.5	16-19
CB (20 Vol %)	18.6	16-17
CB (25 Vol %)	18.6	16-18

3.6.4 Results of cyclic modes of a photo actuator

A laser displacement sensor measures the deflection of the beam by fixing one end of the beam other end is free to move. The photography image of the experimental setup for composite beam deflection measurement is shown in Figure 3.31.
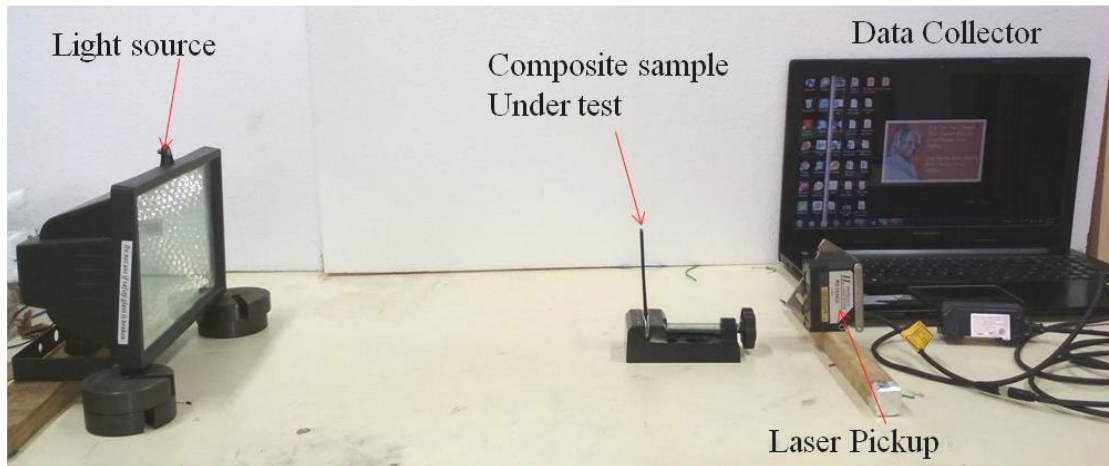
Figure 3.31 Photography image of the experimental setup for composite beam deflection measurement

In this developed composite beam, IR light energy is absorbed by the polymer composite layer and readily converted to heat. Due to heat in the composite material, try to bend or deflect away from the source. The main focus of this work is to evaluate the effect and performance of the fabricated composite beam on the photothermal actuation.

Figure 3.32 shows the experimental and analytical value of the PDMS/CB composite sample for a single cycle. Heat is generated in the membrane by direct irradiation with an IR lamp. The resulting output beam located at 180 mm away from the source input. The experimental values of the deflection were measured using a laser displacement sensor. The period of light ON composite beam bends away from the source and period of light-OFF time back to the original position. As it is observed from experimental data, the composite beam approximately deflects 9 mm of 16-sec duration and takes a long time to settle back. It also predicted that there is a close agreement between the experimental measurement and analytical value at low optical power and confirms that deflection is proration to the intensity of light.
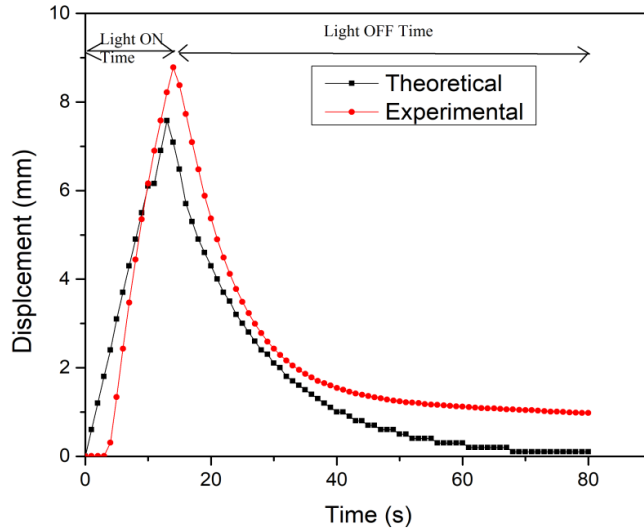
Figure 3.32 Deflection of CB/PDMS composite beam for one cycle

Figure 3.33 shows that steps wear repeated for two cycles and experimentally observed. The photothermal actuation takes immediately as a light source is switched ON. Two cycles of light source switched ON/OFF and found that switching ON time is 16 sec and OFF time 150 sec also repeats.
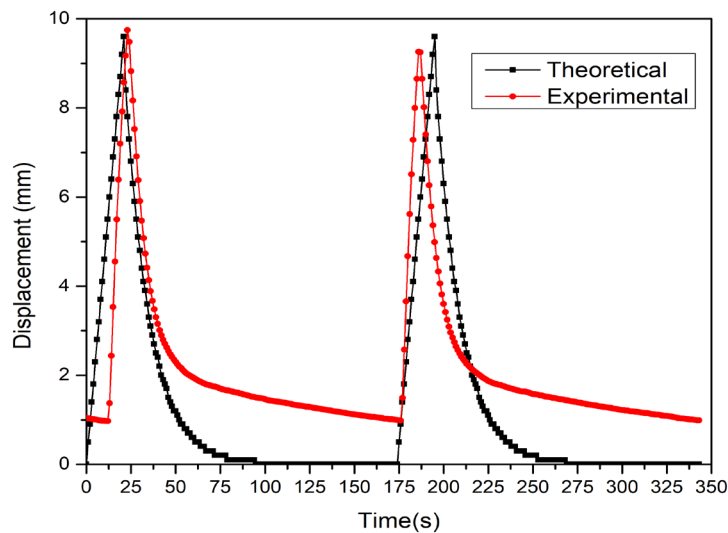
Figure 3.33 Deflection of CB/PDMS composite beam for two-cycle

116

Repeatable photomechanical bending: Deflection of PDMS/CB composite beam repeatability is the key indicator and plays an essential role in evaluating the performance of the photothermal actuator. The multi-cycle irradiation of light source measured the photothermal deflections. Bending repeatability of the proposed composite beam is observed both experimentally and analytically.
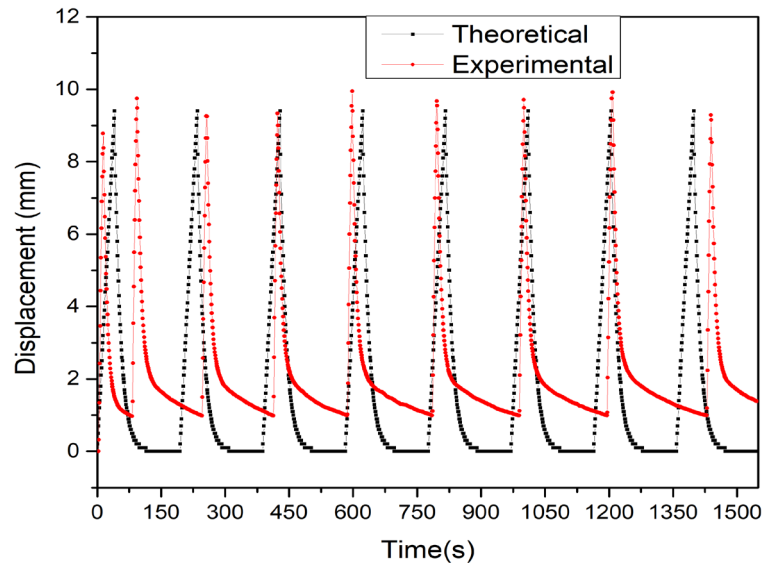
Figure 3.34 Repeatable photo thermal deflection of PDMS/CB composite beam

Figure 3.34 shows that our proposed polymer composite actuator displays the repeatable photothermal deflection. Thus, the composite is qualified with excellent repeatability and promising for the photothermal actuator applications.

3.7 Experimentation on a proposed prototype

At the end of the present study, a prototype of a photoactive switch and a heliotropic tracking mechanism was built. In a laboratory environment, an artificial IR source of 1000 W was used as a light source for illuminating the beam as a substitute for natural sunlight. The composite beam is used for one of the applications that have been successfully tested by constructing a prototype model.

3.7.1 Results of a proposed prototype of a photoswitch

Figure 3.35 shows the experimental test rig up for the proposed photo switch before and after switching ON and OFF of the IR light source. The two parts of the composite sample arranged, as shown in Figure 3.35 (a). The IR light source is used to trigger the load or output. The circuit is connected with an LED bulb through the battery, and the composite switch has closed the circuit. The proposed prototype is successfully tested, and this could be used for photothermal switching applications.

(a)   (b)
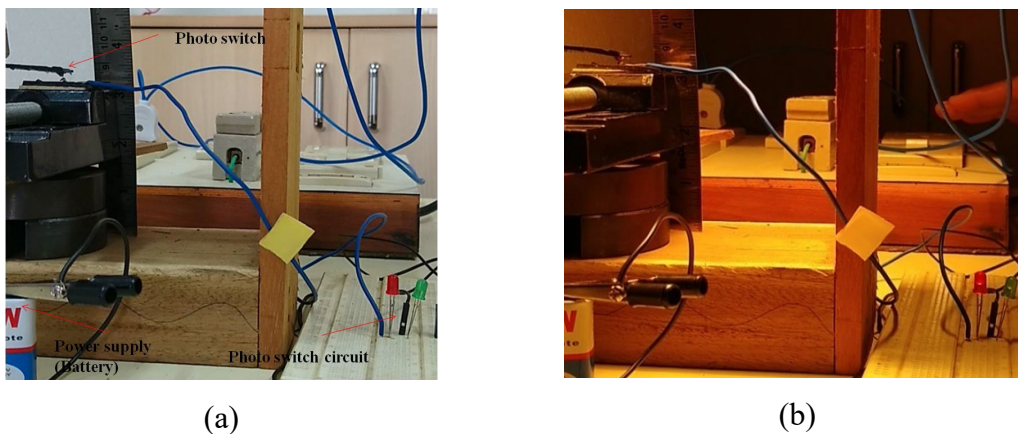
Figure 3.35 Experimental prototype testing of the photoswitch (a) Before, and (b) After the lighting up of the IR light source

3.7.2 Results of a proposed prototype of a heliotropic system

A small solar cell and PDMS/CB composite beams were used for prototype testing. The sun tracking mechanism is constructed to enable the solar receptor to track the sun for 12: 00-hour angle (roughly from 6 am to 6 pm) and tilting the solar cell perpendicular to the equatorial plane. The solar receptor and composite beam arrangement are mounted on the same plane such that the composite beam should tilt the solar cell is shown in Figure 3.36 (a). When the light source is on, the solar cell is tilted towards the light source due to the heat absorbed by the composite beam, as shown in Figure 3.36 (b).

The bilayer beam is used as a tilting beam, due to the difference in the thermal expansion of the material, the beam bends towards the light source. The solar tracking mechanism has been tested successfully, which could be suggested for one of the composite actuators.

| (a) | (b) |
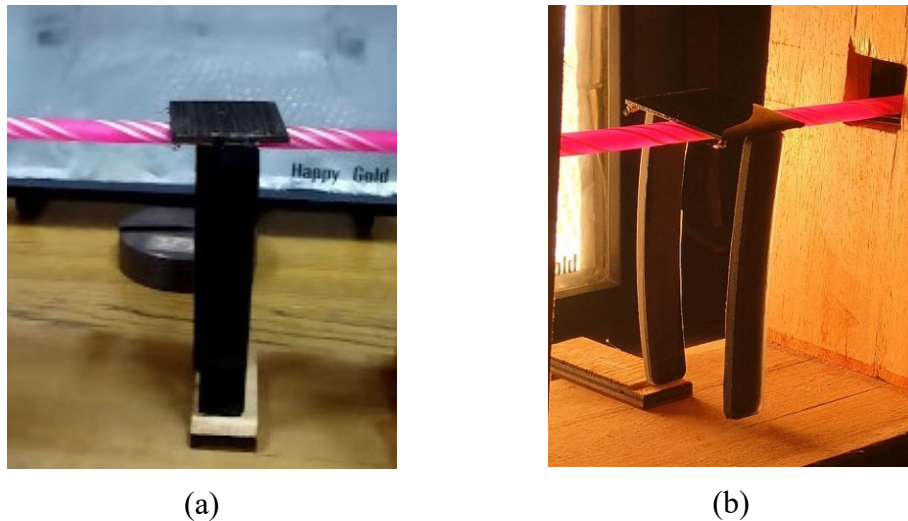
Figure 3.36 Experimental setup for a heliotropic tracking mechanism

The proposed photo actuator concept was successfully tested using polymer composite material. The actuation mechanism is not limited to a specific area; it can be used in various applications of a soft robot, energy harvesting, grippers, as well as where composite-based actuator requires large deformation capacities. The result was inspired by the development of an actuator device with different stimuli and composite content.

Summary of results and discussion

From the results and discuss several essential points that have emerged on the bases of composite material. The empirical, numerical, and analytical modeling results were discussed in detail, and all results showed the positive signs for the development of the actuator. The validation of composite material properties was confirmed with the different empirical as well as a numerical model result. The PDMS/CB composites with different volume percentages were prepared. With regards to the PDMS/CB composite, their

physical, mechanical, thermal, optical, dielectric, and microstructure behaviour discussed in brief. The analytical results on a single layer and bilayer actuation give proof concept for the development of composite material. Numerical results were compared with both analytical and experimental a result, which shows the photo actuator performance.

The investigation clearly shows some improvements in the material with varied content of carbon black composite. The experimental results of single and bilayer composite tested and compared with numerical results. Finally, the proposed prototypes test was conducted successfully and observed the deflection, which gives a positive sign in the developed photo actuator.

The last chapter provides an overall overview of the results of the study and the basic findings of the present research work. The following chapter also suggested certain possible applications of the produced composites. It also outlines various scopes within the related field for future studies.

-----------֍֍֍֍֍------------

CHAPTER 4

CONCLUSION

In this research, an attempt has been made to use a polymer composite beam for photo actuation, composite material characterization, and testing for the prototype system is suggested. The dissertation is broadly composed of material modeling, material characterization, modeling of the actuator, and experimental testing of the actuator, as well as the proposed prototype concept. In the current investigation, developed the polymer based composite for photo actuator, characterization of the composite material, and the deflection of the photo actuator have been successfully implemented.

The empirical and numerical (FE) modeling of the composite material was analyzed for more essential parameters of the actuator. Also, various empirical and numerical models of the composite density, mechanical, thermal, and dielectric properties were used to verify the experimental results. In continuous with this, materials and methods were discussed in detail, and the experiment carried out during this research was presented in brief. Test results on the physical, mechanical, thermal, optical, dielectric, and microstructural characteristics of PDMS and carbon black composites have been reported. Analytical and numerical (FE) methods for single-layer and bi-layer actuators have been studied using carbon black and polydimethylsiloxane composites. This approach was used to demonstrate the layered beams with varying thickness and volume percentage of the filler material, which has a vital impact on the actuator. At the end of the study, the testing method of the photo actuator is included. The results of a single layer and bilayer composite beams are tested on the laboratory scale and validated using an analytical and numerical method. Eventually, the proposed conceptual model for the photo actuation was also presented.

The specific conclusion drawn from the present investigation based on the PDMS/CB composites has led to the important points. The empirical model results show, the proposed

composite material is within the vicinity of the other models, and also, it is successfully correlated with experimental results. Numerical (FE) estimation of the coefficient of thermal expansion and thermal conductivity of carbon black filled PDMS composites are successfully modeled. It has been observed that numerical modeling serves as a perfect correlation with empirical models as well as experimental results for spherical inclusion of varied volume percentages of filler content.

A new class of polydimethylsiloxane based composite reinforce with carbon black has been used for the development of the photo actuator. Successfully fabricated the carbon black particulate filled PDMS composites by solution cast technique. The properties PDMS/CB composite of the physical, mechanical, thermal, optical, dielectric, and microstructure have also been identified. The density of plain PDMS is increased by 5.02% by adding CB filler. Young's modulus of 25% PDMS/CB composite increases by 57% compared to plain PDMS; also, the empirical results show that Young's modulus of a composite is within the acceptable range. The compressive modulus of the composite is approximately 36% greater than PDMS material. The hardness of the composite varied linearly as a percentage of filler increases. The tear strength of the plain PDMS was 0.64 (N/mm), and it enhanced by 1.37 (N/mm) at 25% CB filler content. The composites' thermal conductivity increases with an increase in the amount of CB filler. The coefficient of thermal expansion is decreased by 17.2% compared to plain PDMS. The light absorbance of the PDMS/CB is increasing 20 times compared to the pure PDMS material. Also, the crystallinity of the PDMS/CB composite rises with an increase in filler content. The dielectric permittivity is increased markedly with increases in CB content. At the frequency range of 100Hz to 100 kHz, dielectric permittivity is increased by about 48 %, at 25 Vol% of CB. The dielectric loss in the PDMS/CB composite is marginally very low. Also, the conductivity is nearly constant until a critical frequency, beyond that the conductivity relaxation follows the power law. Microstructure study reveals the bonding as well as the morphology of these composite.

The analytical and FE modeling for single and bilayer deflection of the composite structure with varied thicknesses and filler content is implemented successfully. The bilayer

deflection is found to be higher deflection than the single layer with the different volume fraction of CB as well as thicknesses. The bilayer beam shows 11.48 times more deflection than the single layer at 25 % Vol CB content. Also, at 368K, the bilayer beam deflection is 6.87 times higher than the single layer. The comparative results of the analytical and numerical (FE) model for a single and bilayer are approximately similar to each other. The single and bilayer samples were prepared and tested successfully for photo actuation. The experimental and numerical (FE) modeling results of both the layers deflection shows the almost similar results.

Experimental testing of photo actuation for cyclic mode is observed, and it is correlated with the analytical results. The composite beam approximately deflecting 9 mm in 16-sec duration and takes a long time to settle back. Finally, successfully tested a conceptual model for photo actuation. Hence, this polymer composite could be improved and suggested for photo actuation applications.

The current research work leaves a wide scope for potential researchers to investigate many other aspects of polymer composites loaded with particulate matter. Critical studies on the actuator system need to be explored thoroughly, which is directly produced as the product for societal applications.

-----------❦❦❦❦❦------------

REFERENCES

Agari, Y., and Uno, T. (1985). "Thermal conductivity of polymer filled with carbon materials: effect of conductive particle chains on thermal conductivity." *J. Appl. Polym. Sci.*, 30(5), 2225–2235.

Ahir, S. V., and Terentjev, E. M. (2005a). "Photomechanical actuation in polymer–nanotube composites." *Nat. Mater.*, 4(6), 491–495.

Ahir, S. V, and Terentjev, E. M. (2005b). "Photomechanical actuation in polymer--nanotube composites." *Nat. Mater.*, 4(6), 491.

Ahmedzade, P., and Geckil, T. (2007). "Influence of carbon black on the mechanical and electrical properties of asphalt mixtures." *Indian J. Eng. Mater. Sci.*, 14(5), 358–364.

Asaka, K., and Okuzaki, H. (2013). "Soft Actuators." *Ed. by Tak. Someya*. 151.

Baglio, S., Castorina, S., Fortuna, L., and Savalli, N. (2002). "Modeling and design of novel photo-thermo-mechanical microactuators." *Sensors Actuators, A Phys.*, 101(1–2), 185–193.

Bakshi, S. R., Lahiri, D., and Agarwal, A. (2010). "Carbon nanotube reinforced metal matrix composites - a review." *Int. Mater. Rev.*, 55(1), 41–64.

Camacho-Lopez, M., Finkelmann, H., Palffy-Muhoray, P., and Shelley, M. (2004). "Fast liquid-crystal elastomer swims into the dark." *Nat. Mater.*, 3(5), 307.

Cao, X., Zhang, M., Zhang, Z., Xu, Y., Xiao, Y., and Li, T. (2019). "Review of Soft Linear Actuator and the Design of a Dielectric Elastomer Linear Actuator." *Acta Mech. Solida Sin.*, 32(5), 566–579.

Cerretti, G., Martella, D., Zeng, H., Parmeggiani, C., Palagi, S., Mark, A. G., Melde, K., Qiu, T., Fischer, P., and Wiersma, D. S. (2016). "Towards photo-induced swimming: actuation of liquid crystalline elastomer in water." B. Gu, H. Helvajian, and A. Piqué, eds., 97380T.

Chen, X. G., Guo, J. D., Zheng, B., Li, Y. Q., Fu, S. Y., and He, G. H. (2007). "Investigation of thermal expansion of PI/SiO2 composite films by CCD imaging technique from -120 to 200 °C." *Compos. Sci. Technol.*, 67(14), 3006–3013.

Clifford, M. J., and Eastwood, D. (2004). "Design of a novel passive solar tracker." *Sol. Energy*, 77(3), 269–280.

Dang, Z. M., Yuan, J. K., Zha, J. W., Zhou, T., Li, S. T., and Hu, G. H. (2012).

"Fundamentals, processes and applications of high-permittivity polymer-matrix composites." *Prog. Mater. Sci.*

Deng, J., Li, J., Chen, P., Fang, X., Sun, X., Jiang, Y., Weng, W., Wang, B., and Peng, H. (2016). "Tunable Photothermal Actuators Based on a Pre-programmed Aligned Nanostructure." *J. Am. Chem. Soc.*, 138(1), 225–230.

Dey, T. K., and Tripathi, M. (2010). "Thermal properties of silicon powder filled high-density polyethylene composites." *Thermochim. Acta*, 502(1–2), 35–42.

Dogru, S., Aksoy, B., Bayraktar, H., and Alaca, B. E. (2018). "Poisson's ratio of PDMS thin films." *Polym. Test.*, 69, 375–384.

Du, P., Lin, X., and Zhang, X. (2011). "Dielectric constants of PDMS nanocomposites using conducting polymer nanowires." *2011 16th Int. Solid-State Sensors, Actuators Microsystems Conf. TRANSDUCERS'11*, 645–648.

Duc, N. D., and Minh, D. K. (2012). "Experimental study on Young's modulus E of a polymer composite reinforced by nano titanium dioxide particles." *Vietnam J. Mech.*, 34(1).

Fan, X., Khosravi, F., Rahneshin, V., Shanmugam, M., Loeian, M., Jasinski, J., Cohn, R. W., Terentjev, E., and Panchapakesan, B. (2015). "MoS2 actuators: reversible mechanical responses of MoS2-polymer nanocomposites to photons." *Nanotechnology*, 26(26), 261001.

Ganesh, N. J., Maniprakash, S., Chandrasekaran, L., Srinivasan, S. M., and Srinivasa, A. R. (2011). "Design and development of a sun tracking mechanism using the direct SMA actuation." *J. Mech. Des.*, 133(7), 75001.

Han, B., Zhang, Y.-L., Chen, Q.-D., and Sun, H.-B. (2018). "Carbon-Based Photothermal Actuators." *Adv. Funct. Mater.*, 28(40), 1802235.

Han, D., Meng, Z., Wu, D., Zhang, C., and Zhu, H. (2011). "Thermal properties of carbon black aqueous nanofluids for solar absorption." *Nanoscale Res. Lett.*, 6(1), 457.

Han, X., Zhang, H., Xu, R., Wang, S., and Qin, C. (2015). "Theoretical model of an optothermal microactuator directly driven by laser beams." *J. Micromechanics Microengineering*, 25(7), 75012.

Hu, Y., Liu, J., Chang, L., Yang, L., Xu, A., Qi, K., Lu, P., Wu, G., Chen, W., and Wu, Y. (2017). "Electrically and Sunlight-Driven Actuator with Versatile Biomimetic Motions Based on Rolled Carbon Nanotube Bilayer Composite." *Adv. Funct. Mater.*, 27(44), 1–10.

Hu, Y., Wu, G., Lan, T., Zhao, J., Liu, Y., and Chen, W. (2015). "A Graphene-Based

Bimorph Structure for Design of High Performance Photoactuators." *Adv. Mater.*, 27(47), 7867–7873.

Huang, C., and Zhang, W. (2018). "A Photothermal Soft Actuator Based on MoS2 and PDMS." *2018 IEEE 1st Int. Conf. Micro/Nano Sensors AI, Heal. Robot.*, 1–4.

Huang, J. C. (2002). "Carbon black filled conducting polymers and polymer blends." *Adv. Polym. Technol.*, 21(4), 299–313.

Jeong, O. C., and Konishi, S. (2005). "Fabrication of all PDMS micro pump." *Proc. 2005 Int. Symp. Micro-NanoMechatronics Hum. Sci. Eighth Symp. Micro- Nano-Mechatronics Information-Based Soc. - 21st Century COE Progr*, 130–134.

Jiang, W., Niu, D., Liu, H., Wang, C., Zhao, T., Yin, L., Shi, Y., Chen, B., Ding, Y., and Lu, B. (2014). "Photoresponsive soft-robotic platform: Biomimetic fabrication and remote actuation." *Adv. Funct. Mater.*, 24(48), 7598–7604.

Johnston, I. D., McCluskey, D. K., Tan, C. K. L., and Tracey, M. C. (2014). "Mechanical characterization of bulk Sylgard 184 for microfluidics and microengineering." *J. Micromechanics Microengineering*, 24(3).

Kausar, A., Rafique, I., and Muhammad, B. (2016). "Review of Applications of Polymer/Carbon Nanotubes and Epoxy/CNT Composites." *Polym. - Plast. Technol. Eng.*, 55(11), 1167–1191.

Kaw, A. K. (2005). *Mechanics of composite materials*. CRC press.

Keller, M. W., White, S. R., and Sottos, N. R. (2007). "A Self-Healing Poly(Dimethyl Siloxane) Elastomer." *Adv. Funct. Mater.*, 17(14), 2399–2404.

Kim, D., Lee, H. S., and Yoon, J. (2016). "Highly bendable bilayer-type photo-actuators comprising of reduced graphene oxide dispersed in hydrogels." *Sci. Rep.*, 6, 20921.

Kim, J. U., Lee, S., Kang, S. J., and Kim, T. Il. (2018). "Materials and design of nanostructured broadband light absorbers for advanced light-to-heat conversion." *Nanoscale*, Royal Society of Chemistry.

Kohlmeyer, R. R., and Chen, J. (2013). "Wavelength-selective, IR light-driven hinges based on liquid crystalline elastomer composites." *Angew. Chemie - Int. Ed.*, 52(35), 9234–9237.

Leeladhar, Raturi, P., Kumar, A., and Singh, J. P. (2017). "Graphene-polydimethylsiloxane/chromium bilayer-based flexible, reversible, and large bendable photomechanical actuators." *Smart Mater. Struct.*, 26(9).

Levitsky, I. A., Kanelos, P. T., Woodbury, D. S., and Euler, W. B. (2006). "Photoactuation

from a carbon nanotube-nafion bilayer composite." *J. Phys. Chem. B*, 110(19), 9421–9425.

Li, C., Liu, Y., Huang, X., and Jiang, H. (2012). "Direct sun-driven artificial heliotropism for solar energy harvesting based on a photo-thermomechanical liquid-crystal elastomer nanocomposite." *Adv. Funct. Mater.*, 22(24), 5166–5174.

Li, K., and Cai, S. (2016). "Modeling of light-driven bending vibration of a liquid crystal elastomer beam." *J. Appl. Mech. Trans. ASME*, 83(3), 1–6.

Li, M.-H., Keller, P., Li, B., Wang, X., and Brunet, M. (2003). "Light-Driven Side-On Nematic Elastomer Actuators." *Adv. Mater.*, 15(7-8), 569–572.

Li, M., Lv, S., and Zhou, J. (2014). "Photo-thermo-mechanically actuated bending and snapping kinetics of liquid crystal elastomer cantilever." *Smart Mater. Struct.*, 23(12), 125012.

Li, Y., Verbiest, T., and Vankelecom, I. (2013). "Improving the flux of PDMS membranes via localized heating through incorporation of gold nanoparticles." *J. Memb. Sci.*, 428, 63–69.

Lim, H., Park, T., Na, J., Park, C., Kim, B., and Kim, E. (2017). "Construction of a photothermal Venus flytrap from conductive polymer bimorphs." *NPG Asia Mater.*, 9(7), 1–8.

Liu, H., Niu, D., Jiang, W., Zhao, T., Lei, B., Yin, L., Shi, Y., Chen, B., and Lu, B. (2016). "Illumination-oriented and thickness-dependent photomechanical bilayer actuators realized by graphene-nanoplatelets." *Sensors Actuators, A Phys.*, 239, 45–53.

Loomis, J., Fan, X., Khosravi, F., Xu, P., Fletcher, M., Cohn, R. W., and Panchapakesan, B. (2013). "Graphene/elastomer composite-based photo-thermal nanopositioners." *Sci. Rep.*, 3, 1–10.

Luo, R., Wu, J., Dinh, N. D., and Chen, C. H. (2015). "Gradient porous elastic hydrogels with shape-memory property and anisotropic responses for programmable locomotion." *Adv. Funct. Mater.*, 25(47), 7272–7279.

Maggi, C., Saglimbeni, F., Dipalo, M., Angelis, F. De, and Leonardo, R. Di. (2015). "Micromotors with asymmetric shape that efficiently convert light into work by thermocapillary effects." *Nat. Commun.*, 6, 1–5.

Maragò, O. M., Jones, P. H., Gucciardi, P. G., Volpe, G., and Ferrari, A. C. (2013). "Optical trapping and manipulation of nanostructures." *Nat. Nanotechnol.*, 8(11), 807–819.

Meng, J., Mu, J., Hou, C., Zhang, Q., Li, Y., and Wang, H. (2017). "A flexible metallic actuator using reduced graphene oxide as a multifunctional component." *Nanoscale*, 9(35),

12963–12968.

Mu, X., Sowan, N., Tumbic, J. A., Bowman, C. N., Mather, P. T., and Qi, H. J. (2015). "Photo-induced bending in a light-activated polymer laminated composite." *Soft Matter*, 11(13), 2673–2682.

Nakamura, A., and Kawakami, S. (2019). "An actuator–sensor hybrid device made of carbon-based polymer composite for self-sensing systems." *AIP Adv.*, 9(6), 065311.

Nguyen, T. D., and Duc, N. D. (2016). "Evaluation of elastic properties and thermal expansion coefficient of composites reinforced by randomly distributed spherical particles with negative Poisson's ratio." *Compos. Struct.*, 153, 569–577.

Niu, D., Jiang, W., Liu, H., Zhao, T., Lei, B., Li, Y., Yin, L., Shi, Y., Chen, B., and Lu, B. (2016). "Reversible Bending Behaviors of Photomechanical Soft Actuators Based on Graphene Nanocomposites." *Sci. Rep.*, 6(May), 1–10.

Oosten, C. L. Van, Corbett, D., Davies, D., Warner, M., Bastiaansen, C. W. M., and Broer, D. J. (2008). "Bending dynamics and directionality reversal in liquid crystal network photoactuators." *Macromolecules*, 41(22), 8592–8596.

Pimentel-Domínguez, R., Velázquez-Benítez, A. M., Vélez-Cordero, J. R., Hautefeuille, M., Sánchez-Arévalo, F., and Hernández-Cordero, J. (2016). "Photothermal Effects and Applications of Polydimethylsiloxane Membranes with Carbon Nanoparticles." *Polymers (Basel).*, 8(4).

Pradhan, D. K., Choudhary, R. N. P., and Samantaray, B. K. (2008). *Studies of Dielectric Relaxation and AC Conductivity Behavior of Plasticized Polymer Nanocomposite Electrolytes*. *Int. J. Electrochem. Sci.*

Rivlin, R. S., and Thomas, A. G. (1953). "Rupture of rubber. I. Characteristic energy for tearing." *J. Polym. Sci.*, 10(3), 291–318.

Sharma, M., and Sharma, V. (2016). "Chemical, mechanical, and thermal expansion properties of a carbon nanotube-reinforced aluminum nanocomposite." *Int. J. Miner. Metall. Mater.*, 23(2), 222–233.

Tai, Y., Lubineau, G., and Yang, Z. (2016). "Light-Activated Rapid-Response Polyvinylidene-Fluoride-Based Flexible Films." *Adv. Mater.*, 28(23), 4665–4670.

Tang, Z., Gao, Z., Jia, S., Wang, F., and Wang, Y. (2017). "Graphene-Based Polymer Bilayers with Superior Light-Driven Properties for Remote Construction of 3D Structures." *Adv. Sci.*, 4(5).

Tjahjono, I. K., and Bayazitoglu, Y. (2008). "Near-infrared light heating of a slab by

embedded nanoparticles." *Int. J. Heat Mass Transf.*, 51(7), 1505–1515.

Torras, N., Zinoviev, K., Camargo, C. J., Campanella, H., Esteve, J., Campo, E. M., Marshall, J. E., and Terentjev, E. M. (2011). "Opto-mechanical parameters of liquid crystals elastomers with carbon nanotubes." *Nano-Opto-Mechanical Syst.*, 8107, 810704.

Torres, D., Green, A. J., Wang, T., Sepúlveda, N., Fernández, F. E., and Wang, C. (2015). "Increasing Efficiency, Speed, and Responsivity of Vanadium Dioxide Based Photothermally Driven Actuators Using Single-Wall Carbon Nanotube Thin-Films." *ACS Nano*, 9(4), 4371–4378.

Tsai, P. J., Nayak, S., Ghosh, S., and Puri, I. K. (2017). "Influence of particle arrangement on the permittivity of an elastomeric composite." *AIP Adv.*, 7(1).

Vassalini, I., and Alessandri, I. (2017). "'the phactalysts': Carbon nanotube/TiO2 composites as phototropic actuators for wireless remote triggering of chemical reactions and catalysis." *Nanoscale*, 9(32), 11446–11451.

Wang, E., Desai, M. S., and Lee, S.-W. (2013). "Light-controlled graphene-elastin composite hydrogel actuators." *Nano Lett.*, 13(6), 2826–30.

Wang, Q., Sheng, B., Wu, H., Huang, Y., Zhang, D., and Zhuang, S. (2019). "Composite films of polydimethylsiloxane and micro-graphite with tunable optical transmittance." *Appl. Sci.*, 9(12).

Weng, M., Zhou, P., Chen, L., Zhang, L., Zhang, W., Huang, Z., Liu, C., and Fan, S. (2016). "Multiresponsive Bidirectional Bending Actuators Fabricated by a Pencil-on-Paper Method." *Adv. Funct. Mater.*, 26(40), 7244–7253.

Xu, W., and Allen, M. G. (2009). "fabrication of patterned carbon nanotube (cnt) / elastomer bilayer material and its utilization as force sensors."

Yang, H., Leow, W. R., Wang, T., Wang, J., Yu, J., He, K., Qi, D., Wan, C., and Chen, X. (2017). "3D Printed Photoresponsive Devices Based on Shape Memory Composites." *Adv. Mater.*, 29(33).

Yoon, C. (2019). "Advances in biomimetic stimuli responsive soft grippers." *Nano Converg.*, 6(1).

Zhang, B.-T., Zheng, X., Li, H.-F., and Lin, J.-M. (2013). "Application of carbon-based nanomaterials in sample preparation: a review." *Anal. Chim. Acta*, 784, 1–17.

Zhang, W., Chen, L., Zhang, J., and Huang, Z. (2017). "Design and optimization of carbon nanotube/polymer actuator by using finite element analysis." *Chinese Phys. B*, 26(4).

Zhang, X., Yu, Z., Wang, C., Zarrouk, D., Seo, J. W. T., Cheng, J. C., Buchan, A. D.,

Takei, K., Zhao, Y., Ager, J. W., Zhang, J., Hettick, M., Hersam, M. C., Pisano, A. P., Fearing, R. S., and Javey, A. (2014a). "Photoactuators and motors based on carbon nanotubes with selective chirality distributions." *Nat. Commun.*, 5, 1–8.

Zhang, X., Yu, Z., Wang, C., Zarrouk, D., Seo, J. W. T., Cheng, J. C., Buchan, A. D., Takei, K., Zhao, Y., Ager, J. W., Zhang, J., Hettick, M., Hersam, M. C., Pisano, A. P., Fearing, R. S., and Javey, A. (2014b). "Photoactuators and motors based on carbon nanotubes with selective chirality distributions." *Nat. Commun.*, 5, 2983.

Zhou, S., Cun, F., Zhang, Y., Zhang, L., Yan, Q., Sun, Y., and Huang, W. (2019). "Thermo-Responsive Aluminum-Based Polymer Composite Films with Controllable Deformation." *J. Mater. Chem. C.*

Zhu, L., Gao, M., Peh, C. K. N., and Ho, G. W. (2018). "Solar-driven photothermal nanostructured materials designs and prerequisites for evaporation and catalysis applications." *Mater. Horiz.*, 5(3), 323–343.

Zhu, W., Shelley, M., and Palffy-Muhoray, P. (2011). "Modeling and simulation of liquid-crystal elastomers." *Phys. Rev. E - Stat. Nonlinear, Soft Matter Phys.*, 83(5), 1–11.

-----------֎֎֎֎֎------------

List of Publications based on Ph.D. Research Work

The thesis titled "**Development and Characterization of Polydimethylsiloxane and Carbon black Composites for Photo Actuation**" is the outcome of the research carried at the Department of Mechanical Engineering, National Institute of Technology Karnataka. The research outcomes in the following publications and conference proceedings are provided below

Sl. No.	Title of the paper	Authors (In the same order as in the paper, underline the Research Scholar's name)	Name of the Journal/Conference/Symposium, Vol., No., Pages	Month & Year of Publication	Category*
1	Modelling and Analysis of Thermomechanical Behaviour in Composite Bimorph Actuator	<u>Shivashankar H</u>, S.M. Kulkarni	Materials Science Forum ISSN: 1662-9752, Vol. 928, pp 209-214 2018 Trans Tech Publications, Switzerland	Aug 2018	1
2	Optimization of Bilayer Actuator Based on Carbon Black/Polymer Composites	<u>Shivashankar H</u>, Sangamesh R and S M Kulkarni	IOP Conference Series: Materials Science and Engineering, vol. 522, no. 1, p. 012007. doi:10.1088/1757-899X/522/1/012007	May 2019	1
3	Modelling and Analysis of Polymer Diaphragms for Micro Sensing and Actuation	Sushmita, <u>Shivashankar Hiremath</u>, Satyabodh M Kulkarni	AIP Conference Proceedings 2080, 020004 (2019) doi.org/10.1063/1.5092887	Mar 2019	1
4	Processing and Investigation of Mechanical Characteristics on the Polydimethylsiloxane/Carbon Black Composites	<u>H Shivashankar</u>, R Sangamesh, and S M Kulkarni	Materials Research Express, Volume 6, Number 10. doi.org/10.1088/2053-1591/ab3b7e	Aug 2019	1
5	Analysis of Coefficient of Thermal Expansion in Carbon Black Filled PDMS Composite	<u>Shivashankar H</u>, Sangamesh, S.M. Kulkarni	Materials Science Forum ISSN:1662-9752,Vol,978,pp 237-244 Trans Tech Publications, Switzerland	Feb 2020	1
6	Photomechanical actuation of polydimethylsiloxane/carbon black nanocomposite	<u>Shivashankar Hiremath</u>, Satyabodh. Kulkarni	Micro and Nano Letters, DOI: 10.1049/mnl.2019.0286, ISSN 1750-0443, IET, Journal	Mar 2020	1
7	Modeling and optimization of thermally excited carbon black/polymer composite actuator	<u>Shivashankar H</u>, S.M. Kulkarni	Material Today Proceeding	The publication is in press	3

131

8	Investigations on the Thermal Actuation of Carbon Black Reinforced PDMS Composite Uni-Layer and Bi-Layer Cantilever Beams	**Hiremath Shivashankar**, D, Sushmita; Kulkarni, S M; P, Navin Karanth; Desai, Vijay	Journal of modern manufacturing technology	The publication is in press	1
9	Synthesis, Characterization, and Physico-Mechanical Properties of Carbon Black infused Polymer Composite."	**Shivashankar H**, Sangamesh, Kevin A M, S.M. Kulkarni	Journal of materials processing	Under review	1
10	Investigation on dielectric properties of PDMS based nanocomposites	**Shivashankar H,** Manohar S B S, Kevin A M, S M Kulkarni	Journal of Physica B	Under review	1
11	Theoretical and experimental investigation on dielectric properties of the polymer nanocomposite for electronic applications	**Shivashankar H**, Kevin Amith Mathias, Shrishail M H, S M Kulkarni	IET Nano dielectrics	Under review	1
12	Progression and Characterization of polydimethylsiloxane-carbon black nanocomposites for photothermal actuation	**Shivashankar Hiremath**, Shrishail M H, Satyabodh. Kulkarni	Sensor and Actuator A: Physical	Under review	1

Category*

1: Journal paper, the full paper reviewed 2: Journal paper, Abstract reviewed   3: Conference/Symposium paper, the full paper reviewed 4: Conference/Symposium paper, abstract reviewed 5: others (including papers in Workshops, NITK Research Bulletins, Short notes, etc.) (If the paper has been accepted for publication but yet to be published, the supporting documents must be attached.)

Research Scholar   **Research Guide**

Mr. Shivashankarayya Hiremath   Prof.S.M.Kulkarni

Bio-Data

Name: Shivashankarayya Hiremath
Father 's Name: Mallikarjunayya Hiremath
Mother's Name: Mahadevi Hiremath
Date of Birth: 26 July 1986
Nationality: Indian
Marital Status: Married

Permanent address	Present address
S/o M C Hiremath, #59, 3rd cross Shiradi Nagar UAS, Dharwad, Dharwad-580005 Karnataka, India	Department of Mechatronics Engineering Manipal Institute of Technology, Manipal University, MAHE, Manipal Udupi-576104, Karnataka, India

Mobile Number: +91-9986906205
E-mail ID: sssnitk@gmail.com; sssdait@gmail.com
Orchid-ID: 0000-0001-7613-9832; Scopus-ID: 57205542475

Educational Qualification

- Ph.D. Continued in Mechanical Engineering at National Institute of Technology, Karnataka, India.
- M.Tech in Space Engineering (Instrumentation and control) at Manipal Institute of Technology, Manipal, Karnataka.
- B.E in Instrumentation Technology at Dr. Ambedkar Institute of Technology, Bangalore, Karnataka.

Awards and Recognition

- Received Ph.D. scholarship by the Ministry of Human Resource Development (MHRD), Government of India.
- Received "Young Scientist Travel Grant" from Human Resource Development Group (HTDG), Council of Scientific & Industrial Research (CSIR) for attending, International Conference on Manufacturing Science and Technology at the University of Malaya Malaysia.
- Received travel grant from Alumni association, NITK, Surathkal for attending the International conference on composite material and material engineering held at NUS, Singapore. From 26-28 Jan 2018.
- Best presentation award at International Conference on Manufacturing science and technology (ICMST-18) held at Kuala Lumpur Malaysia, from 11-13 March 2018.